

LINKING ACETYL-COA METABOLISM AND HISTONE ACETYLATION  
TO DYNAMIC GENE REGULATION IN YEAST AND MOUSE HIPPOCAMPUS

Philipp Mews

A DISSERTATION

in

Cell and Molecular Biology

Presented to the Faculties of the University of Pennsylvania

in

Partial Fulfillment of the Requirements for the

Degree of Doctor of Philosophy

2016

Supervisor of Dissertation

Graduate Group Chairperson

---

Shelley L. Berger, Ph.D.

---

Daniel S. Kessler, Ph.D.

Daniel S. Och University Professor

Associate Professor of Cell

Director, Epigenetics Program

and Developmental Biology

Dissertation Committee

Mitchell A. Lazar, M.D., Ph.D., Sylvan H. Eisman Professor of Medicine

F. Bradley Johnson, M.D., Ph.D., Associate Professor of Pathology and Laboratory Medicine

Ben E. Black, Ph.D., Associate Professor of Biochemistry and Biophysics

Kathryn E. Wellen, Ph.D., Assistant Professor of Cancer Biology

LINKING ACETYL-COA METABOLISM AND HISTONE ACETYLATION  
TO DYNAMIC GENE REGULATION IN YEAST AND MOUSE HIPPOCAMPUS

COPYRIGHT

2016

Philipp Mews

This work is licensed under the  
Creative Commons Attribution-  
NonCommercial-ShareAlike 3.0  
License

To view a copy of this license, visit

<http://creativecommons.org/licenses/by-nc-sa/2.0/>

## ABSTRACT

### LINKING ACETYL-COA METABOLISM AND HISTONE ACETYLATION TO DYNAMIC GENE REGULATION IN YEAST AND MOUSE HIPPOCAMPUS

Philipp Mews

Shelley L. Berger

A compelling body of evidence suggests an intimate relationship between metabolic state and chromatin regulation. This link is manifested in key metabolites that participate in biochemical pathways as intermediates, and function as cofactors to regulate chromatin modifying enzymes. Of particular interest is the metabolite acetyl-CoA, given its central role as an intermediate of cellular energy metabolism and key determinant of all histone acetylation. How nuclear acetyl-CoA levels are regulated to, in turn, control histone acetylation is under intense investigation, and holds promise for increased understanding of the molecular mechanisms adapting gene expression to internal and external stimuli. We studied the relationship between histone modification dynamics and the dramatic transcriptional changes that occur during nutrient-induced cell cycle re-entry from quiescence in the yeast *S. cerevisiae*. CHIP-seq and SILAC-based mass spec revealed genome-wide shifts in histone acetylation at growth and stress genes as cells exit quiescence and transcription dramatically changes. Strikingly, however, the patterns of histone methylation remain intact. We conclude that histone acetylation, in contrast to methylation, rapidly responds to metabolic state, driving growth gene transcription in nutrient-induced cell cycle re-entry. Next, we set out to investigate how nuclear acetyl-CoA is regulated to control histone acetylation in mammalian cells. We reveal a previously unknown function of the central metabolic enzyme acetyl-CoA synthetase 2 (ACSS2) as a chromatin-bound transcriptional coactivator that stimulates histone acetylation and gene expression. We show that ACSS2 is a critical and direct regulator of histone acetylation in neurons and of long-term mammalian memory. Genome-wide, ACSS2 binding corresponds with increased histone acetylation and gene

expression of key neuronal genes. Our data indicate that ACSS2 functions as a chromatin-bound co-activator to increase local concentrations of acetyl-CoA, to locally promote histone acetylation for transcription of neuron-specific genes. Remarkably, in vivo attenuation of hippocampal ACSS2 expression in adult mice impairs long-term spatial memory, a cognitive process reliant on histone acetylation. ACSS2 reduction in hippocampus also leads to a defect in upregulation of key neuronal genes involved in memory. These findings reveal a unique connection between cellular metabolism and neural plasticity, and establish a link between generation of acetyl-CoA and neuronal chromatin regulation.

## TABLE OF CONTENTS

<b>CHAPTER 1 INTRODUCTION</b> .....	<b>1</b>
ABOVE AND BEYOND: EPIGENETICS .....	2
AT THE NEXUS OF METABOLIC STATE AND CHROMATIN STRUCTURE .....	6
CHROMATIN: A BONA-FIDE ENERGY SENSOR? .....	11
BEYOND THE ABOVE: EPIGENETIC MECHANISMS IN COGNITION .....	14
<b>CHAPTER 2 HISTONE METHYLATION HAS DYNAMICS DISTINCT FROM THOSE OF HISTONE ACETYLATION IN CELL CYCLE REENTRY FROM QUIESCENCE</b> .....	<b>21</b>
ABSTRACT .....	22
INTRODUCTION.....	23
RESULTS.....	25
<i>Histone methylation does not change globally during cell cycle re-entry</i> .....	25
<i>Histone methylation dynamics are distinct from histone acetylation during exit</i> .....	28
<i>Histone methylation is redistributed genome-wide during quiescence and exit</i> .....	35
DISCUSSION .....	46
<i>Histone methylation as an epigenetic memory mark during metabolic shifts</i> .....	47
<i>Histone methylation in the context of altered metabolism in cancer and stem cells</i> ...	49
MATERIALS AND METHODS .....	51
<b>CHAPTER 3 ACETYL-COA METABOLISM BY ACSS2 REGULATES NEURONAL HISTONE ACETYLATION AND LONG-TERM MEMORY</b> .....	<b>56</b>
ABSTRACT .....	57
INTRODUCTION.....	58
RESULTS.....	59
<i>ACSS2 is localized to nuclei in differentiated neurons</i> .....	59
<i>ACSS2 regulates neuronal gene expression</i> .....	61
<i>ACSS2 is recruited to transcriptionally active chromatin</i> .....	65
<i>ACSS2 functions in neuronal histone acetylation</i> .....	72
<i>ACSS2 regulates long-term memory storage</i> .....	74
<i>ACSS2 regulates dynamic upregulation of early response genes in vivo</i> .....	79
DISCUSSION .....	81
EXPERIMENTAL PROCEDURES .....	85
<b>CHAPTER 4 GENERAL DISCUSSION AND CONCLUSIONS</b> .....	<b>90</b>
<i>Chromatin-localized acetyl-CoA metabolism functions in regulated gene expression</i> .....	91
<i>Role of ACSS2 in neuronal histone acetylation linked to alcohol consumption</i> .....	93
<i>ACSS2 as a therapeutic target in neuropsychiatric disorders</i> .....	95
<b>APPENDIX</b> .....	<b>98</b>
<b>BIBLIOGRAPHY</b> .....	<b>101</b>

## LIST OF ILLUSTRATIONS

### CHAPTER 1

Figure 1.1. Waddington's epigenetic landscape .....	2
Figure 1.2. Atomic structure of the core histones and nucleosome.....	3
Figure 1.3. Post-translational modifications of histone proteins .....	4
Figure 1.4. Model for transcriptional activation and repression .....	5
Figure 1.5. Chromatin-remodeling enzymes 'sense' cellular metabolism .....	7
Figure 1.6. Methodology of SILAC-mass spec analysis of histone modification dynamics.....	8
Figure 1.7. SILAC-mass spec and ChIP-seq work synergistically to capture dynamic aspects of chromatin-mediated gene regulation .....	10
Figure 1.8. Chromatin-mediated transcriptional control by intermediary metabolism .....	12
Figure 1.9. Schematic of hippocampal anatomy and contribution to behavior. ....	16
Figure 1.10. Functional mechanisms of transcriptional activation by CBP/p300.....	17
Figure 1.11. Synthesis of acetyl-CoA in yeast and mammalian cells .....	18

### CHAPTER 2

Figure 2.1. Nutrient availability stimulates histone acetylation and dramatic change in gene expression, but does not alter global histone methylation levels.....	26
Figure 2.2. SILAC-mass spectrometry analysis of histone protein and methylation dynamics in proliferating cells. ....	30
Figure 2.3. Histone methylation, unlike acetylation, remains static during quiescence exit. ....	33
Figure 2.4. Histone methylation is redistributed as proliferating cells enter quiescence, but remains static in early exit from quiescence. ....	36
Figure 2.5. Histone methylation at individual stress and growth genes remains stable upon nutrient replenishment.....	38
Figure 2.6. Box plot analysis shows distinct dynamics of histone acetylation and methylation at growth and stress genes during the early exit. ....	39
Figure 2.7. Scatterplot analyses demonstrate distinct dynamics of histone acetylation and methylation at growth genes. ....	40
Figure 2.8. H3K36me3 retained at growth genes in quiescent yeast is required for rapid transcriptional activation during exit.....	41
Figure 2.9. Histone acetylation and histone methylation levels at stress-responsive RRPE/PAC and nutrient-insensitive genes in quiescence and cell cycle re-entry.....	43
Figure 2.10. Histone methylation patterns correlate genome-wide in quiescence exit. ....	44
Figure 2.11. Schematic model for the distinct dynamics of histone methylation and acetylation during quiescence establishment and exit.....	46

### **CHAPTER 3**

Figure 3.1. ACSS2 localizes to the nucleus upon CAD neuron differentiation. ....	60
Figure 3.2. ACSS2 supports neuronal gene expression. ....	62
Figure 3.3. ACSS2 knockdown does not lower global gene expression .....	64
Figure 3.4. ACSS2 is recruited to transcriptionally active chromatin. ....	66
Figure 3.5. Relationship between ACSS2 enrichment and increased histone acetylation. ....	68
Figure 3.6. UCSC Genome Browser views of ACSS2 ChIP-seq data .....	70
Figure 3.7. Genic enrichment of ACSS2 corresponds to increased gene expression. ....	72
Figure 3.8. ACSS2 functions in neuronal histone acetylation. ....	74
Figure 3.9. ACSS2 is highly expressed in the dorsal CA1 region of the hippocampus .....	76
Figure 3.10. ACSS2 knockdown in dorsal hippocampus impairs object location memory. ....	78
Figure 3.11. ACSS2 regulates retrieval-induced upregulation immediate-early genes in vivo. ....	80

### **APPENDIX**

Figure A1. Histone H4 acetylation labeling in SILAC with heavy EtOH. ....	98
Figure A2. Heavy EtOH-SILAC – Histone acetylation labeling in liver .....	99
Figure A3. Heavy EtOH-SILAC – Histone acetylation labeling in cortex and hippocampus .....	100

**CHAPTER 1**  
**INTRODUCTION**

## ABOVE AND BEYOND: EPIGENETICS

The term epigenetics was coined by Waddington to describe a conceptual solution to a fundamental consideration – and conundrum – in developmental biology<sup>1</sup>. All the different types of cells that make up our bodies, bar certain exceptions in our reproductive and immune systems, have exactly the same genome. Hence, our muscle cells contain the exact same DNA nucleotide sequence as our brain cells. Therefore, a key question is how can the identical DNA template yield distinct cell types like myocytes or neurons? How can two cells have the exact same DNA but produce vastly different gene products? Waddington reasoned there must be a mechanism *above* the level of DNA that controls the readout of genes encoded in its nucleotide sequence – coining the term *epigenetics*. These epigenetic mechanisms specify certain sets of genes that are turned into functional products in neurons, for instance, yet not in myocytes. Diverse epigenetic marks are set up during early cell fate decisions, in due course forming a cellular memory system that perpetuates cellular phenotypes over the lifespan of our bodies. In view of that, classic epigenetics is the study of a change in gene expression or cellular phenotype that is stably inherited by a cell and that is not associated with changes in DNA sequence<sup>2</sup> (Fig. 1.1).

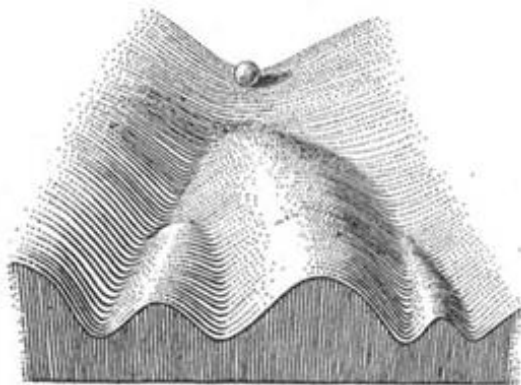


Figure 1.1. Waddington's epigenetic landscape

Conrad Waddington used the concept of the epigenetic landscape to describe the process by which a cell, pictured here as a ball, may follow many different paths of differentiation during development. (Waddington, 1957)<sup>1</sup>

Recent years have seen spectacular advances in the field of epigenetics, and additional aspects of epigenetic control keep emerging that extend its modern definition. These qualities transcend the mechanisms that hard-wire phenotypes at the cellular level during development, and further implicate them in the acute regulation of dynamic gene expression that must be adapted to the ever-changing cellular environment. It is through epigenetic mechanisms that the relatively fixed genetic blueprint can flexibly accommodate variability resulting from environmental stimuli, dietary signals, and other influences. Remarkably, epigenetic regulation is not only critical for basic cellular processes such as neuronal plasticity, but is now being recognized to play important congruent roles in highly complex behaviors such as learning and memory<sup>3,4</sup>.

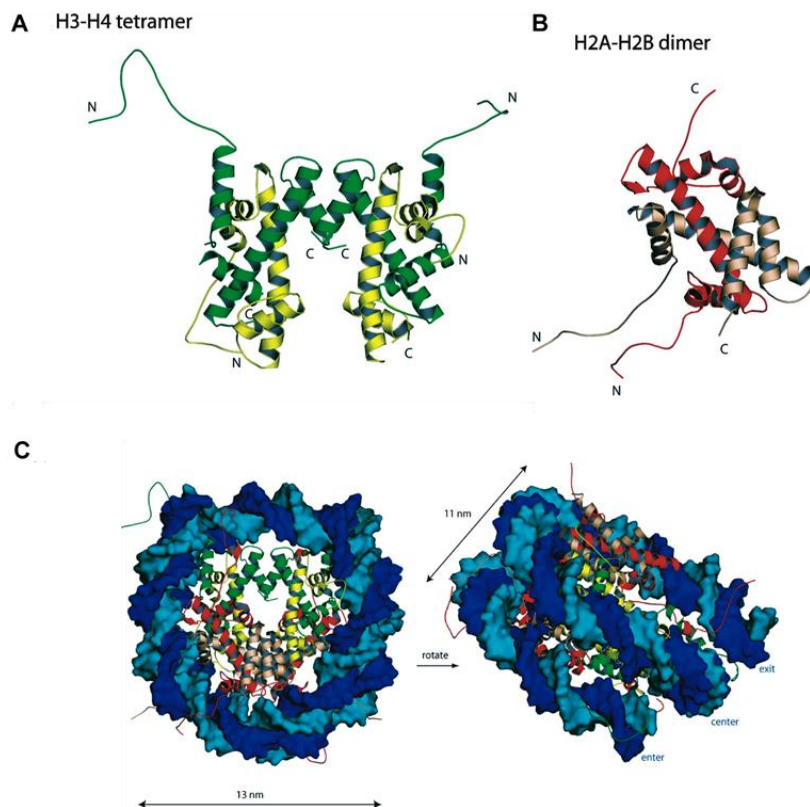


Figure 1.2. Atomic structure of the core histones and nucleosome.

(A) A tetramer of H3 (green) and H4 (yellow). (B) A dimer of H2A (red) and H2B (pink). (C) Nucleosome core particle. Each strand of DNA is shown in a different shade of blue. The DNA makes 1.7 turns around the histone octamer to form an overall particle with a disk-like structure. Histones are colored as in (A) and (B). (adapted from Khorasanizadeh, 2004)<sup>5</sup>



Post-translational modifications of histones elicit structural and functional changes within chromatin and regulate various epigenetic processes. Numerous histone modifications have been identified and include acetylation, methylation, phosphorylation, ubiquitylation, sumoylation, and ADP-ribosylation<sup>6,8</sup> (Fig. 1.3). Acetylation, for instance, along with methylation, is the most extensively studied histone modification, and has broad effects on chromatin function and nuclear signaling pathways<sup>9,10</sup>. Histone acetylation marks are written by histone acetyltransferases (HATs). These enzymes acetylate specific lysine residues of histone proteins, which neutralizes their positive charge, and can thus help to de-condense chromatin leading to active gene transcription<sup>10</sup>. Additionally, histone acetylation marks can be bound by small protein modules called bromodomains, often referred to as ‘readers’. These domains are conserved within many chromatin-associated proteins – including HATs themselves – that regulate transcription-mediated biological processes (Fig. 1.4), and whose aberrant activities are correlated with several human diseases<sup>11–13</sup>. Insight into the kinetic mechanisms of the writers, readers, and erasers of chromatin modifications is anticipated to provide us with novel clinically relevant diagnostic, prognostic, and therapeutic avenues in the treatment of disease, including cancer and neurodegenerative disorders.

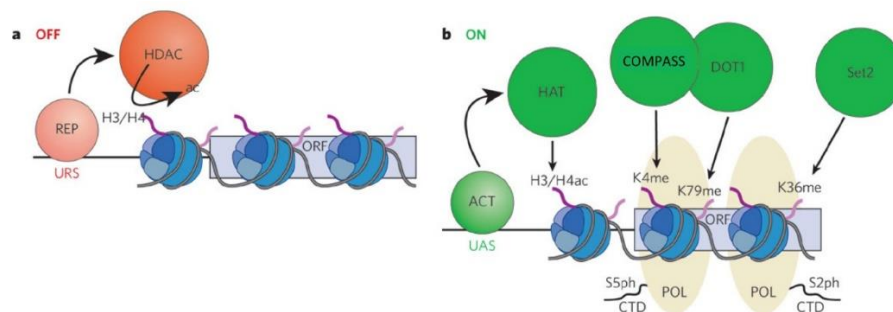


Figure 1.4. Model for transcriptional activation and repression

(A) In the off state, the DNA-bound repressor (REP) at the upstream repressor site (URS) recruits negative modifiers, such as histone deacetylases (HDAC), which remove acetyl groups from histones. (B) In the on state, DNA-bound activator (ACT) at the upstream activator site (UAS) recruits positive modifiers, such as histone acetylases (HAT). Early during elongation, the C-terminal domain (CTD) of the RNA polymerase (POL) is phosphorylated at serine 5, leading to recruitment of the COMPASS complex (Set1, part of the COMPASS complex, methylates H3K4) and DOT1 (which methylates H3K79). Later in elongation the CTD repeat is phosphorylated at serine 2 (S2ph), which recruits Set2 (H3K36 methylase enzyme). (from Berger, 2007)<sup>6</sup>

## AT THE NEXUS OF METABOLIC STATE AND CHROMATIN STRUCTURE

The intimate relationship between metabolic state and chromatin regulation has gained major interest in the field of epigenetics. Cells must continually adapt to metabolic needs and changing environment, and therefore require an acutely responsive system that adjusts chromatin structure and gene transcription to maintain homeostasis. Metabolic homeostasis is maintained by an intricate regulatory circuitry, controlled to a large extent by transcriptional<sup>14–17</sup>. In recent years, a new paradigm of transcriptional regulation has emerged, based on direct sensing of intermediary metabolites by chromatin-modifying enzymes<sup>15,18</sup>. Key metabolites, beside their role in central biochemical pathways as intermediates, also participate as cofactors in chromatin modification, and can therefore dynamically adapt global chromatin structure and gene expression to metabolic change<sup>19</sup> (Fig. 1.5). Advancing our insight into how metabolic state influences chromatin structure thus holds promise for new intervention points in the treatment of diseases that are characterized by epigenetic aberration, including cancer and neurodegenerative disorders. Hence, metabolic pathways and the enzymes that provide metabolites used in chromatin modification have now moved into the limelight of epigenetic studies. In particular, the temporal turnover dynamics of histone modifications – and their dysregulation upon nutritional and metabolic disruption – are of increasing interest.

The endeavor of exploring the dynamic relationship between cellular metabolism and chromatin structure, however, is challenged by technological limitations. The advent of chromatin immunoprecipitation sequencing (ChIP-seq) technology truly revolutionized the field of epigenetics<sup>20–22</sup>, and has become the prevalent method to interrogate the genome-wide binding pattern of epigenetic enzymes and their cognate chromatin modifications. In the past decade, a wave of epigenomic analyses using ChIP-seq generated maps of the epigenetic landscape that greatly expanded our knowledge of chromatin structure and its aberrations in disease. Yet, this now routine method fails to capture important dynamic aspects in epigenetic regulation. Thus, in order to examine how cellular metabolism regulates dynamic change in chromatin structure, we

devised a highly adaptable approach that employs two complementary methods: making use of both high throughput sequencing data to establish the location of changes, and stable isotope tracing using mass spectrometry to evaluate their dynamics.

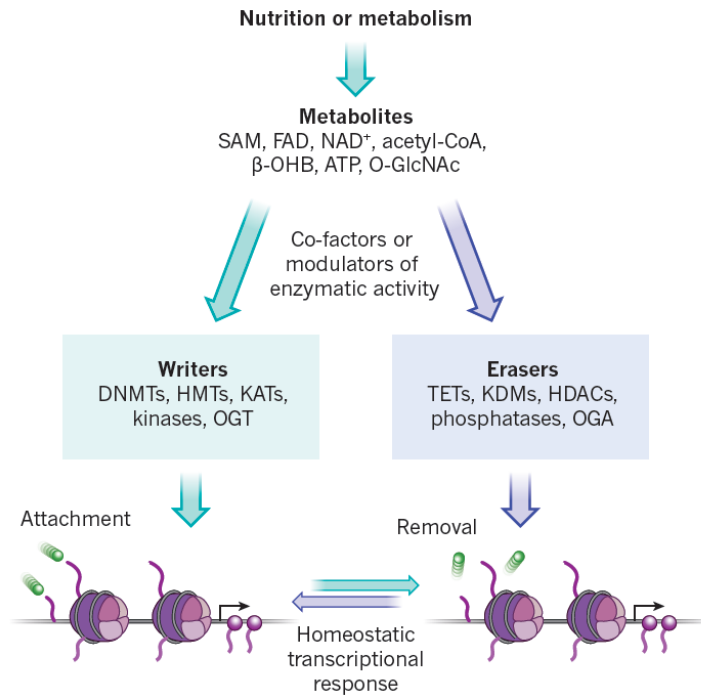


Figure 1.5. Chromatin-remodeling enzymes ‘sense’ cellular metabolism

Homeostatic transcriptional responses are induced by changes in nutrition or fluctuations in metabolism. The enzymatic activity of chromatin-associated proteins is changed in a dose-dependent manner by several intermediary metabolism products. ‘Writer’ enzymes that attach marks covalently to chromatin or DNA and ‘erasers’ that remove these modifications act as metabolic sensors. Chromatin modifications remodel DNA–histone interactions and regulate the recruitment of transcriptional complexes to genes that control cellular function. DNMT, DNA methyltransferases; FAD, flavin adenine dinucleotide; HDACs, histone deacetylases; HMTs, histone methyltransferases; KATs, lysine acetyltransferases; KDMs, lysine demethylases; O-GlcNAc, O-linked N-acetylglucosamine; OGT, O-GlcNAc transferase; OGA, O-GlcNAcase; β-OHB, β-hydroxybutyrate; SAM, S-adenosylmethionine; TET, ten-eleven translocation protein. (from Gut and Verdin, 2013)<sup>19</sup>

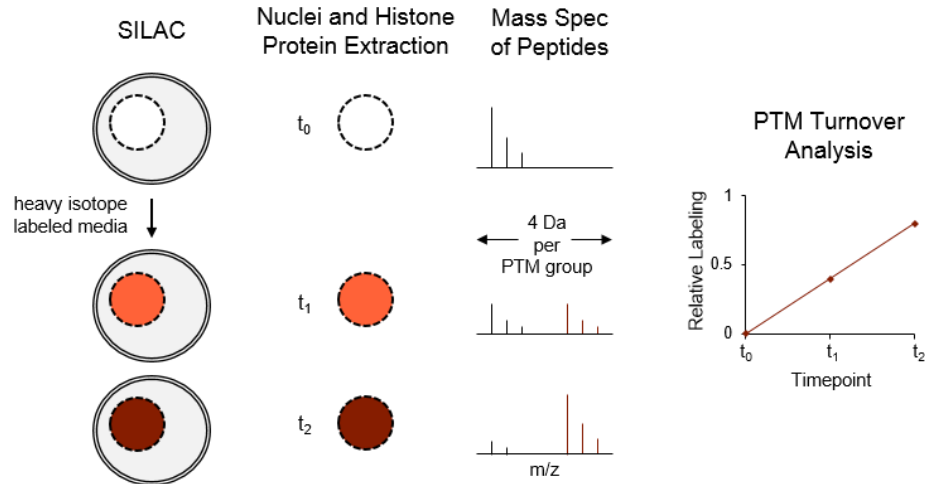


Figure 1.6. Methodology of SILAC-mass spec analysis of histone modification dynamics

Cells are transferred to medium containing heavy [ $^{13}\text{C}$ ]D $_3$ -methionine-labeled medium, and isotope incorporation (orange) into histone methylation pools is monitored over time by tandem mass spectrometry analysis. Specific shifts in the mass-to-charge ( $m/z$ ) ratio are used to distinguish unlabeled from labeled modifications and reveal methylation turnover when measured over time (e.g. 4-Da shift per methyl group).

Quantitative proteomics using Stable Isotope Labeling using Amino acids in Cell culture (SILAC) is a popular quantitative proteomics approach that relies on the endogenous translational machinery of living cells to incorporate tagged chemical analogs of molecular building blocks into chromatin<sup>23,24</sup>. In the classical SILAC experiment, two cell populations are compared<sup>24</sup>. These populations are grown in different media containing distinct forms of amino acids that are either of natural isotopic abundance or heavy labeled stable isotopes. Incorporation of these light and heavy amino acids into de novo synthesized proteins creates proteomes that can be discerned by their specific mass differences. Mass spectrometry is used to measure the relative abundance of light and heavy peptides in pooled samples, which allows for the detection and quantification of differential changes in protein expression. In order to study temporal turnover dynamics of chromatin modifications, we adapted the classic SILAC approach to analyze site-specific dynamics of different histone modifications<sup>25</sup>. Our labeling approach provides an effective marker to distinguish pre-existing from newly catalyzed chromatin modifications, and permits the monitoring over time for dynamic turnover, when coupled with advanced quantitative liquid

chromatography-mass spec technology<sup>26,27</sup> (Fig. 1.6). Quantitative modeling allowed us to characterize the steady-state kinetics of histone modifications globally – thus providing a sensitive metric to study gene regulatory mechanisms in different physiological and metabolic states.

SILAC-based mass spec technology provides sought-after insight into the residue-specific turnover dynamics of histone modifications. These turnover dynamics remain obscured in classic Western blot analysis that measures only the total relative abundance of specific histone modifications. SILAC therefore presents a valuable tool to reveal whether particular modification pools acutely respond to altered metabolic flux. However, neither SILAC nor Western blot approaches illuminate the genome-wide distribution of the examined histone modifications. Therefore, in order to monitor epigenomic change over time, the genome-wide enrichment of histone modifications needs to be investigated with modern ChIP-sequencing technology. Such insight into the epigenetic landscape by ChIP-seq is critical when examining chromatin-based mechanisms of gene regulation. For instance, changes in gene expression can result from metabolic activities that alter the turnover of particular histone modifications. Monitoring turnover using SILAC-mass spec may indicate whether particular histone modifications are created *de novo*, but ChIP-seq is needed to gain insight into their genomic location in order to distinguish (1) localized dynamic turnover from (2) epigenomic restructuring that involves regional gains and losses, both of which may be coupled to altered gene expression, as outlined in Figure 1.7. Likewise, increases in global histone acetylation and methylation may be detected by either Western blot or SILAC analysis, but only ChIP-sequencing provides information regarding their genomic location, and whether such change is linked to altered gene expression (Figure 1.7.E and F). Therefore, SILAC-mass spec and ChIP-seq technologies are especially powerful when applied together, and work in concert to afford novel insight into chromatin-mediated mechanisms of transcriptional control by metabolic state.

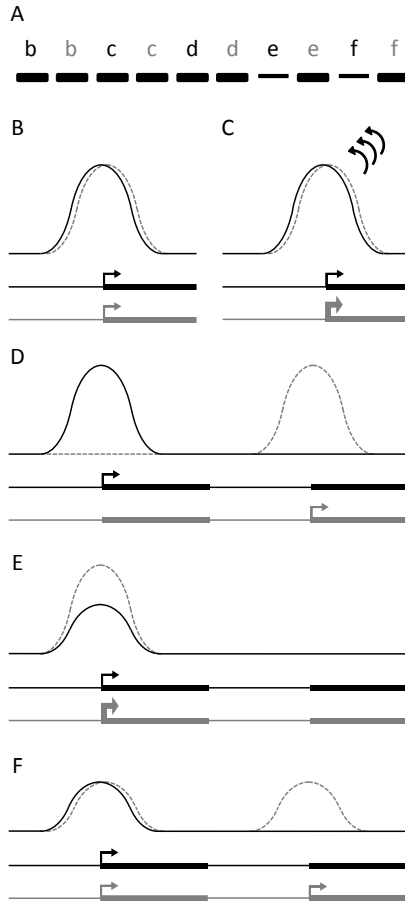


Figure 1.7. SILAC-mass spec and ChIP-seq work synergistically to capture dynamic aspects of chromatin-mediated gene regulation

(A) Hypothetical Western blot analysis of global histone modification levels for theoretical chromatin state alterations illustrated in B-F (from black to grey), demonstrating the inherent limitations of Western method when a dynamic change in chromatin structure is analyzed. (B-D) Enrichment of a histone modification over the promoter region of a gene. Shifts in metabolic state may alter the turnover dynamics of particular histone modifications, coupled to changes in gene expression. Whereas SILAC-mass spec analysis indicates whether or not histone modifications are created *de novo* (example B vs. C, D), this method on its own is inadequate to distinguish localized dynamic turnover (example C) from epigenomic restructuring involving both regional gains and losses of enrichment (example D). These outcomes can be distinguished by ChIP-seq, which provides important information on the genomic location of histone modifications. Conversely, ChIP-seq does not yield insight into their turnover dynamics that may respond to metabolic state (example B vs. C). Notably, none of these changes in chromatin structure can be detected by classic Western blot analysis (in A, a-d are identical levels). (E, F) Increases in total abundance of histone modification may be detected with either Western or SILAC analysis. Yet, only ChIP-seq technology may determine the location of such epigenetic change, and whether it is associated with altered gene transcription.

One context in which a combined approach of SILAC and ChIP-seq is poised to yield novel insight are studies of oncogenic lesions and the metabolic adaptations they precipitate, which ultimately alter chromatin structure and epigenome. For instance, in many cancers, deregulated metabolism resulting in aberrant histone methylation has been implicated in tumorigenesis<sup>28–30</sup>. Specifically, mutations in the metabolic enzymes isocitrate dehydrogenase 1 and 2 are found in a variety of tumors and cause neomorphic catalytic activities that generate 2-hydroxyglutarate, an oncometabolite that alters the histone methylation landscape and disrupts regulated gene expression<sup>31</sup>. Similarly, a large body of evidence has shown that acetyl-CoA metabolism and histone acetylation are frequently dysregulated in cancer<sup>32,33</sup>. Therefore, in order to develop novel therapeutic approaches that target cellular metabolism to alter the tumor epigenome, it is key to understand how chromatin is regulated by metabolic state in health and disease. Our two-pronged approach is of particular advantage when interrogating how such metabolic and oncogenic mutations influence the dynamic relationship between metabolism, nutritional environment, and chromatin regulation.

## CHROMATIN: A BONA-FIDE ENERGY SENSOR?

Cells constantly sense and integrate environmental cues to maintain homeostasis and control proliferative growth. In response to unfavorable environmental conditions such as nutrient depletion, eukaryotic cells enter a resting state termed quiescence. Nutrient availability stimulates the return into the cell cycle and initiates a growth response that involves histone acetylation and dramatic change in gene expression (Fig. 1.8). We applied the SILAC and ChIP-seq technologies described above to study metabolically controlled gene regulation in the context of nutrient-induced growth and cell cycle re-entry from quiescence in the yeast *Saccharomyces cerevisiae*<sup>27</sup>. Budding yeast, providing a flexible and rapid genetic system, has proved to be an excellent model organism for studying such cellular events<sup>34–36</sup>. In both mammalian and yeast cells, histone acetylation – key modulator of transcriptional activation and elongation – has been found to be exquisitely responsive to the cellular nutritional and metabolic states<sup>37–39</sup>. Accordingly, acetylation

can be considered an energy-sensitive protein modification that integrates a range of nutrient signals to reprogram transcription. However, the genome-wide pattern of glucose-induced histone acetylation have not been examined, and the roles of targeted and untargeted acetylation in the transcriptional response during cell cycle re-entry remain elusive. Using a powerful combination of Western blotting, SILAC-mass spec, CHIP-seq, and RNA-seq, we set out to investigate how nutritional status and metabolic state impact the genome-wide pattern of individual histone modifications, and their turnover.

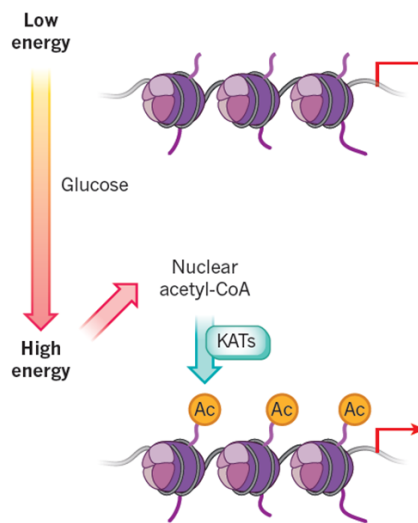


Figure 1.8. Chromatin-mediated transcriptional control by intermediary metabolism

During feeding or under high glucose conditions, acetyl-CoA from glycolysis is exported to the nuclear-cytosolic compartment. In the nucleus, increased acetyl-CoA – rate-limiting to the catalytic activity of HAT enzymes – is allowing for increased histone acetylation. In that way, rising acetyl-CoA creates a permissive state for transcription of genes involved in glucose uptake and glycolysis constituting a feed-forward loop acetyl-CoA transmits the signal of increased nutrient supply. (adapted from Gut and Verdin, 2013)<sup>19</sup>

ChIP-seq is a valuable technology enabling the study of a broad range of chromatin phenomena on a genome-wide scale, and provides position- and gene-specific mapping. Nonetheless, ChIP-seq does not capture the temporal dynamics of histone modification turnover. SILAC-mass spec, in contrast, is a formidable tool that permits detection and quantification of relative differential changes in histone modifications over time. We successfully applied this

technology to interrogate the reciprocal relationship between glucose uptake, glycolytic metabolism, and regulated histone acetylation. In combination, ChIP-seq and SILAC-mass spec allowed comprehensive profiling of chromatin during changing nutritional and metabolic environments. Used together, these technologies yielded superior insight that each approach on its own could not provide.

Our findings from SILAC and ChIP-seq provided the first unequivocal evidence that nutrients induce an immediate histone acetylation response at growth-related genes, driven by external glucose. Notably, whereas solid evidence showed that specific histone acetylation can translate metabolic signals into alterations in chromatin structure and transcription, the relationship between metabolic state and the uniquely multifaceted methylation of histones remained virtually unexplored. We thus set out to investigate whether metabolism modulates histone methylation to control gene expression in the transition from quiescence to cell proliferation, akin to histone acetylation.

Histone methylation is a far more complex process than acetylation. Histone methyltransferase (HMT) and demethylase (HDM) enzymes regulate mono-, di-, and trimethylation states of multiple histone lysine residues that have diverse functions in transcriptional control<sup>40</sup>. HMT enzymes have striking target specificity – usually modifying one single lysine on a single histone – and their output can be either activation or repression of transcription. To methylate histones, methyltransferases are dependent on the metabolic intermediate and sole methyl group donor S-adenosyl methionine (SAM)<sup>41</sup>. Histone methylation could in theory reprogram gene expression in function of the metabolic milieu, based on its dependence on metabolic SAM, whose availability is governed by the intracellular energy content. The SAM precursor methionine is an essential amino acid that mammal cells cannot synthesize *de novo*<sup>42</sup>. For that reason, SILAC-based studies are an excellent approach to probe the relationship between cellular metabolism and epigenetic control of histone methylation. Thus, when heavy stable isotope form of methionine, L-Methionine-methyl-<sup>13</sup>C, D<sub>3</sub>, is used in the cell

culture medium, heavy-methyl groups will be introduced by methyltransferases into lysine and arginine residues on histone proteins. This labeling technology coupled with quantitative mass spectrometry technology facilitates the study of complex site-specific methylation dynamics on histone proteins<sup>26,43</sup>.

Interestingly, our application of both SILAC and ChIP-seq technology demonstrated that histone methylation – in contrast to highly dynamic histone acetylation – remains exceptionally stable and uncoupled from rapid metabolic and transcriptional reprogramming as yeast cells exit quiescence. Instead, our studies revealed that the methylation landscape is extensively restructured genome-wide only at a later time, in conjunction with genome replication and ensuing cell division<sup>27</sup>. Notably, as global histone methylation levels do not change immediately in the exit from quiescence, these dynamic changes in genome-wide methylation patterns would have remained obscured when analyzed by Western blot alone. Thus, the combination of SILAC-mass spec with ChIP-seq provided distinct interpretations of the dynamics of histone acetylation compared to histone methylation during re-entry into the cell cycle.

## BEYOND THE ABOVE: EPIGENETIC MECHANISMS IN COGNITION

The ability to store information over long periods of time lies at the heart of cellular identity. Cellular memory – encoded in the epigenetic signatures that govern gene expression – ensures that cells do not drift when moving along elaborate pathways in cellular development and differentiation. In analogy, our own mental identity relates to memories that make sure we remember who we are when navigating the incredibly complex world that surrounds us. The elemental question of how the exceptional variety of stimuli submitted to neurons are converted into higher order brain functions such as memory storage, however, continues to perplex in the field of neuroscience. Today, deepening our understanding of the molecular machinery that underlies long-term memory consolidation and storage is a primary goal in contemporary studies of cognition.

It is fascinating that one potential molecular mechanism by which behavioral memories may be fixed and persist in a structure as dynamic as our brain may ultimately be of epigenetic nature<sup>44–48</sup>. Learning-induced epigenetic modifications at the cellular level could serve to support memory in the adult brain, through stable alterations in the chromatin structure of neurons<sup>44</sup>. Changes in chromatin occur during the earliest stages of neuronal development, and epigenetic mechanisms play critical roles in neurogenesis, the specification of neuronal fates, and the development of neural circuitry in the brain. Without a doubt, such epigenetics-related molecular mechanisms are functionally active in terminally differentiated, non-dividing neurons of the adult brain. In fact, current research strongly supports the prevailing hypothesis that neuronal plasticity involves epigenetic regulation. Recent studies highlight alterations in chromatin structure, via histone modifications, as critically important for the long-term stability of plastic changes at the circuit and behavioral levels<sup>49–52</sup>. Epigenetic modifications have now been implicated in neuronal plasticity, neurodegeneration, and psychiatric conditions, such as drug addiction<sup>53–56</sup>. In fact, there are several types of epigenetic modifications that have been associated with cognitive functions, including DNA methylation, RNAi, and post-translational modification of histone proteins by acetylation, methylation, phosphorylation<sup>45,48,56,57</sup>. Yet histone acetylation in particular has spurred considerable interest, and is most robustly associated with promoting memory formation.

As early as 1979, that is, nearly two decades before the first nuclear HAT was discovered<sup>58</sup>, it was found that the acetylation state of histones is altered when rats undergo memory consolidation<sup>59</sup>. More recent evidence confirmed these findings, showing that specific forms of associative learning – contextual fear conditioning and latent inhibition – correlate with increased histone acetylation<sup>50</sup>. Following contextual fear conditioning, acetylation of H3K14 was significantly increased in the hippocampus proper, the cornu ammonis (CA1; Fig. 1.9), whereas acetylation of H4 was unchanged. Conversely, H4 acetylation was selectively increased after latent inhibition training. While Schmitt and Matthies used C14-labeled acetate to study histone acetylation<sup>59</sup>, these later studies used immunoblotting to detect bulk levels of histone

modifications. The mechanistic insight from such early observations is limited since they do not allow to identification of the genomic regions in which altered histone acetylation takes place. However, importantly, these early results not only highlighted that histone acetylation accompanies memory consolidation, but show that different learning paradigms elicit distinct epigenetic signatures in the brain. Many follow-up studies have corroborated the implied link between histone hyper-acetylation and memory formation for different memory types and phases, such as reconsolidation and extinction<sup>49,60–65</sup>.

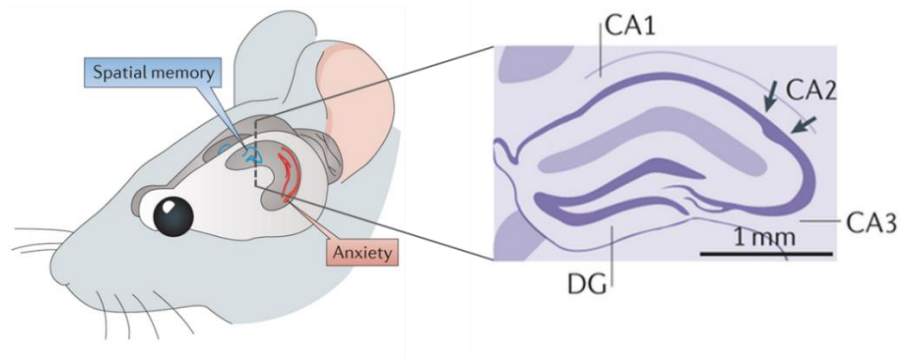


Figure 1.9. Schematic of hippocampal anatomy and contribution to behavior.

Drawing of the hippocampal formation in mouse, located in the medial temporal lobe. The frontal cross-section depicts the histological subdivision of the hippocampus by Nissl stain in the frontal cross-section, and delineates the CA1, CA2, and CA3 regions together with the dentate gyrus (DG). The dorsal and ventral hippocampus have distinct contributions to behaviour. Subregion specific, cytotoxic lesions have fractionated the hippocampus in terms of their behavioural effects. The dorsal hippocampus subserves the spatial memory functions of the hippocampus (for example, in the water maze and radial maze), whereas the ventral hippocampus underlies the anxiolytic effects of hippocampal lesion. (adapted from Bannerman et al., 2014)<sup>65</sup>

For instance, newer studies using chromatin immunoprecipitation have revealed that memory-induced histone acetylation is specific to certain genes. These include genes that are important for learning and memory, such as the immediate-early genes *Erg1*, *Creb* and *Bdnf*, which showed an increase in expression following contextual fear learning, concomitant with the increase in histone acetylation<sup>52,64,65</sup>. Relevantly, phosphorylation of the transcription factor cAMP-response element-binding protein (CREB) is critical during these time windows for long-term memory. These windows of CREB phosphorylation coincide with sensitive periods during

which inhibition of transcription impairs memory storage<sup>66</sup>. Notably, recent evidence showed that CREB phosphorylation alone is not sufficient to drive such gene expression. Instead, it is the interaction between phosphorylated CREB and the histone acetyltransferase CREB-binding protein (CBP/KAT3A) that is critical for memory formation, and that is associated with increased histone acetylation levels at CREB target genes (Fig. 1.10).

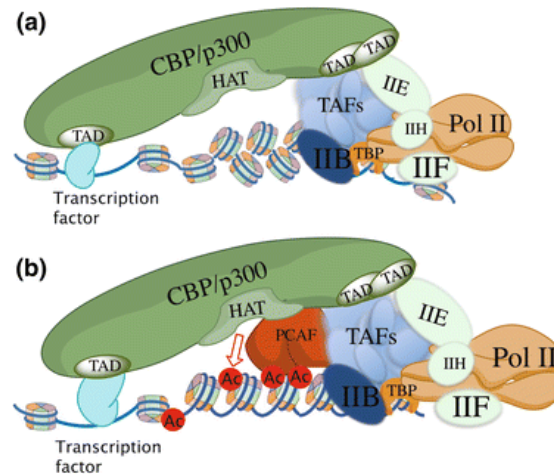


Figure 1.10. Functional mechanisms of transcriptional activation by CBP/p300

CBP/p300 promotes transcriptional activity by recruiting transcriptional machinery to the promoter, and by modifying chromatin structure to facilitate transcription. (a) CBP/p300 functions as a “bridge”, linking the DNA-bound transcription factors (activators) to basal transcription machinery through direct interactions with TFIID, TFIIB, and RNA Pol II, thus promoting pre-initiation complex (PIC) assembly. (b) CBP/p300 acetylates histones through its HAT domain, resulting in chromatin remodeling and relaxation of chromatin structure to enable transcription. CBP/p300 also recruits the coactivators PCAF and GCN5. (from Wang et al, 2013)<sup>67</sup>

The functional relevance of histone acetylation for memory formation was first demonstrated via genetic mouse models in which the activity of CBP was reduced<sup>51,52,68</sup>. These mutant mice displayed impaired memory consolidation, a finding that has been reproduced in various mouse models in which CBP activity was altered<sup>52,69,70</sup>. Additionally, it was found that pharmacological inhibition of HDACs in the hippocampus enhances the consolidation of associative memories in rodents<sup>50,71–74</sup>, requiring the interaction of CREB and CBP. Surprisingly, data in which ChIP-qPCR for specific histone-modifications was analyzed during memory

formation are sparse. The current state of the art method to study chromatin marks across the entire genome is ChIP followed by next-generation sequencing. A recent study performed a genome-wide analysis of H4K5ac via ChIP-sequencing and found that H4K5ac correlates with learning-induced gene expression<sup>75</sup>. In general, increments in histone acetylation have consistently been shown to favor learning and memory. In contrast, an inability to acetylate has been causally implicated in cognitive impairments in neurodevelopmental disorders, neurodegeneration and ageing<sup>44,46,68,76–78</sup>.

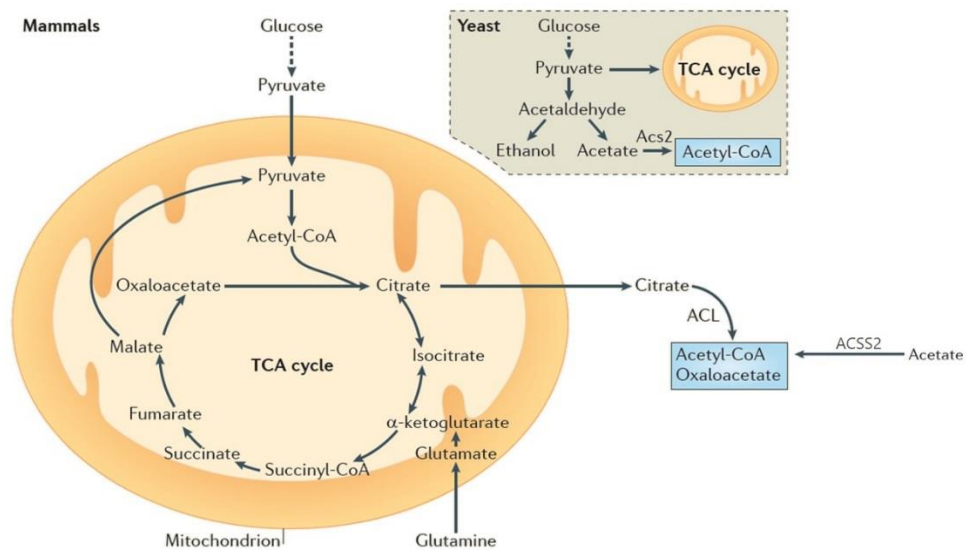


Figure 1.11. Synthesis of acetyl-CoA in yeast and mammalian cells

In mammalian cells, mitochondrial acetyl-CoA is produced from pyruvate by the pyruvate dehydrogenase complex or by the  $\beta$ -oxidation of fatty acids, and then feeds into the tricarboxylic acid (TCA) cycle. Citrate can be exported from mitochondria into the cytoplasm, where it freely diffuses into and out of the nucleus. The extra-mitochondrial pool of acetyl-CoA, which is used for protein acetylation or for lipogenesis, is synthesized from citrate by ATP citrate lyase (ACL) or from acetate by acetyl-CoA synthetase 2 (ACSS2). Because these enzymes use different substrates for generating acetyl-CoA, the relative importance of ACL and ACSS2 in non-mitochondrial acetylation may depend on differences in carbon source utilization. Similar to mammalian cells, yeast generate acetyl-CoA via pyruvate metabolism in mitochondria. However, in yeast, nucleocytoplasmic acetyl-CoA is exclusively provided by the catalytic activity of acetyl-CoA synthetase enzymes. Although the enzymes and mechanisms of acetyl-CoA generation are different between mammalian cells and yeast, in both cases acetyl-CoA is produced through more than one route and in different subcellular compartments. (adapted from Wellen and Thompson, 2012)<sup>16</sup>

On the whole, there is a substantial body of data demonstrating that enzymes regulating histone acetylation have critical roles in memory function. In view of the novel paradigm of chromatin-mediated transcriptional control by cellular metabolism, we were interested whether such mechanism may operate in the adult nervous system – particularly in the context of dynamically increased histone acetylation regulating memory formation. To catalyze the histone acetylation reaction, HAT enzymes depend on the central metabolite acetyl-CoA as the sole acetyl group donor. In mammals, nuclear acetyl-CoA that contributes to histone acetylation is principally produced by two enzymes: ATP citrate lyase (ACL) utilizing citrate to generate acetyl-CoA<sup>79</sup>, and the acetate-dependent acetyl-CoA synthetase ACSS2<sup>80–82</sup>. Intriguingly, ACSS2 has been shown to localize primarily to the nucleus throughout development, and its expression was found to be maintained at high levels in the adult nervous system<sup>83</sup>. In contrast, ACL predominantly locates to the cytoplasm, and is highly expressed in tissues with substantial levels of lipogenesis, including the developing brain<sup>84,85</sup>.

Acetyl-CoA is the principle building block for *de novo* lipogenesis, a process that is particularly important in the developing brain, mostly for myelination. Both ACL and ACSS2 are believed to contribute acetyl-CoA to this process in development. Interestingly, ACL expression was found to be lower in the adult brain, reflecting reduced levels of *de novo* lipogenesis. However, ACL expression persists at high levels in cholinergic neurons of the brain stem and spinal cord<sup>83</sup>, suggesting a role in acetylcholine synthesis, which is indeed stimulated by supplementation of the ACL substrate citrate<sup>86</sup>. Collectively, these findings suggest that the primary source for acetyl-CoA functioning in neuronal histone acetylation is catalytic ACSS2. This hypothesis is supported by our findings in the yeast *S. cerevisiae*. In yeast, the homolog of the evolutionary highly conserved ACSS2 is the acetyl-CoA synthetase Acs2p<sup>87</sup>. Notably, in contrast to mammalian cells, yeast Acs2p is essential and the exclusive enzymatic source of nucleocytoplasmic acetyl-CoA during growth on glucose<sup>88</sup>. In fact, using SILAC and CHIP-seq, we showed unequivocally that the Acs2p-dependent histone acetylation response to nutrient feeding

is driven by metabolized external glucose. All the more, earlier studies showed that virtually all Acs2p is present in the nucleus, localizing into distinct nuclear clusters including the nucleolus<sup>88</sup>.

These data caused us to hypothesize that chromatin-localized production of acetyl-CoA by ACSS2 regulates histone acetylation and gene transcription in post-mitotic neurons. Specifically, we hypothesized that ACSS2 is required for dynamic histone acetylation and gene expression involved in long-term memory formation. Our data show that ACSS2 is a critical and direct regulator of histone acetylation in neurons and of long-term mammalian memory. Our findings from comprehensive ChIP-seq analyses in neuronal cell culture indicate that ACSS2 functions as a chromatin-bound co-activator, locally promoting histone acetylation for transcription of neuron-specific genes. Remarkably, *in vivo* attenuation of hippocampal ACSS2 expression in adult mice impairs long-term spatial memory, associated with defective induction of key neuronal genes involved in memory. These results reveal a unique connection between cellular metabolism and neural plasticity, providing new mechanistic insight that may lead to novel pharmacological strategies in treating neurodegenerative and neuropsychiatric disease.

## **CHAPTER 2**

# **HISTONE METHYLATION HAS DYNAMICS DISTINCT FROM THOSE OF HISTONE ACETYLATION IN CELL CYCLE REENTRY FROM QUIESCENCE**

## ABSTRACT

Cell growth is attuned to nutrient availability to sustain homeostatic biosynthetic processes. In unfavorable environments, cells enter a non-proliferative state termed quiescence, but rapidly return to the cell cycle once conditions support energetic needs. Changing cellular metabolite pools are proposed to directly alter the epigenome via histone acetylation. Here we studied the relationship between histone modification dynamics and the dramatic transcriptional changes that occur during nutrient-induced cell cycle re-entry from quiescence in the yeast *S. cerevisiae*. SILAC-based mass spectrometry showed that histone methylation – in contrast to histone acetylation – is surprisingly static during quiescence exit. ChIP-seq revealed genome-wide shifts in histone acetylation at growth and stress genes as cells exit quiescence and transcription dramatically changes. Strikingly, however, the patterns of histone methylation remain intact. We conclude that the functions of histone methylation and acetylation are remarkably distinct during quiescence exit: acetylation rapidly responds to metabolic state while methylation is independent. Thus, the initial burst of growth gene reactivation emerging from quiescence involves dramatic increases of histone acetylation, but not of histone methylation.

## INTRODUCTION

Cells constantly sense and integrate environmental cues to control proliferative growth, but the underlying molecular mechanisms remain unclear. Eukaryotic cells, including adult stem cells, typically exist in a state of growth arrest – quiescence – that is distinguished by two principal qualities: quiescent cells both safeguard cell identity and retain the ability to resume proliferation once external cues become favorable<sup>35,89,90</sup>. Remarkably little is known about the molecular processes that mediate quiescence exit and the transition to proliferative growth, which requires massive changes in cell metabolism and reprogramming of global gene expression<sup>91–93</sup>.

Recent evidence suggests that the metabolic state is a principle regulator of quiescence establishment and exit via epigenetic changes that alter gene expression<sup>15,94,95</sup>. A clear example is that nutrient-induced increases in acetyl coenzyme A (acetyl-CoA) pools promote chromatin acetylation and growth gene transcription<sup>38,39</sup>. Rhythmic fluctuations of acetyl-CoA levels are characteristic of the metabolic cycle that budding yeast cells enter during growth in nutrient-limiting conditions. In such a milieu, recurrent bursts of acetyl-CoA production by the enzyme acetyl-CoA synthase Acs2p have been linked to increased histone acetylation and growth gene expression, indicating a functional connection between metabolic state and gene transcription via chromatin acetylation<sup>38</sup>. Indeed, studies in both the yeast *S. cerevisiae* and activated lymphocytes indicate that glucose-induced histone acetylation is a critical and highly conserved driver of quiescence exit<sup>39,96,97</sup>. In mammalian cells, acetyl-CoA synthesis by ATP-citrate lyase (ACL) has been shown to link nutrient-dependent histone acetylation and cellular growth. These findings suggest a model of transcriptional control via conserved connections between metabolic and epigenetic states<sup>18,37,98</sup>.

Even though metabolic activities are coupled to histone acetylation and growth gene transcription, it is uncertain whether cellular metabolites also influence histone methylation to dynamically regulate transcription. Notably, histone methylation is a far more complex process than acetylation. Histone methyltransferase (HMT) and demethylase (HDM) enzymes regulate

mono-, di-, and trimethylation states of multiple histone lysine residues that have diverse functions in transcriptional control <sup>40</sup>. Histone methylation is dependent on the central metabolite S-Adenosyl-Methionine (SAM). Based on this, it has been speculated that intracellular SAM concentrations may modulate chromatin structure in response to the metabolic milieu <sup>99</sup>. The high-energy methyl donor SAM is generated from methionine by methionine adenosyltransferase (MAT) enzymes in an ATP-consuming reaction, and its chromatin-localized synthesis concentration is believed to fine-tune histone methylation <sup>100</sup>. Recent evidence suggests that threonine metabolism may selectively influence di- and trimethylation of histone H3 lysine 4 (H3K4me3) specifically in mouse embryonic stem cells (mESCs) by supplying acetyl-CoA for SAM synthesis during mESC colony growth <sup>101</sup>.

Overall, it remains unknown whether histone methylation is a broad energy sensing modification that adapts transcription relative to the metabolic state, akin to histone acetylation. The dynamics of histone methylation have not been examined in cells transitioning from minimal to high metabolic activity, and methods to reliably determine residue-specific methylation dynamics using mass spectrometry have been only recently developed <sup>26</sup>. To explore the role of histone methylation as a putative energy sensor in the context of massive metabolic and transcriptional reprogramming, we investigated the temporal dynamics of global histone methylation during cell cycle re-entry of quiescent budding yeast *S. cerevisiae*. Our results show that histone methylation operates in stark contrast to highly dynamic glucose-induced histone acetylation, with methylation levels remaining highly stable during quiescence exit.

## RESULTS

### **Histone methylation does not change globally during cell cycle re-entry**

Nutrient abundance induces quiescence exit and stimulates vast changes in cellular metabolism. Presently, the metabolic state is under intense investigation as a principle regulator of both chromatin and gene expression<sup>94</sup>. Indeed, previous observations show that global histone acetylation is dramatically altered during nutrient starvation and re-feeding<sup>39</sup>. During nutrient-induced quiescence exit, glycolytic metabolism has been found to be the central driver of bursts of histone acetylation<sup>39</sup>. We investigated the unexplored changes in histone methylation that may occur upon quiescence establishment and during cell cycle re-entry.

Quiescence establishment in yeast is a gradual process involving the stepwise acquisition of various quiescence traits culminating in the final cessation of proliferation. In order to obtain a homogenous population of quiescent cells and eliminate contamination of slowly cycling subpopulations, we achieved quiescence, as previously described<sup>102</sup>, by transferring cells from carbon-exhausted media into water to ensure complete nutrient starvation prior to the induction of quiescence exit. To investigate and compare chromatin modification dynamics over the course of this process, we examined proliferating cells (LOG), cells in the quiescent state (Q), early exiting cells before DNA replication (E 30 min), and late exiting cells after DNA replication commences (E 240 min) (Fig. 2.1A). We measured changes in global histone methylation abundance by western blot and Stable Isotope Labeling using Amino acids in Cell culture (SILAC)-mass spectrometry (hereafter referred to as SILAC). We then used chromatin immunoprecipitation followed by massive parallel sequencing (ChIP-seq) to examine changes in local genic modification patterns. In each of these experimental approaches we compared histone methylation to histone acetylation, which is known to undergo dramatic fluctuations in cell cycle exit and re-entry.

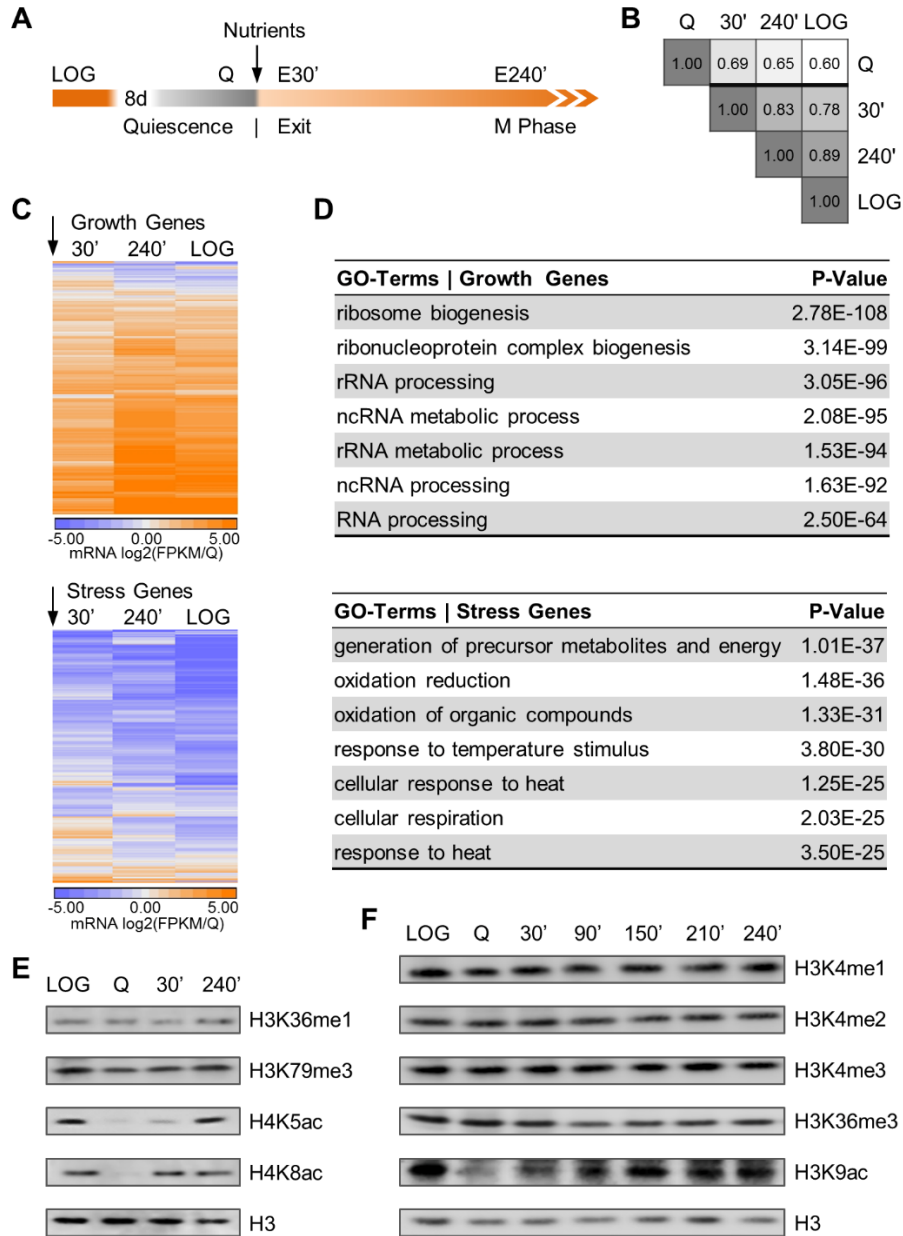


Figure 2.1. Nutrient availability stimulates histone acetylation and dramatic change in gene expression, but does not alter global histone methylation levels.

(A) Schematic of yeast culturing and quiescence exit protocol. Yeast are grown in rich medium (LOG) until carbon exhaustion, and are then transferred to water to ensure a completely starved, homogeneous quiescent cell population (Q) prior to nutrient-induced quiescence exit on day 8. An arrow indicates nutrient feeding and subsequent sampling times 30 minutes and 240 minutes after nutrient feeding (E30 and E240, respectively). (B) mRNA-sequencing data show that nutrient feeding (indicated by an arrowhead) induces vast transcriptional reprogramming in the transition from quiescence to cellular growth. Following nutrient

replenishment, 475 growth genes are drastically up-regulated (indicated in orange), whereas a core set of 463 stress genes are rapidly down-regulated (blue). Data are clustered by time points into columns, and rows that represent genes, ranked by FPKM values normalized to quiescence sample FPKM and log<sub>2</sub>-transformed. (C) GO-term enrichment analysis shows that growth genes are involved in processes critical to growth. Stress genes cluster in classic stress response categories. (D, E) western blot analysis of lysates from yeast over the course of quiescence exit reveals that total levels of histone acetylation are diminished in quiescent cells and rapidly increase following nutrient replenishment. In contrast, global histone methylation levels remain stable throughout quiescence establishment and do not increase during quiescence exit.

First, to confirm that quiescence exit results in expected dramatic gene expression changes in our experiments, we performed RNA sequencing. As previously noted by gene expression microarray analysis<sup>91-93</sup>, we observed that during the exit from quiescence, nutrients trigger a massive transcriptional response that involves one third of yeast genes. The rapid transformation of the global gene expression program produces an mRNA transcriptome in the early exit (E30) that closely resembles the transcriptional profile of cycling cells (LOG), as shown in a Pearson correlation matrix (Fig. 2.1B). Thus, the massive changes in transcription do not require replication. Following nutrient feeding, a core set of roughly 500 growth genes is immediately and dramatically up-regulated (Fig. 2.1C, top panel), whereas another group of nearly 500 stress genes is promptly down-regulated (Fig 1C, bottom panel). As expected, Gene Ontology (GO) enrichment analyses indicate that nutrient-induced growth genes are involved in processes critically important for growth, including ribosome biogenesis, rRNA processing and translational regulation (Fig. 2.1D). In contrast, genes that are actively transcribed in quiescent cells and become rapidly down-regulated after nutrient-feeding are highly overrepresented in classic stress response categories, such as oxidation reduction and response to heat (Fig. 2.1D).

The induction of growth genes has been shown to correlate with glucose-dependent increases in histone acetylation<sup>38,39</sup>. We confirmed by western blot analysis that transcriptionally relevant histone acetylation levels drop dramatically during quiescence and then robustly and rapidly increase after nutrient refeeding as the cells exit quiescence (Fig. 2.1E, H4K5ac and

H4K8ac; Fig. 2.1F, H3K9ac). Strikingly, western blot analysis revealed that for all of the abundant methylation sites relevant to transcription (K4, K36 and K79), there was no global change during nutrient starvation and replenishment (Fig. 2.1E, F). Thus, in stark contrast to histone acetylation that is connected to transcription, global histone methylation levels remain constant in nutrient-stressed quiescent cells and do not increase during nutrient-induced cell cycle re-entry.

### **Histone methylation dynamics are distinct from histone acetylation during exit**

While western blot analysis measures the total relative abundance of specific histone modifications, this technique is unable to measure either turnover dynamics or changes in genome-wide distribution of those modifications. Although the kinetics have not been previously reported in exiting cells, it has been speculated that turnover dynamics of various histone modifications correspond to cellular metabolism<sup>18,99</sup>. To investigate methylation dynamics, we performed SILAC in quiescent and quiescence-exiting cells.

SILAC is a popular quantitative proteomics approach that relies on the endogenous translational machinery of living cells to incorporate tagged chemical analogs of molecular building blocks into chromatin<sup>23,24</sup>. In the classical SILAC experiment, two cell populations are compared<sup>24</sup>. These populations are grown in different media containing distinct forms of amino acids that are either of natural isotopic abundance or heavy labeled stable isotopes. Incorporation of these light and heavy amino acids into de novo synthesized proteins creates proteomes that can be discerned by their specific mass differences. Mass spectrometry is used to measure the relative abundance of light and heavy peptides in pooled samples, which allows for the detection and quantification of differential changes in protein expression. In order to study temporal turnover dynamics of chromatin modifications, we adapted this classic SILAC approach to analyze site-specific dynamics of histone acetylation and methylation<sup>25</sup>. Our labeling approach provides an effective marker to distinguish pre-existing from newly catalyzed chromatin modifications, and permits the monitoring of time for dynamic turnover, when coupled with advanced quantitative liquid chromatography-mass spec technology<sup>26,27</sup>.

To track and quantify histone protein turnover, as well as newly acetylated and methylated histones, we cultured cells in media with isotopically heavy lysine ( $^{15}\text{N}_2$ - $^{13}\text{C}_6$ -lysine), glucose ( $^{13}\text{C}_6$ -glucose), or methionine ( $^{13}\text{CD}_3$ -methionine), respectively, prepared nuclei, and isolated histones (Fig. 2.2A, left panels). While the stable heavy isotopes do not perturb the system<sup>26,103</sup>, label incorporation rate into histone modification pools can be monitored by tandem mass spectrometry analysis. Specific shifts in the mass-to-charge ( $m/z$ ) ratio are used to distinguish unlabeled from labeled histone peptides and to reveal modification turnover rates when measured with respect to time of continuous isotopic labeling (Fig. 2.2A, right panels). In contrast to a shift in  $m/z$ , the incorporation of the heavy isotopes generally does not induce a significant shift in retention time and thus histone peptides with light, heavy, or a combination of both isotopes generally co-elute by reversed phase liquid chromatography. By measuring the metabolic rate of labeled isotope incorporation into histone modifications, we determined the residue-specific dynamics of acetylation and methylation in the context of major transcriptional reprogramming during quiescence exit.

To establish conditions and explore histone methylation by SILAC, we first examined turnover of both histone protein and histone methylation in proliferating cells. First, to track turnover of histone proteins in cycling cells, we performed SILAC using heavy lysine (Fig. 2.2B). Following the transfer of proliferating cells to heavy media, any histones that have incorporated isotopically heavy  $^{13}\text{C}_6$ - $^{15}\text{N}_2$  lysines can be distinguished as 'newly' synthesized histone proteins. We found that the half-max labeling time ( $t_{1/2}$ ) of histone proteins corresponds to approximately one budding yeast cell cycle of 130 minutes, confirming by SILAC that doubling of the histone protein pool occurs once with every cell division (Fig. 2.2B).

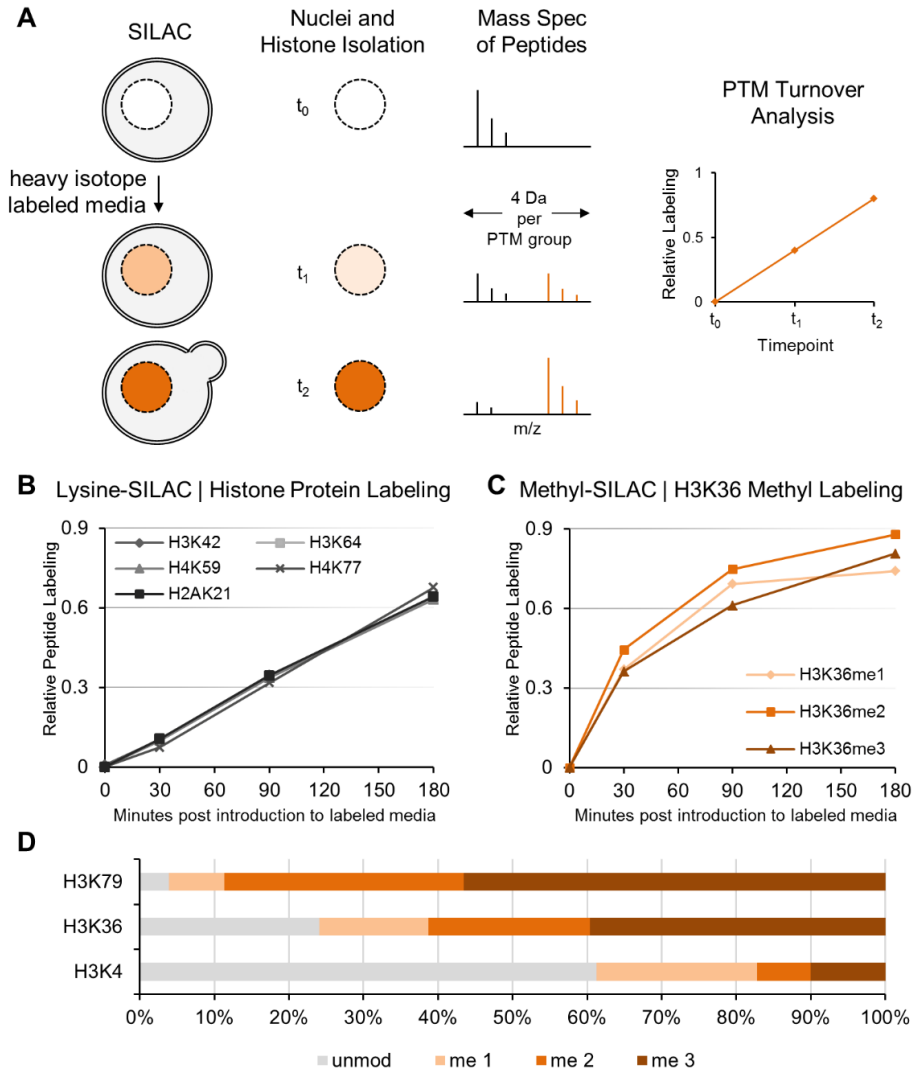


Figure 2.2. SILAC-mass spectrometry analysis of histone protein and methylation dynamics in proliferating cells.

(A) Methodology of SILAC-based quantitative mass spec. Cells are cultured in media containing labeled heavy isotopes (e.g.  $^{13}\text{CD}_3$  methionine to track methylation). Isotope incorporation (shown in orange) into histone peptides or modification pools is monitored by tandem mass spec analysis. Specific shifts in the mass to charge ( $m/z$ ) ratio are used to distinguish unlabeled from labeled histone peptides or modifications and reveal turnover dynamics when measured over time (e.g. 4 Da shift per methyl group). (B) SILAC with L-lysine- $^{13}\text{C}_6$  in proliferating cells shows relative distributions and half-max labeling time of newly synthesized H3, H4, and H2A peptides, confirming doubling of the histone pool with every cell division ( $\sim 130$  minutes). (C) Methyl-SILAC with heavy  $^{13}\text{CD}_3$ -methionine in proliferating cells shows rapid incorporation of  $^{13}\text{CD}_3$ -methionine into histone methylation of H3K36 (y-axis represents total methylation labeling, e.g. 0.9 denotes 90% labeling) (D) SILAC mass spec reveals the percentage of unmodified and mono-, di-, and tri-methylated histone H3 at residues K79, K36, and K4 in proliferating cells.

Next, to examine residue-specific methylation dynamics in proliferating cells, we utilized heavy methionine SILAC. This method involves mass spectrometry detection of *in vivo* incorporation of labeled S-adenosyl methionine (SAM), originating from metabolized exogenous  $^{13}\text{CD}_3$ -methionine into endogenous methylation substrates. The SAM precursor methionine is an essential amino acid that mammal cells cannot synthesize *de novo*. Thus, when heavy stable isotope form of methionine,  $^{13}\text{CD}_3$ -methionine, is used in the cell culture medium, heavy-methyl groups will be introduced by methyltransferases into lysine and arginine residues on histone proteins. Indeed, heavy methionine was rapidly metabolized to SAM, and we detected histone methylation labeling within minutes of transfer to heavy media (Fig. 2.2C). We detected ratios of mono-, di-, and tri-methylated histone H3 that are consistent with their abundance and prevalent functions at promoters (K4), over partial gene bodies (K36), and over entire gene bodies (K79) (Fig. 2.2D).

Methylated peptide species are commonly denoted for each methylation residue with X:Y, where X is the number of total methyl groups, and Y is the number of labeled methyl groups. For instance, H3K36me1:0 refers to unlabeled monomethylated H3K36, and H3K36me1:1 refers to labeled monomethylated H3K36. In order to reveal the distribution of differently labeled species within a methylation state, their relative abundance is calculated after all methylation intermediates for a specific methylation state of a particular residue have been determined. For instance, the abundance of H3K36me1:0 would be determined with respect to H3K36me1:0 and me1:1. This calculation is based on the logic that growth conditions should not change with  $^{12}\text{CH}_3$ - or  $^{13}\text{CD}_3$ -methionine, and that the total abundance of each methylated species does not change<sup>20</sup>. The relative distribution can then be used to quantify half-maximal times of the formation of labeled peptides ( $t_{1/2}$ ). The half-maximal time provides a measure of how quickly a particular species is formed, and thus is predictive of the overall rate of methylation for that species.

Having established SILAC in proliferating cells to study histone modification dynamics, we then applied this method to quiescent cells that were induced to re-enter the cell cycle by nutrient feeding. First, as a control for the method, we examined glucose-dependent histone acetylation in quiescence exit by utilizing heavy glucose SILAC. Similar to Methyl-SILAC, this method relies on mass spectrometry to detect and quantify heavy carbon labeling of histone acetylation at several time points, resulting from the glycolytic breakdown of heavy [ $^{13}\text{C}_6$ ]-glucose in the labeling media. By mass spectrometry, we detected a burst of histone acetylation that occurs immediately after nutrient replenishment, resulting from the glycolytic breakdown of heavy-labeled  $^{13}\text{C}_6$ -glucose from fresh media (Fig. 2.3A). Specifically, new histone H3K9/K14 acetylation takes place within minutes (Fig. 2.3A, red), thus supporting the turnover dynamics of previously reported Western blot analyses that show rapid increases in histone acetylation (Fig. 2.1E, F) <sup>39</sup>.

We found that labeling of N-terminal histone H2A acetylation occurs only after several hours into the exit (Fig. 2.3A, blue). N-terminal acetylation is a prevalent and highly conserved eukaryotic protein modification that is mediated co-translationally; hence our data indicate that histone protein synthesis commences late in the exit and is concurrent with DNA replication. Consistent with this observation, label incorporation into the histone protein pool via alanine residues also occurs very late upon cell cycle return (Fig. 2.3A, grey). These data demonstrate the absence of a slowly cycling subpopulation of cells and indicate homogeneity of the quiescent population.

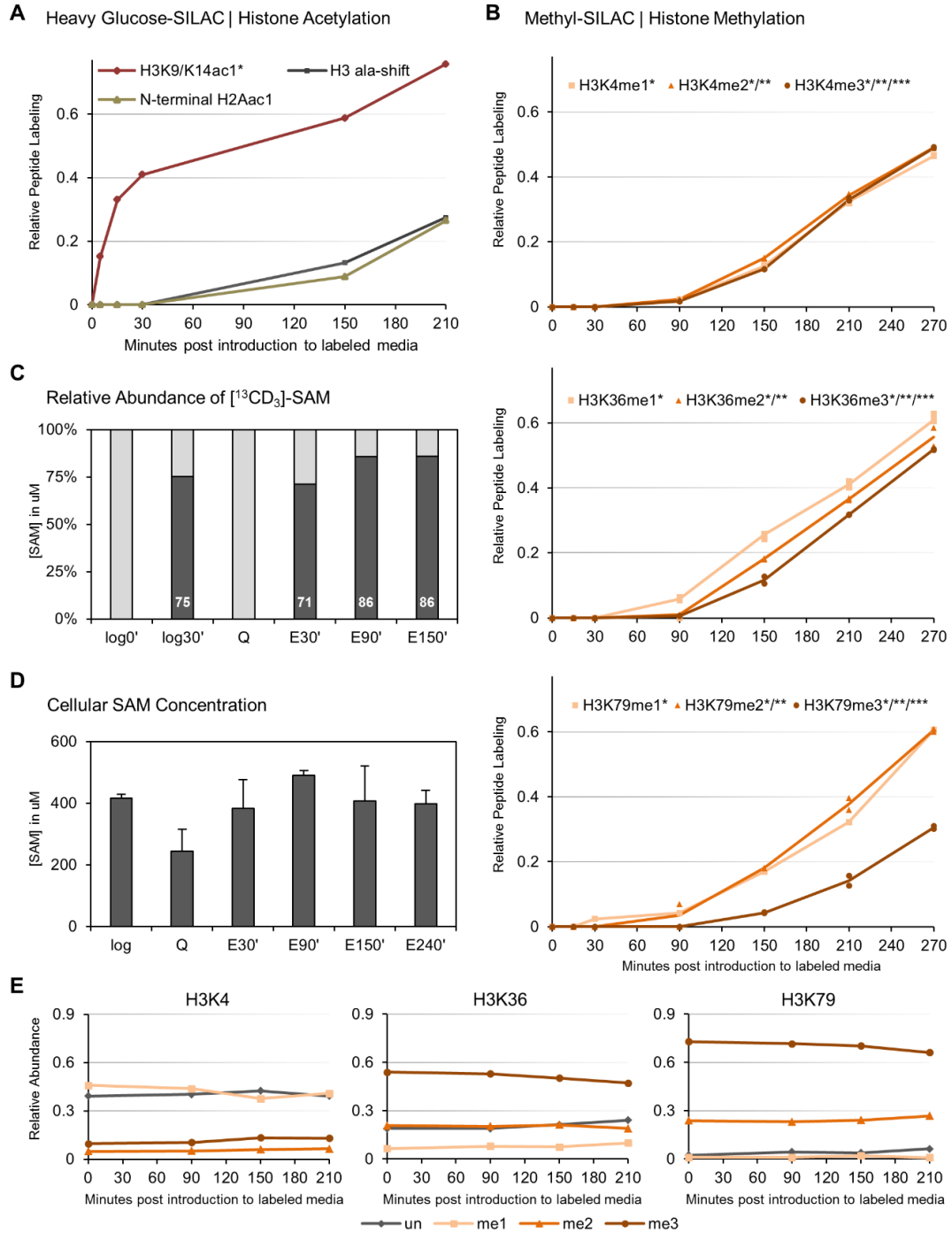


Figure 2.3. Histone methylation, unlike acetylation, remains static during quiescence exit.

(A) <sup>13</sup>C<sub>6</sub>-glucose-SILAC shows an immediate nutrient-induced increase in labeling of histone H3 acetylation (H3K9/K14ac1\*). N-terminal histone H2A acetylation is mediated co-translationally and becomes labeled only late in exit, concurrently with alanine labeling of newly synthesized histone proteins. (B) Methyl-SILAC during quiescence exit shows that all H3 K4, K36, and K79 methylation states remain remarkably static during

nutrient-induced cell cycle re-entry, and new methylation occurs only late in exit concomitantly with histone protein synthesis. (C) Mass spectrometry confirms rapid labeling of cellular SAM pools by  $^{13}\text{CD}_3$ -methionine in proliferating cells (log0' and log30') and upon nutrient replenishment in quiescent cells when histone methylation remains static. (D) Levels of methyl-donor SAM were assessed. Cellular SAM levels are slightly lowered in quiescence, but rise during early quiescence exit to levels characteristic of cycling cells. (E) Mass spectrometry shows that the overall levels of the corresponding methylated H3 peptides remain constant.

We then examined histone methylation dynamics with methyl-SILAC as the cells re-entered the cell cycle. Intriguingly, histone methylation remains remarkably static throughout quiescence exit. This trend was true of all H3K4, K36, and K79 methylation states, representing all of the abundant transcriptionally-linked histone methylation sites in yeast (Fig. 2.3B). Indeed, *de novo* histone methylation occurs only late during cell cycle re-entry, well after the burst of histone acetylation (compare Fig. 2.3B to 3A). We again confirmed that histone proteins are synthesized late in the exit, as assessed above by heavy glucose SILAC (Fig. 2.3A, grey), and here by heavy lysine SILAC (data not shown). Thus, new histone methylation occurs coincidentally with histone protein synthesis late in the exit when cells resumed replication.

We wanted to test a trivial explanation for the lack of change of methylation compared to acetylation in the early exit. It is possible that saturation of *in vivo* SAM pools with exogenous  $^{13}\text{CD}_3$ -methionine is slower than saturation of *in vivo* acetyl-CoA pools with exogenous  $^{13}\text{C}_6$ -glucose in yeast cells undergoing quiescence exit. This would result in an apparently slower rate of pulse labeling of methyl groups compared to acetyl groups. To address this, we tested by mass spectrometry of SAM whether  $^{13}\text{CD}_3$ -methionine was rapidly taken up and incorporated into SAM pools during re-feeding. We found that heavy labeling of SAM occurs early in the exit by 30 minutes (E30' in Fig 3C) and is comparable to labeling of SAM in cycling cells during log growth (log30' in Fig. 2.3C). We further confirmed that cellular SAM levels in cells exiting quiescence are similar to proliferating cells (Fig. 2.3D). While the SAM concentration is slightly lower in quiescent cells, cellular SAM pools readily rise during the early exit to levels typical for cycling cells (Fig. 2.3D), at a time when massive transcriptional changes occur in the absence of novel histone

methylation as shown by heavy-methyl SILAC (Fig. 2.3B). In addition to the absence of dynamic increase in histone methylation upon quiescent exit, we also noted by mass spectrometry that overall levels of the corresponding methylated peptides are constant (Fig. 2.3E), validating our findings by western blot analysis (Fig. 2.1E, F). Taken together, the SILAC analysis shows that histone methylation is surprisingly static during quiescence exit and is wholly different from the dramatic induction of histone acetylation during massive changes in gene expression. New histone methylation only appears late, concurrent with replication and concomitant histone protein synthesis.

### **Histone methylation is redistributed genome-wide during quiescence and exit**

We were surprised that histone methylation remains static in the backdrop of massive metabolic and transcriptional change. While genome-wide histone acetylation patterns have been investigated in nutrient-stressed cells<sup>39</sup>, the histone methylation status of growth and stress genes during quiescence and exit is unknown. We investigated the genome-wide distribution of histone modifications during quiescence and exit, focusing on two core groups of genes that have been previously described by microarray analysis as prominently transcribed during growth and during nutrient stress<sup>92,93,104</sup>, which we confirmed by our RNA-analysis (Fig. 2.1C, D).

We performed ChIP-seq in the same time-course to examine and compare histone acetylation and histone methylation. Histone acetylation at growth genes becomes greatly diminished in quiescence (Fig. 2.4A left). When these growth genes are induced upon nutrient replenishment, H3K9ac (Fig. 2.4A, left) and H4K12ac (Fig. 2.4B, left) rapidly increases at these loci. In contrast, H3K9ac and H4K12ac in quiescent cells is enriched at stress genes that are induced upon nutrient starvation, and then diminishes in E30, E240, and LOG (Fig. 2.4A and 2.4B right). Thus, our findings confirm observations previously made in similar conditions of nutrient limitation and environmental stressors<sup>38</sup>.

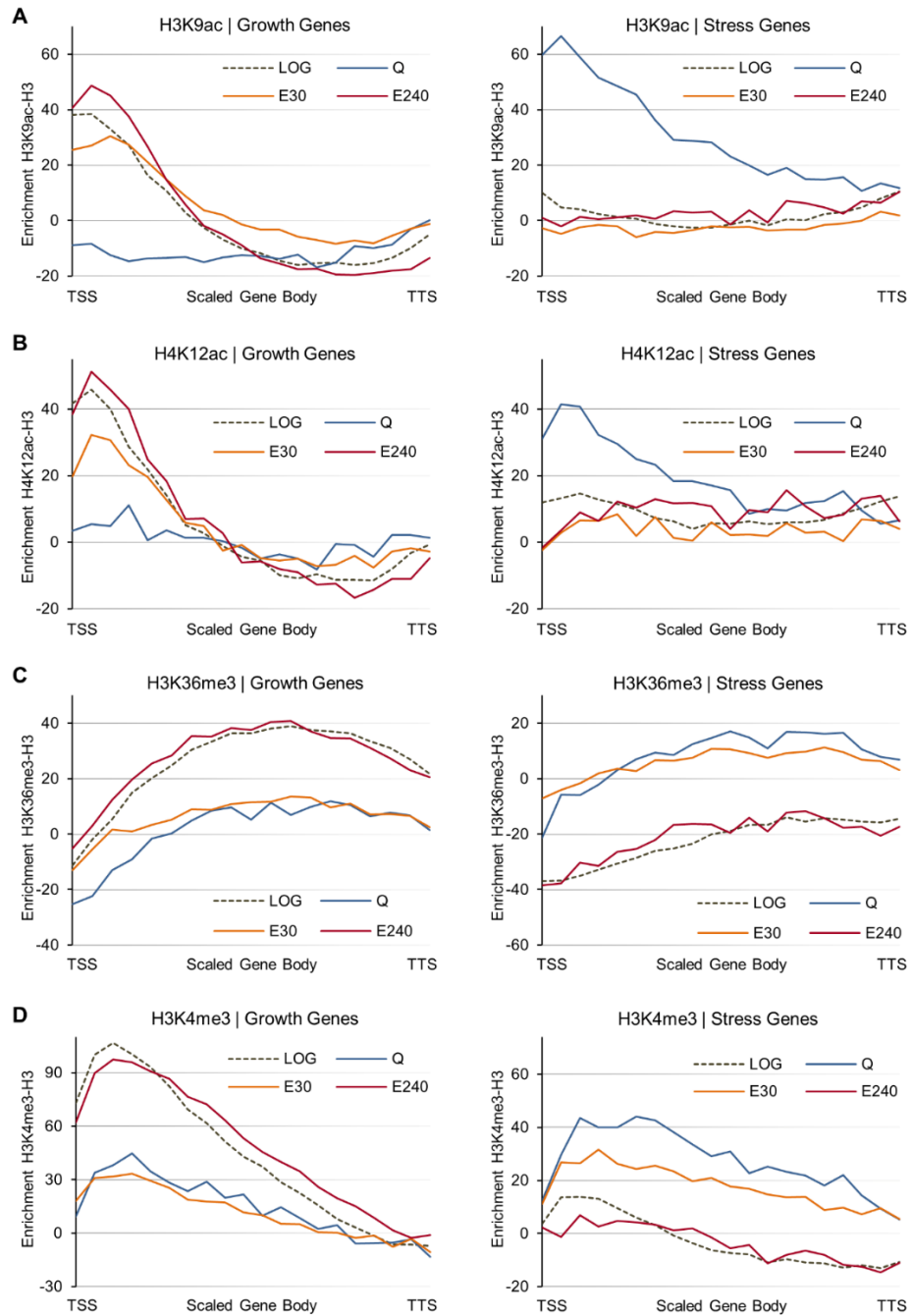


Figure 2.4. Histone methylation is redistributed as proliferating cells enter quiescence, but remains static in early exit from quiescence.

Average ChIP-seq enrichment of H3K9ac (A), H3K36me3 (B), and H3K4me3 (C) over scaled bodies (from the transcriptional start site “TSS” to the transcriptional termination site “TTS”; normalized to H3 ChIP signal) of all growth and stress genes characterized in Fig. 2.1 reveals differences between histone acetylation and methylation levels at these two distinct gene groups during quiescence establishment and exit.

We then analyzed genome-wide enrichment patterns of H3K4me3 and H3K36me3, which are associated with active gene expression. While overall global methylation levels remain stable, as shown by western blot analysis and mass spectrometry (Fig. 2.1F and 2.3E), we detect genome-wide shifts in the methylation status of growth and stress genes when we compare cells that have gone through the long process of establishing the quiescent state: note that the dotted/red lines (LOG and E240) are distinct from the blue/orange (Q and E30) (Fig. 2.4C and 2.4D). Specifically, histone methylation at growth genes is decreased during quiescence (Fig. 2.4C and 2.4D, left), whereas methylation at stress genes is increased (Fig. 2.4C and 2.4D, right). Strikingly, this new methylation pattern established during quiescence remains largely intact through early exit (i.e. Q and E30 lines are very similar) despite the enormous changes in transcription and histone acetylation that occur after re-feeding (Fig. 2.1). We do note that, at stress genes, H3K4me3 drops partially at E30, which might be related to the down-regulation of these genes as the cells leave quiescence. Importantly, new histone methylation at growth genes occurs only during the late exit (E 240 min) when the cell cycle is fully engaged (Fig. 2.4C and 2.4D, left). To confirm these genome-wide methylation data, we performed ChIP qRT-PCR in time-course for H3K4me3 and H3K36me3 for individual growth and stress genes (Fig. 2.5).

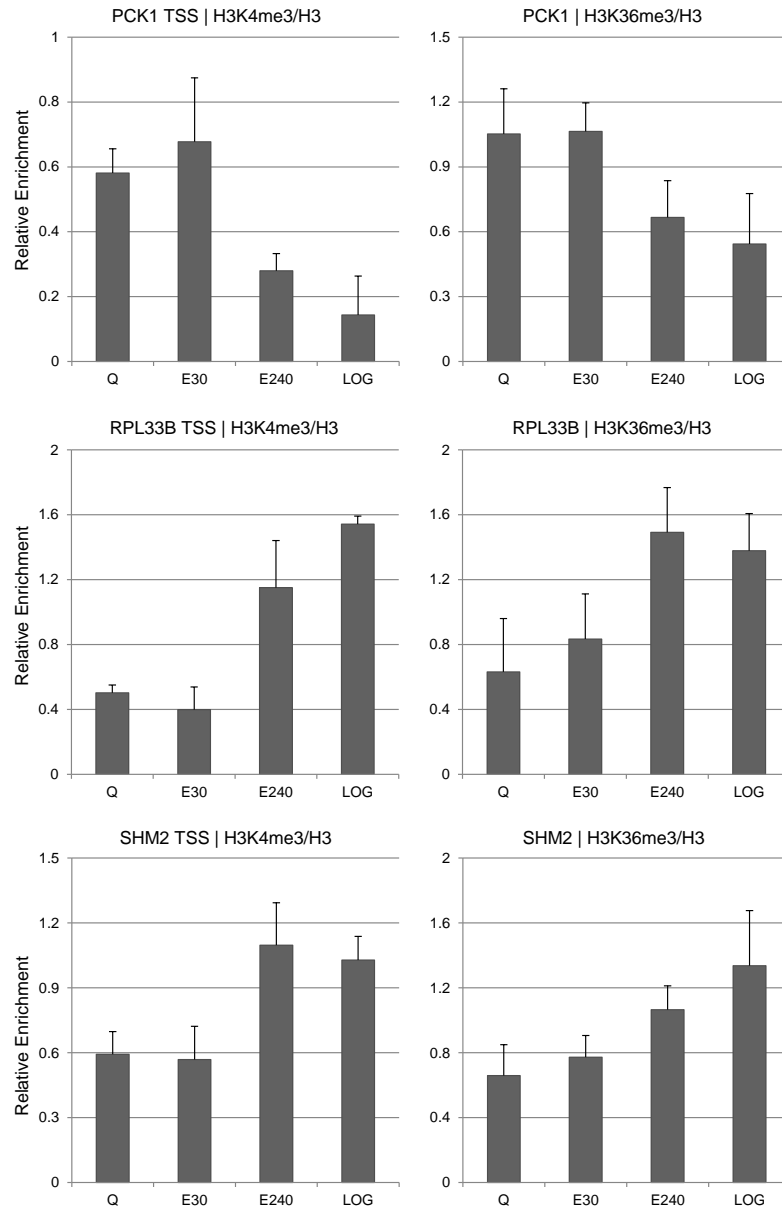


Figure 2.5. Histone methylation at individual stress and growth genes remains stable upon nutrient replenishment.

ChIP-qPCR was performed in time-course to reveal H3K4me3 and H3K36me3 at a representative stress gene, PCK1 (A), and two representative growth genes, RPL33B and SHM2 (B), confirming that methylation levels remain unchanged during the early exit. Data are shown as ratios of modification to total histone H3. ChIP-qPCR data are the average of three biological replicates, and error bars represent standard deviation from the mean.

The clear quantitative contrast between genome-wide acetylation and methylation is most easily visualized by box plot analysis (Fig. 2.6). H3K9ac drops at stress genes between Q and E30 and increases at growth genes between Q and E30. In contrast, H3K4me3 and K36me3 remain constant at both stress and growth genes between Q and E30. Importantly, these ChIP-seq findings for histone methylation agree with our methyl-SILAC data showing that catalytic histone methylation is altered late (at E240) but not early (at E30) after quiescence exit (Fig. 2.3B).

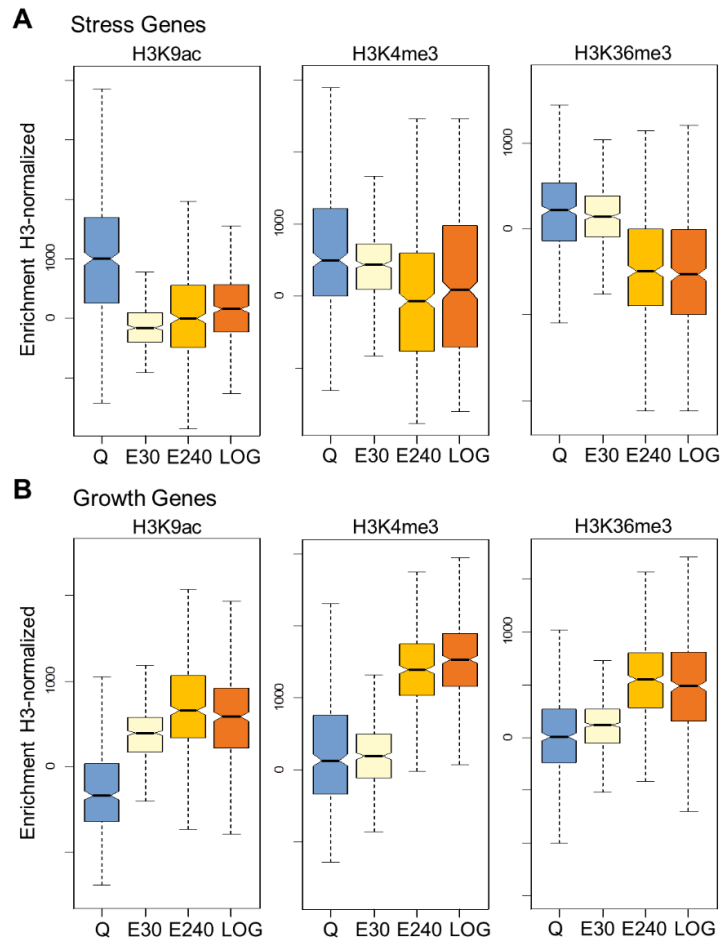


Figure 2.6. Box plot analysis shows distinct dynamics of histone acetylation and methylation at growth and stress genes during the early exit.

H3K9ac drops at stress genes (A) between Q and E30 and increases at growth genes (B) between Q and E30. In contrast, H3K4me3 and K36me3 remain constant at both stress and growth genes between Q and E30.

Indeed, further analysis of the ChIP-seq histone modification profiles at growth genes confirms stark dissimilarities during the exit. The dynamic histone acetylation profiles at these genes correlate with gene expression changes upon nutrient-induced cell cycle re-entry (Fig. 2.1C; Fig. 2.7A). In proliferating cells, such a correlation is also found between histone methylation and growth gene expression (Fig. 2.1C; Fig. 2.7B, left). However, the altered methylation profiles in the quiescent state Q remain unchanged in the early exit E30: even though both acetylation and expression of growth genes are greatly increased in the early exit E30, their methylation profiles remain unchanged (Fig. 2.7B, right) and do not correlate with gene expression in the early exit E30 (Fig. 2.7C).

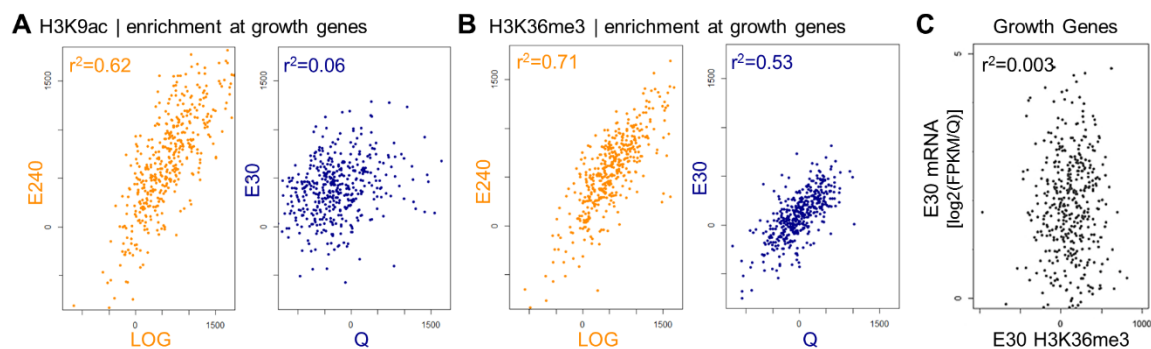


Figure 2.7. Scatterplot analyses demonstrate distinct dynamics of histone acetylation and methylation at growth genes.

(A, B) Scatterplots contrasting the enrichment of H3K9ac (A) and H3K36me3 (B) at growth genes: histone acetylation correlates well between LOG and E240 cells (A, orange), but not between Q and E30 cells (A, blue). In contrast, histone methylation not only correlates well between the LOG and E240 time points (B, orange), but also between Q and E30 (B, blue), which illustrates that histone methylation remains static in the early exit. (C) Growth gene expression levels (y-axis) and H3K36me3 enrichment (x-axis) do not correlate in the early exit from quiescence when growth genes are induced and methylation remains stable. Each dot represents one growth gene.

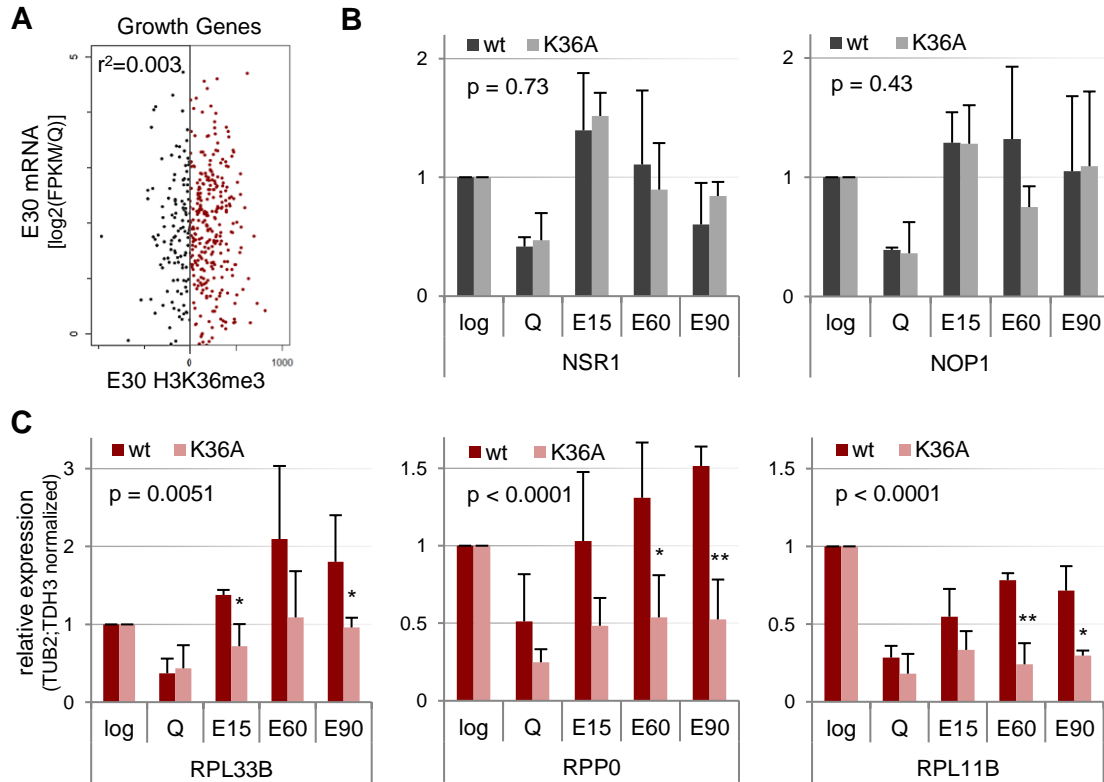


Figure 2.8. H3K36me3 retained at growth genes in quiescent yeast is required for rapid transcriptional activation during exit.

(A) Growth gene expression levels (y-axis) and H3K36me3 enrichment (x-axis) do not correlate in the early exit from quiescence. Many growth genes are induced while methylation remains stable (black). A set of growth genes does not follow this trend and partially retain their histone methylation throughout quiescence and the early exit (red). Each dot represents one growth gene. (B) RT-qPCR analysis in wildtype and H3K36A mutant yeast shows that growth genes that naturally lose methylation in wildtype quiescent cells (NSR1 and NOP1) are induced normally in the H3K36A mutant strain upon refeeding. (C) In contrast, the re-feeding induction kinetics of growth genes that naturally retain methylation during quiescence (RPL33B, RPP0, and RPL11B) are delayed in the mutant strain compared to wildtype cell. Asterisks indicate significance.

Interestingly, while methylation is largely unchanging through quiescence exit, it is indeed present over several growth genes even in quiescence (Fig. 2.8C, red dots). Thus, we were intrigued at the possibility that histone methylation may be retained at certain growth genes to assist in rapid transcriptional induction upon quiescence exit. To examine this, we conducted a time-course expression analysis through quiescence exit using yeast mutants that bear a

methylation site histone substitution. We sampled certain growth genes that fully lose methylation (Fig. 2.8C, black dots) to compare them to growth genes that retain methylation (Fig. 2.8C, red dots) in quiescence, and investigated the induction kinetics of these genes after adding nutrients to induce cell cycle re-entry. The induction of three genes that typically retain methylation in wild type cells during quiescence is delayed to varying degrees in the histone mutant expressing H3K36A (Fig. 2.8D, RPP0, RPL11A, RPL33B, in red shades). In contrast, two genes that largely lose methylation during quiescence are induced at an earlier time-point and show a profile of gene activation in the H3K36A cells that is comparable to wild-type cells (Fig. 2.8E, NSR1, NOP1, in grey shades). Taken together, our ChIP-seq and histone mutagenesis results thus point to histone methylation functioning as a partial memory mark that facilitates transcriptional induction of certain growth genes following nutrient replenishment as the cells exit quiescence.

We then investigated histone acetylation and methylation in another group of environmentally regulated genes that has been previously found to exhibit highly dynamic and stress responsive histone acetylation induced by H<sub>2</sub>O<sub>2</sub> treatment<sup>92,105</sup>. Again, we found that histone acetylation is rapidly increased at E30 upon nutrient replenishment, whereas histone methylation remains static and does not follow these dynamics (Fig. 2.9A). As a control, we determined that neither histone acetylation nor methylation changes at nutrient insensitive genes during the early exit E30 (Fig. 2.9B).

We then examined methylation patterns over one kilobase windows genome-wide in Q, E30, E240 and LOG by scatterplot analysis. As expected from the box plot analysis, methylation patterns are highly correlated between E240/LOG and Q/E30, but are very different between Q/LOG (Fig. 2.10A, top panels). Prominently, the correlation of genome-wide H3K36 methylation between Q/E30 (Fig. 2.10A, top right) is strikingly contrasted in by the highly dissimilar H3K9 acetylation pattern between Q/E30 cells (Fig. 2.10A, lower right).

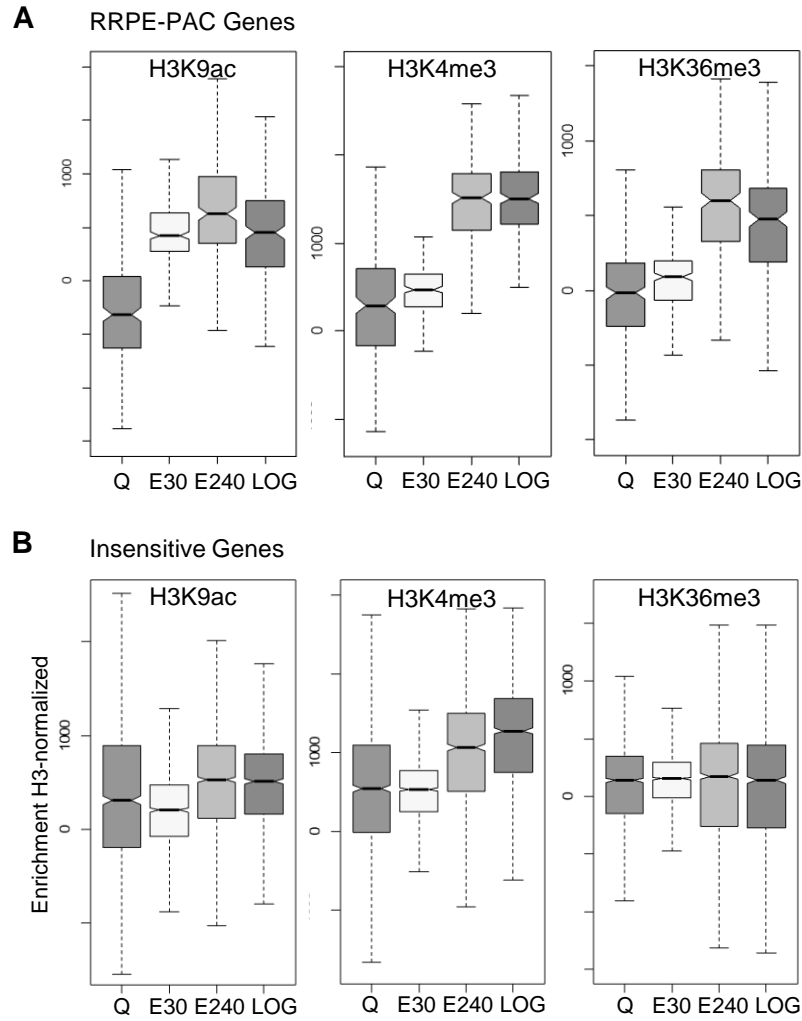


Figure 2.9. Histone acetylation and histone methylation levels at stress-responsive RRPE/PAC and nutrient-insensitive genes in quiescence and cell cycle re-entry.

(A) Genes that are characterized by the presence of RRPE and PAC promoter elements exhibit dynamic changes in histone acetylation, but not histone methylation. In quiescent cells, H3K9ac is greatly diminished, but rapidly increases at E30 upon nutrient replenishment. H3K4me3 does not follow these dynamics and remains unchanged in the early exit (264 genes; RRPE - rRNA processing element; PAC - polymerase A and C). (B) Both histone acetylation and methylation remains largely unaffected at nutrient-insensitive genes in the early quiescence exit.

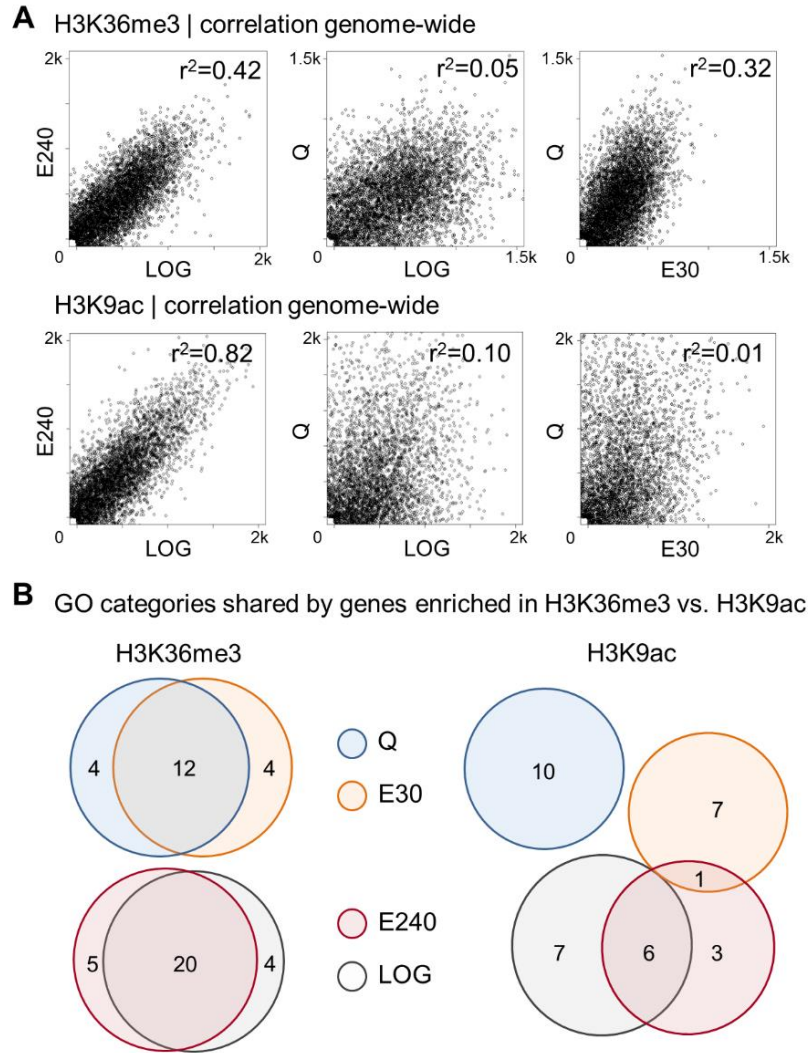


Figure 2.10. Histone methylation patterns correlate genome-wide in quiescence exit.

(A) Genome-wide ChIP-seq enrichment correlations can be seen between proliferating cells (LOG) and cells in late quiescence exit (E240) for both H3K36me3 and H3K9ac. The H3K36me3, but not H3K9ac, enrichment pattern is highly correlated in quiescent yeast (Q) and early exit (E30). Each dot represents a 1000 base pair window of the genome. (B) Genes enriched for H3K36me3 in proliferating cells (LOG) and genes methylated in late exit cells (E240) cluster into shared GO categories (see Suppl. Table 1; categories are related to growth, e.g. regulation of translation, ribosome biogenesis, nuclear export). Genes that are methylated in quiescent (Q) and early exit cells (E30) also share GO categories (related to stress, e.g. cell death, response to abiotic stimuli). Genes enriched for H3K9ac in quiescent cells (Q) cluster into stress categories that are not shared by genes that are acetylated in E30, E240, or LOG (see Suppl. Table 2). Genes that are acetylated in E240 and LOG cluster into shared categories that are linked to ribosome biogenesis and translational regulation.

We further investigated the relationship of histone methylation enrichment to different gene families, examining H3K36me3 during LOG/Q/E30/E240 using unbiased gene ontology (GO) enrichment analysis. We queried GO terms that link to the top methylated genes; we found that LOG cells and E240 cells share categories that are related to cell growth and proliferation (Fig. 2.10B, left, red and grey circles). Remarkably, genes that are methylated in Q and E30 share GO terms associated with stress (Fig. 2.10B, left, blue and orange circles), despite their decidedly distinct expression and histone acetylation profiles. In contrast, GO terms that link to the top acetylated genes in Q do not overlap with GO terms associated with genes that are acetylated in the early exit E30 (Fig. 2.10B, right).

Thus, by ChIP-seq, we uncovered genome-wide changes in histone methylation that are obscured in western and SILAC analyses. First, during quiescence establishment, our genome wide analysis revealed that stress genes become methylated when their expression is induced, whereas growth genes experience extensive methylation losses when they are not transcribed. Second, during exit, ChIP-seq revealed two key features of the location of dynamic histone methylation changes determined by SILAC: (1) quiescence-specific methylation patterns remain remarkably intact through early exit E30, but (2) change in the course of replication initiation at E240, when de novo histone methylation occurs exclusively at growth genes. These results, taken together with our SILAC analyses above, underscore the differences in the roles of histone methylation and acetylation in the dramatic gene expression changes following quiescence exit. Histone acetylation rapidly responds to metabolic state, but histone methylation remains stable through quiescence exit and undergoes genome-wide re-distribution with de-novo growth gene methylation linked to the initiation of cellular replication.

## DISCUSSION

The epigenome is hypothesized to provide an interface between the cellular environment and gene expression. One of the most important environmental factors that must be synchronized with gene transcription is the availability of caloric energy. Indeed, glucose-derived acetyl-CoA is thought to function as a modulator of histone acetylation and growth-related gene expression<sup>38</sup>. Previous studies suggest that histone acetylation is exquisitely responsive to the nutritional state of cells. In fact, our findings from SILAC demonstrate that certain histone acetylation sites and, by default, their acetylation enzymes operate as *bona fide* energy sensors, providing unequivocal evidence that nutrients induce an immediate histone acetylation response, driven by external glucose (Fig. 2.3A).

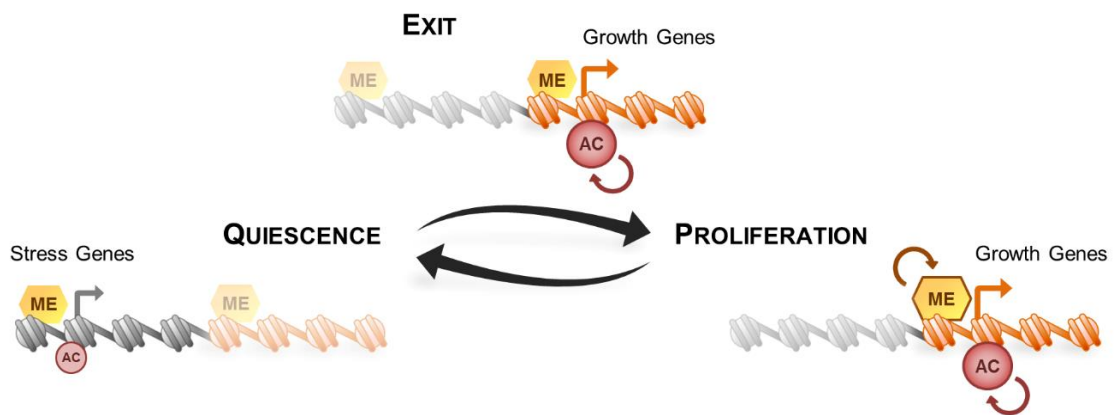


Figure 2.11. Schematic model for the distinct dynamics of histone methylation and acetylation during quiescence establishment and exit.

The methylation landscape is changed genome-wide in cellular quiescence. In nutrient-induced cell cycle re-entry, this methylation pattern remains strikingly intact – in contrast to dynamic histone acetylation that is linked to gene transcription. Upon cell cycle return, the methylation landscape is restructured only very late in conjunction with genome replication and ensuing cell division.

Histone methylation also has an important role in gene regulation in all eukaryotes. Chemically, methylation is more stable than acetylation and is known to be less dynamic in cells. Hence, a key question is whether histone methylation responds to nutritional status. Like histone acetylation, histone methylation is speculated to be synchronized with metabolic information in order to regulate gene expression<sup>19,94,99</sup>. Here, we performed a comprehensive investigation of methylation profiles during quiescence exit, when cells undergo a dramatic shift in gene regulation as a result of the drastic change in metabolic state from nutrient starvation into regrowth. We observe that histones become enriched for acetylation at certain genes both globally (by western blot) and locally (by ChIP-seq). Indeed, similar observations have represented a paradigm for how metabolic changes can alter the epigenome<sup>38,39</sup>. Our rigorous examination, additionally by SILAC, fully confirms that histone acetylation responds immediately to increased nutrition after starvation. Thus, this nutrient-induced transition from quiescence to proliferation represents an ideal scenario to examine metabolic signaling to histone methylation.

### **Histone methylation as an epigenetic memory mark during metabolic shifts**

To investigate histone methylation during quiescence exit, we used three approaches: (1) western blot analysis with methyl-specific antibodies, as was previously used to demonstrate global changes in histone acetylation<sup>39</sup>, (2) quantitative mass spectroscopy using heavy-labeled precursors to distinguish new histone methylation immediately following re-feeding, and (3) ChIP-seq with methyl-specific antibodies, as was previously used to examine site-specific acetylation in metabolic cycling yeast<sup>38</sup>. Interestingly, we found that histone methylation, irrespective of the residue or methylation states, is exceptionally stable, and is uncoupled from rapid changes in the metabolic state as cells exit quiescence (Fig. 2.3B). Western blot and SILAC show that the overall global levels of methylation do not change and do not turnover as the cells emerge from quiescence. Furthermore, ChIP-seq revealed that there are no localized changes in genomic distribution during quiescence exit until cell replication commences. In contrast, these same approaches provide clear evidence that histone acetylation is dynamic: new acetylation is

detected by SILAC immediately following re-feeding and well before replication (Fig. 2.4). Finally, ChIP-seq shows that acetylation is rapidly enriched at genes that are induced and depleted at genes that are repressed.

Thus, our observations revealed that yeast cells that return to the cell cycle in nutrient-rich conditions exhibit a strikingly stable methylation landscape despite major metabolic and transcriptional reprogramming. Historically, histone methylation is thought to be a static modification based on studies that have demonstrated similar turnover rates for methyl groups and histone proteins<sup>106,107</sup>; however, in the past decade, the notion that histone methylation is enzymatically irreversible has been challenged by the identification of numerous HDMs, specifically the lysine-specific demethylase 1 (LSD1) and Jumonji C demethylases<sup>41,108,109</sup>. Remarkably, both domain classes of HDMs require high-energy metabolic cofactors – flavin adenine dinucleotide (FAD) and alpha ketoglutarate (α-KG), respectively. Thus, the coenzymes of both HMTs and HDMs are positively regulated by high energy levels, an apparent paradox that likely imposes further regulation should these enzymes be integrated in metabolic control. In contrast, HATs and HDACs are regulated by high and low energy levels, respectively, adapting histone acetylation to dynamic metabolic processes through acetyl-CoA generation and the cellular redox state.

Our results confirm that histone acetylation quickly drives growth gene transcription in relation to transient caloric availability when emerging from quiescence, whereas histone methylation remains surprisingly static during the early exit. We cannot exclude the possibility that metabolic fluxes may directly modify methylation later, i.e. during cell replication when we detect new methylation. Thus, histone methylation may not play a role in the initial re-activation of growth genes, but may function in the late cell cycle re-entry to provide transcriptional marking and coordinate gene expression following genome replication. This is a particularly intriguing possibility, given our observation of de-novo methylation late after quiescence exit.

Furthermore, our results show that histone methylation is indicative of transcriptional potential but not necessarily current transcriptional activity. Indeed, we confirm that enrichment of H3K4me3 at promoters correlates with gene activity in proliferating yeast <sup>110,111</sup>; however, we also show that H3K4me3 does not directly correlate with gene expression in the quiescent cell state, (i.e. we detect H3K4me3 at both active stress genes and inactive growth genes). In fact, previous observations in mammalian cells showed that H3K4me3 is actually present at a majority of promoters and is not strictly predictive of transcriptional activity <sup>112,113</sup>.

In summary, we find that acetylation is lost nearly completely at growth genes during quiescence and – driven by metabolic state - is very rapidly reinstated in the early exit. In contrast, full re-methylation at growth genes occurs only at the time of cell replication following quiescence exit. Accordingly, although diet, exercise, and circadian rhythms are all known to readily manipulate histone acetylation to maintain metabolic homeostasis, they may not easily modify long-term histone methylation.

### **Histone methylation in the context of altered metabolism in cancer and stem cells**

It is interesting to compare our results with recent investigations of histone methylation in higher eukaryotic cells in the context of proliferative states. In many cancers, deregulated histone methylation has been implicated in tumorigenesis <sup>29,30</sup>. In a variety of tumors, the metabolic enzymes isocitrate dehydrogenase 1 (IDH1) and IDH2 were found to bear mutations that result in neomorphic activities that generate 2-hydroxyglutarate (2HG) <sup>31</sup>. As an oncometabolite, 2HG inhibits a family of Jumonji-C domain histone demethylases (JHDMS) and is thought to disrupt gene expression patterns through alterations in the histone methylation landscape <sup>31</sup>.

In addition, recent findings suggest a mechanistic link between reprogrammed cancer metabolism and an altered methylation landscape <sup>114</sup>. Certain cancer cells aberrantly express high levels of the metabolic enzyme nicotinamide N-methyltransferase (NNMT) and exhibit global methylation defects when methionine is limited. Under these conditions, the increased catalytic

capacity of NNMT may drain cellular SAM pools by creating stable 1-methylnicotinamide and thereby impairs histone and other protein methylation <sup>114</sup>. However, it is unclear when, during the cell cycle, elevated NNMT activities may actually affect histone methylation, and how broad alterations in the methylation landscape eventually promote oncogenesis. Therefore, in order to develop novel therapeutic approaches that target cellular metabolism and alter the tumor epigenome, it is key to understand how chromatin may be metabolically regulated in non-cancerous cells.

Interestingly, histone methylation may not only be influenced by metabolic alterations in tumors, but may also be manipulated by metabolic adaptations in stem cells, where methylation has critical functions in transcriptional regulation and self-renewal <sup>115,116</sup>. Current evidence suggests that the pluripotency of mouse embryonic stem cells (ESCs) is dependent on their distinct mode of threonine catabolism and its effect on SAM metabolism and H3K4me3 <sup>101</sup>. When proliferating mESCs are cultured in threonine-depleted media, SAM levels become lowered and H3K4me3 levels – but not other methylation – decrease, which results in slowed growth and increased differentiation <sup>101</sup>. However, as threonine dependency is specific to mouse ESCs, it remains unclear whether histone methylation is similarly influenced by metabolic activities in other stem cell populations like human ESCs or adult human stem cells. Notably, histone methylation may be under metabolic influence only at specific times, e.g. when quiescent adult human stem cells are induced to return to the cell cycle and initiate cell replication for clonal expansion.

From our findings in the yeast model, histone methylation may also have distinct functions from those of histone acetylation in the orchestrated cell cycle re-entry in induced stem cells, fibroblasts, or lymphocytes. Unlike acetylation, methylation may regulate gene expression independently of the metabolic milieu during early cell cycle return. Rather, it may function as an epigenetic marker of cellular transcriptional identity during genome replication and cell division.

## MATERIALS AND METHODS

**Quiescence establishment and exit protocol.** Western blot, SILAC, RNA-seq, and ChIP-seq experiments were performed in BY4741 (*MATa his3Δ1 leu2Δ0 met15Δ0 ura3Δ0*; Invitrogen). To establish quiescence, yeast cells were cultured in 2% synthetic complete media (SC media; 2% glucose–0.5% ammonium sulfate–0.2% SCM supplement (Bufferad)–0.17% yeast nitrogen base (Bufferad)) for 72h before their transfer into water for complete nutrient starvation and quiescence establishment at 30°C, ensuring a homogenous non-dividing cell population, as previously described<sup>102</sup>. Quiescence exit was induced on day 8 by re-suspending pelleted quiescent cells into fresh 30°C-prewarmed 2% SC media at OD<sub>600</sub> 0.4. At the indicated time points, culture aliquots were taken and cells harvested by centrifugation or microfiltration and stored at -80°C for subsequent analyses as outlined below.

**Yeast whole-cell extract preparation and western blotting analysis.** Yeast cells were harvested by centrifugation at 4,000 rpm for 4 min at 4°C. Cells were washed with ice-cold water once and broken in 50 mM Tris-HCl (pH 7.4)–300 mM NaCl–0.5% NP40–10% glycerol–1 mM EDTA (pH 8)–protease inhibitor cocktail (Complete; Roche) using silica beads and bead beater (Bio-Spec). The lysate was sonicated (Bioruptor; Diagenode) for 5 min and cleared by centrifugation at 14,000 rpm at 4°C for 15 min. The supernatant was collected and stored at -80°C. Protein estimation was determined using Bradford dye. Extracts were resolved on SDS-polyacrylamide gels, western blotting performed by standard methods and images of the western blots were taken with a Fujifilm LAS-4000 imager.

**Antibodies.** The primary antibodies used are as follows: anti-H3 (Abcam, ab1791, 1:1000), anti-H3K9ac (Active Motif, 39137, 1:1000), anti-H3K4me1 (Abcam, ab8895, 1:500), H3K4me2 (Active Motif, 39141, 1:1000), anti-H3K4me3 (Abcam, ab8580, 1:1000), anti-H3K36me1 (Abcam, ab9048, 1:1000), anti-H3K36me3 (Active Motif, 61101, 1:1000), anti-H3K79me3 (Abcam, ab2621, 1:1000), anti-H4K5ac (Millipore, 07-327, 1:1000), anti-H4K8ac (Millipore, 07-328, 1:1000).

**Cell culture and SILAC.** For the methyl-SILAC and lysine-SILAC time course experiments, quiescent cell cultures were pelleted at 4,000 rpm for 3 min at 30°C and resuspended with 2% SC media that was depleted of unlabeled methionine or lysine (SC Dropout Mixtures, Sunrise Science Products) and supplemented with equimolar amount of L-methionine-methyl- $^{13}\text{CD}_3$  (Sigma-Aldrich) or  $^{13}\text{C}_6^{15}\text{N}_2$ -lysine (Cambridge Isotope Laboratories), respectively. In order to assess histone acetylation turnover by heavy glucose-SILAC, quiescent cells were resuspended in SC media supplemented with 2% of isotopically heavy  $^{13}\text{C}_6$ -glucose (Sigma-Aldrich). Aliquots were taken at the indicated time points, and cells collected by centrifugation at 4,000 rpm for 3 min, flash frozen, and stored at -80°C for the subsequent nuclei preparation and histone protein purification as outlined below.

**Purification of histone proteins for mass spectrometry.** Preparation of nuclei was based on published methods <sup>117,118</sup>. In brief,  $10^{10}$  cells were washed in 1 M Sorbitol–50 mM potassium phosphate (pH 6.8)–14 mM  $\beta$ -mercaptoethanol at 30°C. In order to achieve complete digestion of the cell wall, cells were resuspended in the same buffer supplemented with Zymolase 100T (0.4 mg/ml) at 30°C for 30 min to 1.5 h. The digestion was monitored by adding 1% SDS to 20  $\mu\text{l}$  of the digestion reaction and considered complete once the  $\text{OD}_{600}$  dropped by 95%. Spheroplasted cells were washed in 1 M sorbitol, and cell lysis was achieved in 18% Ficoll–20 mM potassium phosphate (pH 6.8)–1.0 mM  $\text{MgCl}_2$ –0.5 mM EDTA–100 mM Na butyrate–protease inhibitor cocktail (Complete; Roche) by 60 strokes of Wheaton Dounce homogenizer on ice. Nuclei were collected after centrifugation at 4000 rpm from supernatant and pelleted by ultracentrifugation at 50,000 x g for 30 min at 4°C. Pelleted nuclei were resuspended in 0.34 M Sucrose–20 mM Tris-HCl (pH 7.4)–50 mM KCl–5.0 mM  $\text{MgCl}_2$  and purified by ultracentrifugation on 2 M sucrose cushion at 30,000 x g for 30 min at 4°C. Acid extraction to enrich for basic histone proteins was achieved by resuspending nuclei in 10 mM Tris-HCl (pH 8.0)–400 mM NaCl–100 mM Na butyrate after three washes in 10 mM Tris-HCl (pH 8.0)–0.5% NP40–75 mM NaCl–100 mM Na butyrate, and protein precipitation by addition of 20% trichloroacetic acid (TCA), followed by centrifugation,

and two washes in acetone–0.1% HCl and acetone alone. The pellet was briefly dried, and proteins were resuspended in water for derivatization.

**Histone sample preparation for mass spectrometry.** Purified histones were derivatized with propionic anhydride and digested with sequencing grade trypsin as described before <sup>26,119</sup>. Due to the relative hydrophilicity of the H3 3-8 peptide spanning H3K4 and thus reduced retention and resolution using reversed phase liquid chromatography (unpublished data), aliquots from the same histone protein sample were derivatized with benzoic anhydride rather than propionic anhydride. After derivatization with either reagent, both sample preparations were separately diluted in 0.1% acetic acid for desalting before mass spectrometric (MS) analysis using homemade C18 STAGE tips as previously described <sup>119</sup>.

**Mass spectrometry analysis and peptide quantification.** Histone peptides were loaded by an Eksigent AS2 autosampler onto silica capillary C18 columns and resolved by an Agilent 1200 binary HPLC system as previously reported <sup>26</sup>. Peptides were electrosprayed into a linear quadrupole ion trap-Orbitrap mass spectrometer. All MS and MS/MS spectra were analyzed with Qual Browser (version 2.0.7, Thermo Scientific) and peptide abundances were obtained by peak integration of the extracted ion chromatograms as previously described <sup>26</sup>.

**SAM labeling assay and SAM fluorometry quantification.** Cells were harvested by filtration, and selected reaction monitoring (SRM) analysis by mass spectrometry was performed as described in Zee et al. 2012 and Bajad et al. 2006 <sup>120,121</sup>. To quantify SAM levels, the Bridge-It® SAM fluorescence assay (Mediomics) was used according to manufacturer's instruction.

**RNA preparation, qRT-PCR, and RNA-seq.** RNA was purified using the Dynabeads® mRNA DIRECT™ Kit (61011, Ambion®, Life Technologies) according to the manufacturer's instructions. For qRT-PCR analysis, reverse transcription was performed using the Applied Biosystems high-capacity RNA-to-cDNA kit (4387406). cDNA was quantified using standard procedures on a 7900HT Fast-Real-Time PCR machine (ABI). During vegetative growth, quiescence, and

quiescence exit, mRNA levels were normalized to TUB2 and GAPDH. Three independent biological replicates were analyzed, and each data point acquired by qPCR was the average from three independent PCRs. Error bars in the figures are standard errors of the means (SEM), and asterisk designate significance (\* $p \leq 0.01$ , \*\* $p \leq 0.001$ ). ANOVA analyses assessed the significance of gene expression defects in the histone mutant (p value in the panels). RNA-seq libraries were prepared using the ScriptSeq™ v2 RNA-Seq Library Preparation Kit (SSV21124, Epicentre) according to the manufacturer's recommendations, and sequencing was performed on the Illumina Hi-Seq (50 bp single-end reads) platform. RNA-seq data were aligned using the software TopHat<sup>122</sup>, and gene expression levels and differences were calculated using Cuffdiff<sup>123</sup>. Reads per million reads sequenced per kilobases of exons in the transcript (RPKM) values for exit and log phase samples were normalized to quiescence scores, log-transformed and visualized using the Partek Genomics Suite™ (Partek Incorporated).

**ChIP-seq.** Approximately 50 OD600 units of cells were cross-linked in 1% formaldehyde for 10 min at 25°C, quenched with addition of glycine to 125 mM for 5 min at 25°C, and washed with water. Cells were resuspended in FA lysis buffer 50 mM HEPES (pH 7.5) –150 mM NaCl–2 mM EDTA–1% Triton X-100–0.2% SDS–CPI Mini EDTA- protease inhibitor cocktail (Complete; Roche). One milliliter of silica beads was added to each tube, and cells were disrupted twice for 3 min each for the LOG sample and four times for 3 min each for the Q, E30' and E240' samples at maximum speed with intermediate incubation at –20°C for 3 min (Mini-Beadbeater 96; Biospec). Chromatin was washed twice with FA lysis buffer and sonicated for 30 cycles (30 s “on” at high level and 30 s “off” per cycle) (Bioruptor; Diagenode). Cellular debris was removed by centrifugation at 14,000 rpm for 15 min at 4°C. ChIP was performed as previously described<sup>124</sup>; ChIP using H3K9ac and H4K12ac antibodies for quiescence extracts were completed with 5-fold the input used for all other ChIP experiments. Per each ChIP, 30  $\mu$ l of Protein G Dynabeads (Invitrogen, 100.02D) were prepared using 5  $\mu$ g of antibody. Controls with IgG and no antibody were routinely performed. The ChIP DNA was used to make sequencing libraries using standard

Illumina library single-end construction procedures. Sequencing was performed on the Illumina Hi-Seq (50 bp single-end reads) platform.

**Sequencing analysis.** ChIP-seq reads were aligned to the sacCer2 assembly of the *S. cerevisiae* genome using the Bowtie alignment software <sup>125</sup>. For growth and stress gene boxplot analysis, each gene of the respective group was assigned a score by computing the area-under-the-curve (AUC) of the ChIP-seq signal over the gene body (H3K36me3), or TSS+/-250bp (H3K4me3, H3K9ac, H3K12ac). Scores for a given locus in a given state were computed by normalizing the number of tags aligned to the locus by the total number of bases sequenced per-barcoded sample as well as by total histone and locus length. Boxplots were generated in R. Yeast transcription start site (TSS) and open reading frame (ORF) locations were obtained by querying the Ensembl database ([www.ensembl.org](http://www.ensembl.org)).

**Gene Ontology and Venn diagrams.** Gene Ontology (GO) analysis was performed using DAVID (<http://david.abcc.ncifcrf.gov/>). The GO terms were clustered using the tool VENNY (<http://bioinfogp.cnb.csic.es/tools/venny/>), and Euler diagrams were generated using the EulerAPE drawing tool (<http://www.eulerdiagrams.org/eulerAPE/>) that were subsequently edited for color in PowerPoint 2010 (Microsoft).

**CHAPTER 3**

**ACETYL-COA METABOLISM BY ACSS2 REGULATES  
NEURONAL HISTONE ACETYLATION AND LONG-TERM MEMORY**

## ABSTRACT

Metabolic production of acetyl-CoA has been linked to histone acetylation and gene regulation, however the mechanisms are largely unknown. We show that the metabolic enzyme acetyl-CoA synthetase 2 (ACSS2) is a critical and direct regulator of histone acetylation in neurons and of long-term mammalian memory. We observe increased nuclear ACSS2 in differentiating neurons in vitro. Genome-wide, ACSS2 binding corresponds with increased histone acetylation and gene expression of key neuronal genes. These data indicate that ACSS2 functions as a chromatin-bound co-activator to increase local concentrations of acetyl-CoA and to locally promote histone acetylation for transcription of neuron-specific genes. Remarkably, in vivo attenuation of hippocampal ACSS2 expression in adult mice impairs long-term spatial memory, a cognitive process reliant on histone acetylation. ACSS2 reduction in hippocampus also leads to a defect in upregulation of key neuronal genes involved in memory. These results reveal a unique connection between cellular metabolism and neural plasticity, and establish a link between generation of acetyl-CoA and neuronal chromatin regulation.

## INTRODUCTION

Memory formation is manifested in long-lasting synaptic restructuring requiring coordinated expression of neuronal genes<sup>126,127</sup>. The regulatory mechanisms that control neuronal gene transcription during memory formation include chromatin-modifying processes that are incompletely understood<sup>47,128</sup>. Histone acetylation, one of the best-characterized chromatin regulatory mechanisms, has emerged as a regulator of memory storage<sup>44</sup>.

Early studies showed that, following training, chromatin becomes progressively acetylated in specific brain regions involved in learning and memory, and prominently in the hippocampal formation<sup>59</sup>. More recent studies confirm that transcriptional regulation by histone acetylation is critical to long-term memory consolidation. In particular, the transcription factor CREB and its coactivator CREB binding protein (CBP) have been linked to synaptic plasticity<sup>129</sup>. Indeed, the histone acetyltransferase (HAT) activity of CBP is required for long-term memory consolidation<sup>51,52,69</sup>. In addition, intra-hippocampal injections of histone deacetylase inhibitors enhance memory consolidation<sup>50</sup>. However, in spite of these important observations, a comprehensive understanding of the complex mechanisms that regulate neuronal histone acetylation in long-term memory remains elusive.

Recent studies have identified a new paradigm of transcriptional regulation, based on direct sensing of intermediary metabolites by chromatin-modifying enzymes such as acetyltransferases to dynamically adapt chromatin structure and gene expression<sup>15,18</sup>. Histone acetylation can be readily manipulated by altered intracellular pools of acetyl-CoA, the key metabolite used as a cofactor in all protein acetylation<sup>37,38,130</sup>. Accordingly, metabolic enzymes that provide nuclear acetyl-CoA have been postulated to directly control chromatin acetylation and, consequently, gene expression<sup>19,131</sup>.

In mammalian cells there are two enzymes that principally generate nuclear acetyl-CoA to contribute to histone acetylation: acetate-dependent acetyl-CoA synthetase 2 (ACSS2) and

ATP-citrate lyase (ACL), which uses mitochondria-derived citrate to generate acetyl-CoA<sup>79</sup>. The relative importance of these producers of acetyl-CoA for nuclear histone acetylation apparently differs by tissue type, developmental state, and disease<sup>79</sup>. Interestingly, while ACL is important for global histone acetylation in non-neuronal cell lines, contributions by ACSS2 are secondary in these proliferating cells<sup>37</sup>. Indeed, the relative roles of ACL and ACSS2 for chromatin acetylation in post-mitotic neuronal cells remains to be elucidated.

Based on high levels of ACSS2 in mouse hippocampus (Allen Brain Atlas<sup>132</sup>), we investigated a neuronal role for ACSS2 in histone acetylation and gene expression and hypothesized that it may directly associate with chromatin to locally fuel catalytic HAT activity. Our results suggest a strong correlation between acetate metabolism and neuronal chromatin regulation, and provide evidence for direct chromatin association of ACSS2 connected to up-regulation of neuronal gene expression. We further demonstrate that hippocampal ACSS2 expression is essential for the acquisition of long-term memories *in vivo*, a process known to be dependent on neuronal histone acetylation and gene expression. Together, our observations provide novel and fundamental insight into molecular mechanisms that underlie neuronal gene expression and memory consolidation.

## RESULTS

### **ACSS2 is localized to nuclei in differentiated neurons**

Neuronal gene transcription underlies memory storage and is regulated by histone acetylation<sup>44</sup>. To investigate the neuronal function of the acetyl-CoA-producing enzyme ACSS2, we used the Cath.-a-differentiated (CAD) cell line, a valuable *in vitro* model for studies of neuronal biology<sup>133</sup>. Upon serum deprivation in culture, these CNS catecholaminergic cells undergo morphological differentiation to form neuronal processes<sup>134</sup>. Electrophysiological characterization confirms that differentiated CAD neurons are excitable and behave similarly to fully functional neurons, indicating that they capture key aspects of neuronal biology<sup>135,136</sup>.

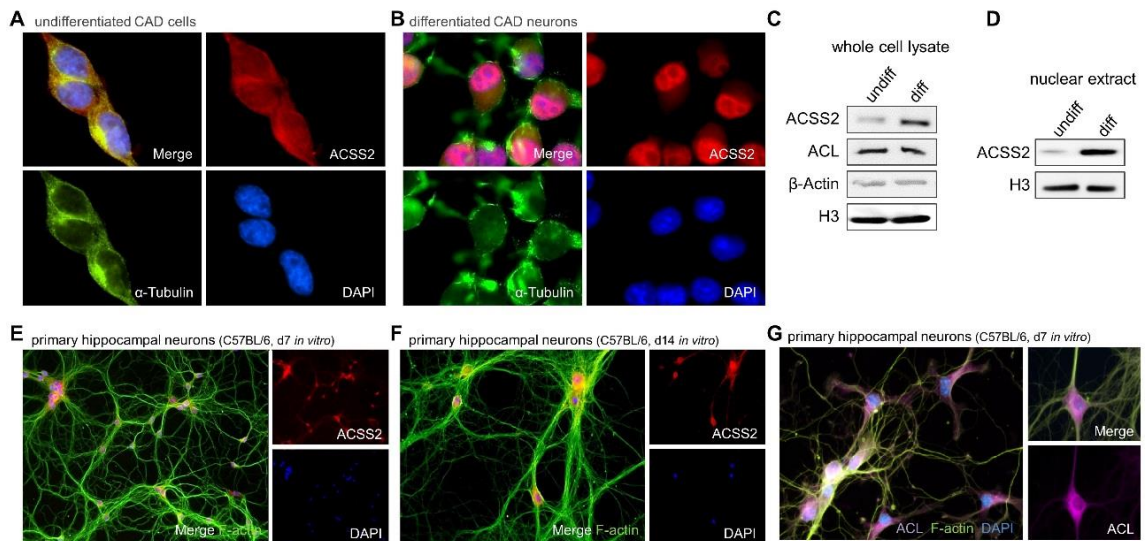


Figure 3.1. ACSS2 localizes to the nucleus upon CAD neuron differentiation.

(A) Subcellular localization of ACSS2 in CAD cells was imaged by immunofluorescence microscopy. Nuclei and cytoplasm are visualized by DAPI (4',6'-diamidino-2-phenylindole) stain and  $\alpha$ -Tubulin immunostaining, respectively. (B) ACSS2 immunostaining shows that ACSS2 localizes to the nucleus of differentiated CAD neurons (5 days post-serum withdrawal). (C) Western blot analysis of whole cell lysates in undifferentiated CAD cells and differentiated CAD neurons for ACSS2, ACL,  $\beta$ -actin, and Histone H3. (D) Western blot analysis of nuclear protein extracts shows that ACSS2 protein expression is increased in nuclei of differentiated CAD neurons. (E, F) Immunofluorescence in primary hippocampal neurons isolated from C57BL/6 embryos at day 7 (E) and day 14 (F) of *in vitro* differentiation culture. ACSS2 locates predominantly to nuclei in differentiated primary neurons. (G) Immunofluorescence shows that ACL is chiefly localized to the cytoplasm of primary hippocampal neurons.

We examined the subcellular localization of ACSS2 in CAD neurons using deconvolution microscopy and imaged endogenous ACSS2 protein expression by immunofluorescence. In undifferentiated CAD cells, ACSS2 expression is observed primarily in the cytoplasm with only a small fraction in the nucleus (Fig. 3.1A). Upon CAD neuronal differentiation a striking change occurs where ACSS2 becomes primarily localized to the nucleus (Fig. 3.1B). To confirm relocalization of ACSS2 upon differentiation, we assessed ACSS2 protein levels by western blot analysis of whole cell lysates and nuclear extracts. Whole cell levels of ACSS2 protein increased upon CAD neuronal differentiation (Fig. 3.1C), associated with higher levels of ACSS2 protein in the nuclear extract (Fig. 3.1D).

We used immunofluorescence to determine whether ACSS2 is also localized to the nucleus in differentiated primary neurons. Indeed, ACSS2 localized to nuclei of both hippocampal and cortical neurons (Fig. 3.1E). Notably, ACSS2 localization persists in nuclei even in longstanding cultures of differentiated primary neurons (Fig. 3.1F). We assessed the specificity of this nuclear ACSS2 localization by examining the localization of the enzyme ACL (adenosine triphosphate (ATP)–citrate lyase), which also supplies acetyl-CoA in mammalian cells, by conversion of mitochondria-derived citrate to acetyl-CoA<sup>37</sup>. In contrast to what we observed for ACSS2, immunofluorescence of ACL showed predominant localization in the cytoplasm of primary neurons, with only a small amount of protein in the nucleus (Fig. 3.1G). Additionally, in contrast to ACSS2, ACL protein expression does not become upregulated during CAD neuronal differentiation (Fig. 3.1C). Based on these results, we conclude that ACSS2, in contrast to ACL, is primarily localized to the nuclei of differentiated neurons.

### **ACSS2 regulates neuronal gene expression**

We assessed global gene expression changes upon neuronal differentiation in CAD cells, via mRNA-seq. RNA-seq tags were aligned to the mm10 reference genome, and mapped to genomic features using cufflinks (n=2; replicates are highly correlated with spearman  $r > 0.8$ ; Fig. 3.3C and 3.3F). Transcriptome analysis identified 894 genes upregulated upon CAD cell differentiation (Fig. 3.2A; red dots depicting genes with >1.6-fold increase). As anticipated, genes upregulated upon differentiation are neuron specific; Gene Ontology (GO) analysis revealed enrichment for genes involved in neuron differentiation, synaptic transmission, ion transport, and neuron projection morphogenesis (Fig. 3.2B; fold enrichment > 3.5, FDR < 0.005).

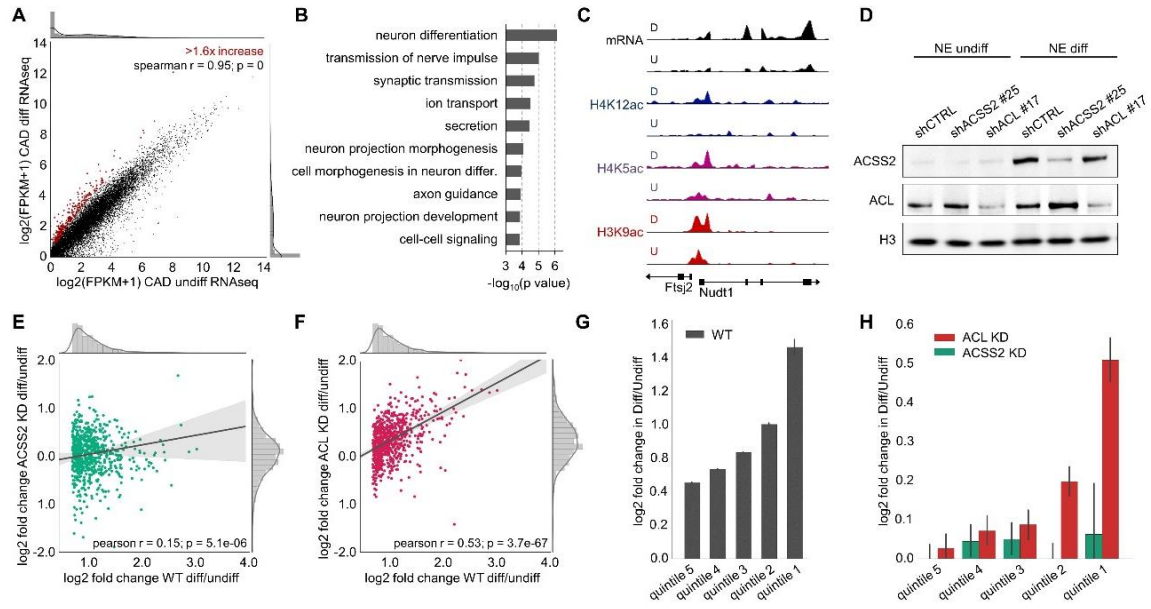


Figure 3.2. ACSS2 supports neuronal gene expression.

(A) RNA-seq identified 894 genes that become upregulated in differentiated CAD neurons (red dots depict genes with >1.6-fold increase). (B) Gene ontology (GO) enrichment analysis. Functional categories of upregulated genes are shown, as assigned by DAVID 6.7 (FE > 3.5, FDR < 0.005). (C) ChIP-seq was performed to reveal regions occupied by H4K12ac, H4K5ac, and H3K9ac in undifferentiated and differentiated CAD neurons. RNA-seq and ChIP-seq UCSC genome-browser track view with annotations of mm10 genomic transcript loci, over *Nudt1* locus (chr5: 140,327,500-140,339,000). (D) CAD cells were infected with lentiviral control or knockdown vector. Western blots of nuclear lysates from stably infected cells were probed with the indicated antibodies. (E) ACSS2 knockdown results in reduced induction of neuronal gene expression program. Scatter plot contrasts the fold-change FPKM of upregulated genes from (A) between WT and ACSS2 knockdown. Marginal distributions show histogram and kernel density estimation. Ordinary least squares linear regression is displayed with 95% confidence interval. (F) Same as (E) but comparing fold-induction in WT to ACL knockdown. (G) Quintiles of upregulated genes (red dots in Fig. 3.2A) with the greatest fold-change increase in WT. (H) Corresponding gene quintiles depict fold-change FPKM in ACL and ACSS2 knockdown.

Typically, transcriptionally active genes are characterized by increased levels of histone acetylation that dynamically upregulate gene expression via altered chromatin structure and recruitment of transcription factors and cofactors. To determine whether histone acetylation is changed at neuronal genes upon CAD differentiation, we performed chromatin immunoprecipitation followed by high-throughput DNA sequencing (ChIP-seq) for several key

histone acetylation sites associated with transcription: acetylation of lysine 9 on histone H3 (H3K9ac), and acetylation of lysines 5 and 12 on histone H4 (H4K5ac and H4K12ac, respectively). ChIP-seq for total histone H3 and sequencing of input DNA served as normalization controls (see Experimental Procedures for additional details). All three histone acetylation modifications greatly increased at the upregulated neuronal genes during CAD cell differentiation, as shown in a genome browser track view in Fig. 3.2C (compare undifferentiated to differentiated tracks for each modification at *Nudt1*, which is upregulated 3.3-fold in the RNAseq dataset). When compared to all other genes, this set of upregulated and neuron-specific genes is distinguished by greatly elevated histone acetylation levels (Fig. 3.3G).

Histone acetylation is catalyzed by histone acetyltransferase (HAT) enzymes that depend on the central metabolite acetyl-CoA as a substrate for their activity. To determine whether ACSS2-mediated or ACL-mediated acetyl-CoA biosynthesis supports gene expression in CAD neuron differentiation, we reduced the level of ACSS2 or ACL gene expression prior to CAD cell differentiation using short hairpin RNAs (shRNA), and validated the knockdown by western blot (Fig. 3.2D). We performed mRNA-seq in the ACSS2 and ACL knockdown cell lines in duplicate to determine the transcriptional response upon CAD neuron differentiation (Fig. 3.3A, 3.3B, 3.3D, 3.3E). Computational analysis showed reduced induction of the neuronal gene expression program described above in the ACSS2 knockdown, as visualized by a low correlation of transcriptional fold change between ACSS2 knockdown compared to WT cells (pearson  $r = 0.15$ ; Fig. 3.2E). This failure of induction was most dramatic when compared to the same analysis for the ACL knockdown, which retained a much stronger correlation in transcriptional fold change compared to WT cells (pearson  $r = 0.53$ ; Fig. 3.2F).

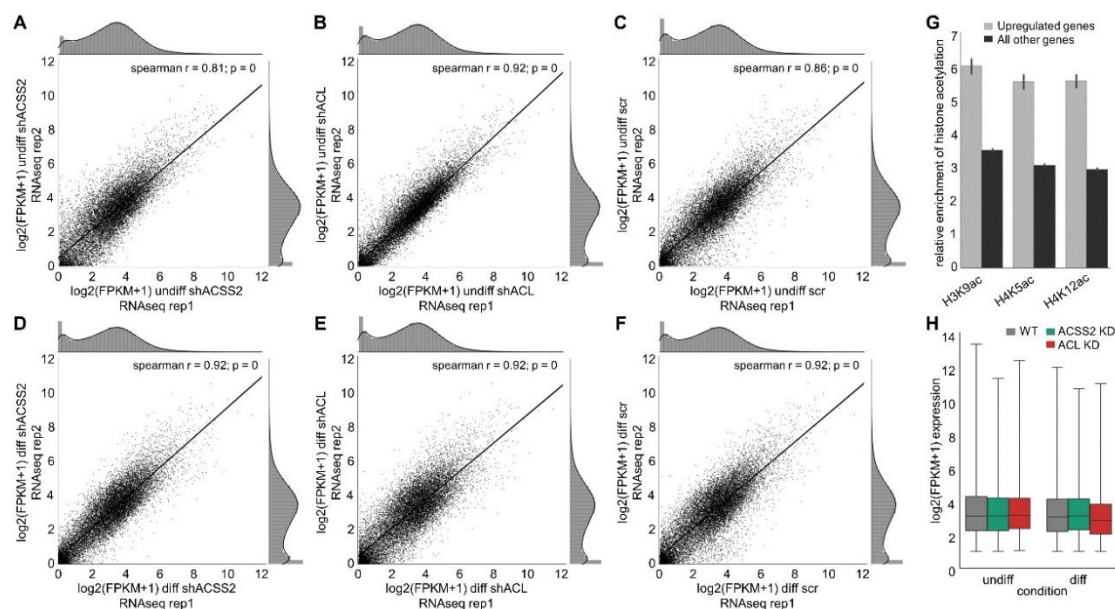


Figure 3.3. ACSS2 knockdown does not lower global gene expression

(A-C) Correlation plots of replicate RNA-seq in undifferentiated CAD cells for ACSS2 knockdown (A), ACL knockdown (B), and scramble control (C). (D-F) Correlation plots of replicate RNA-seq in differentiated CAD neurons for ACSS2 knockdown (D), ACL knockdown (E), and scramble control (F). (G) Bar plot shows the relative genic enrichment of H3K9ac, H4K5ac, and H4K12ac at genes that are upregulated in the CAD neuron differentiation (>1.6-fold, grey bars) versus all other genes (black bars). (H) Boxplot of global mRNA transcript levels in undifferentiated (undiff) and differentiated (diff) CAD neurons from RNA-seq in WT (scramble control knockdown; grey), ACSS2 KD (shACSS2 #25 knockdown; green), and ACL KD (shACL #17 knockdown; red). Genome-wide transcript levels are reduced in diff ACL KD when compared to diff WT ( $p = 1.91e-07$ , Mann-Whitney U test).

To more easily visualize the prominent defect in gene expression caused by ACSS2 knockdown, we analyzed transcriptional induction of the genes upregulated in WT CAD neuron differentiation when stratified into quintiles (Fig. 3.2G-H). In WT neurons, each quintile represents increased expression fold change (log<sub>2</sub> transformed) in the previously described set of upregulated genes (Fig. 3.2G show the upregulated genes, red dots in Fig. 3.2A). We then measured the expression fold change of the same genes in either ACSS2 or ACL knockdown (Fig. 3.2H). ACSS2 knockdown shows highly significant reduction in gene expression induction in

all quintiles, and this was particularly clear in the top most upregulated quintiles ( $p = 7.2 \times 10^{-252}$ , Wilcoxon rank-sum test; Fig. 3.2H, green bars compared to wild type quintiles in 2G).

Interestingly, when comparing transcript levels genome-wide, global gene expression was not lowered in the ACSS2 knockdown in differentiated neurons (Fig. 3.3H). By contrast, in the ACL knockdown, each quintile shows the same upward trend for expression fold change compared to WT. However, we note that the overall fold change is lower in ACL than in WT, nonetheless, it contrasts with the severe defect observed in the neurons harboring ACSS2 knockdown ( $p = 1.1 \times 10^{-25}$ , Wilcoxon rank-sum test; Fig. 3.2H, red bars). In fact, transcript levels were reduced globally when compared to WT ( $p = 1.91 \times 10^{-7}$ , Mann-Whitney U test; Fig. 3.3H), contrasting the more specific and globally far less significant effect in the ACSS2 knockdown ( $p = 0.04$ , Mann-Whitney U test; Fig. 3.3H). Based on these observations, we conclude that ACSS2 is required for the normal induction of the neuronal gene expression program upon CAD neuron differentiation. In contrast, although the overall transcriptional response is not as robust as in WT, ACL knockdown does not abrogate gene induction of neuron-specific genes.

### **ACSS2 is recruited to transcriptionally active chromatin**

The observations from our knockdown experiments indicate that ACSS2 is required for normal gene induction upon CAD neuron differentiation, and that induced genes acquire transcription-associated histone acetylation. We investigated whether ACSS2 might directly associate with neuron-specific genes to increase histone acetylation. We reasoned that direct recruitment of ACSS2 to genes would both increase availability of acetyl-CoA for catalytic HAT enzymes, and would also concurrently lower CoA levels (which restricts HAT enzyme activity via product inhibition), leading to an overall increase in the gene-proximal ratio of acetyl-CoA to CoA. To test this model of chromatin-localized ACSS2 function, we performed ACSS2 ChIP-seq experiments to assess its chromatin binding, using two different antibodies in biological replicates of CAD neuron differentiation.

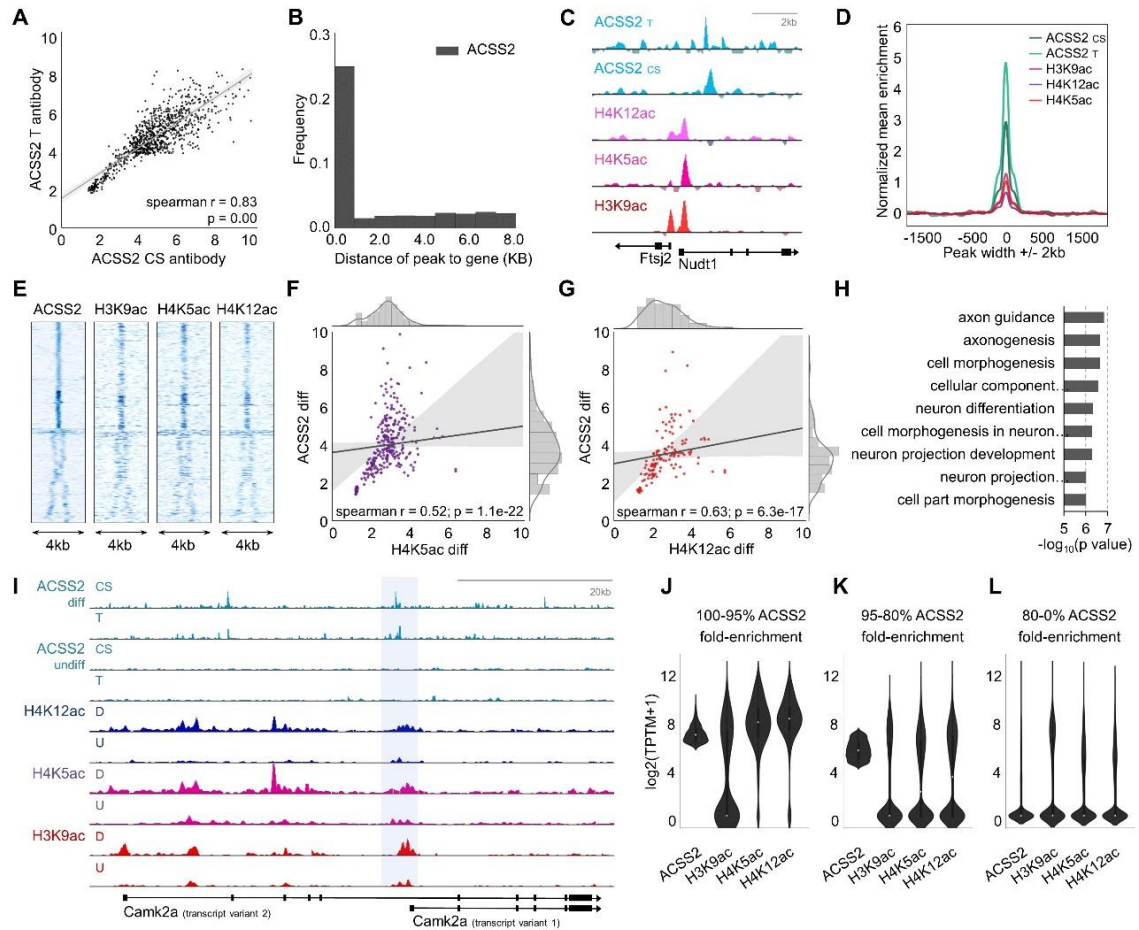


**Figure 3.4. ACSS2 is recruited to transcriptionally active chromatin.**

(A) ChIP-seq in differentiated CAD neurons was performed in replicate with two different antibodies to ACSS2. Correlation plot displays relative enrichment over corresponding MACS peaks (default parameters with Input used as control). (B) Distance distribution plot showing frequency of ACSS2 peak to closest gene distance (1400 peaks total). (C) UCSC Genome Browser views of delta ChIP-seq tracks show that, upon CAD neuron differentiation, increases in H4K5, H4K12, and H3K9 acetylation over the NUDT1 gene locus co-occur with ACSS2 enrichment (chr5: 140,327,500-140,339,000). (D) Meta-peak plot displays mean read enrichment over the center of ACSS2 peaks (intersected set of MACS peaks from ACSS2 CS and T ChIP-seq). (E) Heat-maps depict enrichment of reads mapped over the ACSS2 peak center (+/- 2kb). (F, G) Intersection of ACSS2 and acetyl broad peaks using MACS. (H) GO term enrichment analysis of top 5% genes that become ACSS2-bound in CAD neuron differentiation. (I) UCSC Genome Browser views of ChIP-seq tracks demonstrate that increases in H4K5, H4K12, and H3K9 acetylation co-occur with proximate ACSS2 enrichment over the Camk2a locus upon CAD neuron differentiation (U – undiff, D – diff; chr18: 60,920,000-60,990,000). (J-L) Violin-contour plots display ChIP occupancy for the indicated percentiles of genes that were ranked according to dynamic ACSS2 binding upon CAD neuronal differentiation.

We measured ACSS2 peak enrichment using MACS (see Experimental Procedures for additional details). Importantly, genome-wide comparison of the separate ACSS2 ChIP-seq datasets confirmed high correlation both for MACS overlapping peaks (spearman  $r = 0.82$ ; Fig. 3.4A), and for global enrichment over 1kb genomic windows (spearman  $r = 0.73$ ; Fig. 3.5A). We examined whether histone acetylation is increased at sites of chromatin-bound ACSS2, by comparing to the genome-wide histone H3 and H4 acetylation data from the CAD neuron ChIP-seq described above. An example of ACSS2 peak enrichment is shown in the genome browser track view of the TAB2 (TGF-Beta Activated Kinase 1/MAP3K7 Binding) gene locus, with striking enrichment in differentiated CAD neurons relative to undifferentiated neurons (Fig. 3.5B). Binding of ACSS2 upstream of the activated TAB2 gene is concurrent with prominent increases in histone H3K9, H4K5, and H4K12 acetylation at the Tab2 promoter (Fig. 3.5B). Likewise, at the NUDT1 gene locus, increases in H4K5, H4K12, and H3K9 acetylation that we described earlier (Fig. 3.2C) co-occur with ACSS2 binding upon neuronal differentiation (Fig. 3.3C).

To assess whether chromatin-bound ACSS2 is generally located at or nearby genes in differentiated CAD neurons, as observed in the case of Nudt1 and Tab2, we inspected the distribution of ACSS2 peak-to-gene distance genome-wide. Indeed, the largest cohort of ACSS2 peaks are within 1kb of genes in differentiated neurons (Fig. 3.3B). We identified genes that are closest to ACSS2 peaks (within 10 kb of ACSS2 peak; see Experimental Procedures), and determined by GO enrichment analysis whether ACSS2 binding is related to the neuronal gene expression program in CAD cell differentiation. Strikingly, the genes proximal to ACSS2 binding sites are involved in neuronal differentiation and function, and are enriched for representative categories such as axonogenesis, neuron projection morphogenesis, and synapse function (Fig. 3.5C). These data suggest that chromatin-associated, promoter-proximal ACSS2 may support histone acetylation in differentiated neurons as a local source of acetyl-CoA, by supplying cofactor directly for catalysis by HAT enzymes.

Based on these observations, we tested whether ACSS2 binding is correlated with locally increased histone acetylation. Quantitative enrichment analysis revealed that histone acetylation was markedly increased over all ACSS2 peaks, as evident in a meta-peak plot (Fig. 3.3D). Importantly, visualization of histone acetylation enrichment over ACSS2 peaks in heat-maps confirmed that this positive correlation is not produced by a subset of chromatin-bound ACSS2, but an overall clear trend (Fig. 3.3E). Most importantly, this correspondence is not evident when histone acetylation peaks are surveyed in their entirety genome-wide, suggesting that ACSS2 is not simply enriched wherever histone acetylation is present (Fig. 3.5D-G). These data indicate a positive relationship between ACSS2 binding and increased histone acetylation enrichment patterns.

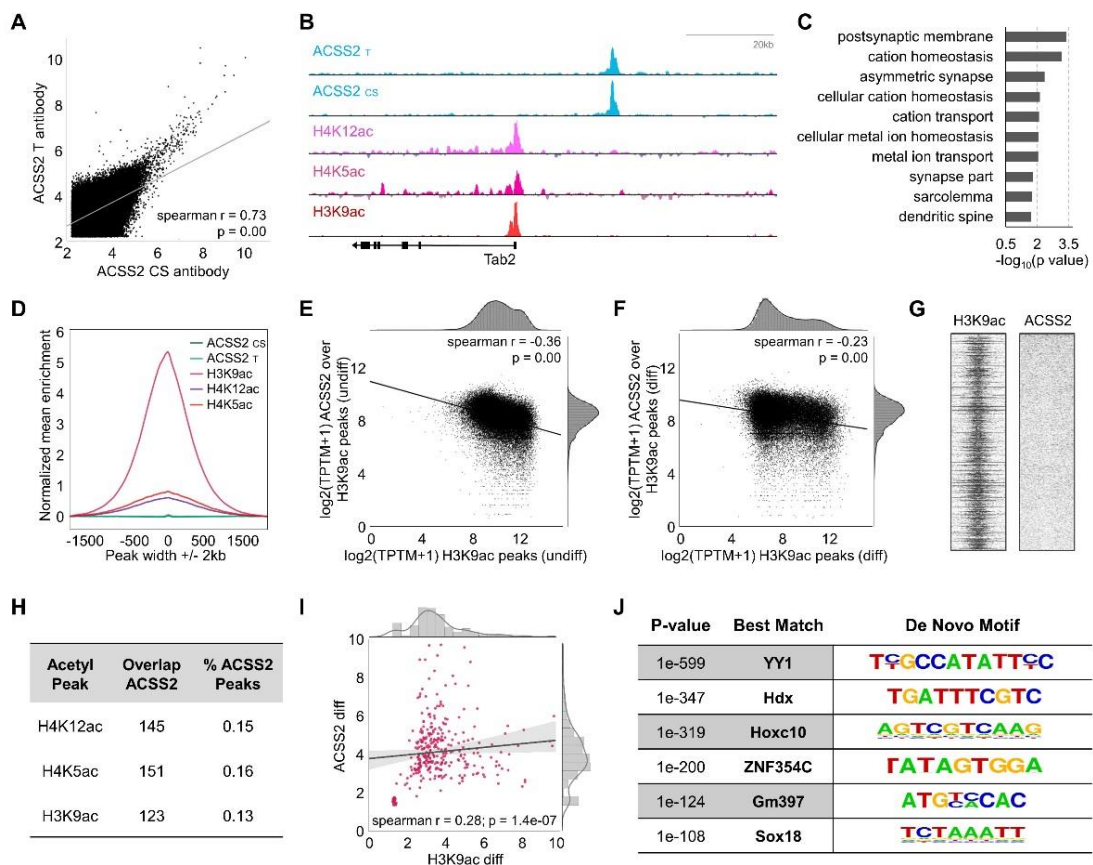


Figure 3.5. Relationship between ACSS2 enrichment and increased histone acetylation.

(A) ChIP-seq in differentiated CAD neurons was performed in replicate with two different antibodies to ACSS2. Correlation plot displays relative enrichment genome-wide. (B) Overlaid UCSC Genome Browser views of indicated ChIP-seq tracks in undifferentiated CAD cells (dark shade) and differentiated CAD neurons (light shade) over Tab2 locus (chr10: 7,875,000-8,004,000). (C) GO enrichment analysis of the genes most proximate to ACSS2 peaks demonstrates that neuron-specific genes are enriched. (D) Meta-peak plot displays mean read enrichment over the center of H3K9ac peaks. (E, F) Correlation plots show ACSS2 ChIP occupancy over H3K9ac broad MACS peaks in undifferentiated CAD cells (E), and in differentiated CAD neurons (F). (G) Heat-maps depict enrichment of reads mapped over the H3K9ac peak center (+/- 2kb). (H) Table shows % direct overlap of ACSS2 peaks with H3K9ac, H4K5ac, and H4K12ac broad MACS peaks. (I) Intersection of ACSS2 and H3K9ac broad peaks using MACS. (J) Discovered de novo motifs for transcription factor binding sites predicted by HOMER from all ACSS2 ChIP-seq peaks called by MACS in differentiated CAD neurons.

Next, we examined more closely the amount of overlap between ACSS2 and histone acetylation peaks. Remarkably, while the majority of ACSS2 peaks are proximal to histone acetylation peaks, a substantial number – nearly 15% of all ACSS2 peaks genome-wide – directly overlap with peaks of H3 and H4 acetylation (Fig. 3.5H). Moreover, we found that ACSS2 peak height is positively correlated with that of intersected histone acetylation peaks, suggesting that ACSS2 becomes bound to chromatin in proximity to HAT enzymes that enact transcriptionally activating histone acetylation (Fig. 3.3F, G; Fig. 3.5I). We next explored whether ACSS2 ChIP-seq peaks are enriched for particular transcription factor binding motifs, using the motif discovery tool in HOMER (Fig. 3.5J). We found highly enriched sequences that are specifically bound by transcription factors typically expressed in neuronal tissue. The motif for transcription factor Yin Yang1 (YY1) binding was the most significantly enriched motif in this list (Suppl. Fig 3I; YY1,  $p = 1e-599$ ). Intriguingly, YY1 has been found to exist in a large complex *in vivo*, and is known to function in transcriptional activation through recruitment of the two HAT enzymes CBP (CREB-binding protein) and p300<sup>137–139</sup>. Both of these co-activators depend on acetyl-CoA for their catalytic activity. Accordingly, chromatin-localized production of acetyl-CoA by ACSS2 may fuel nearby catalytic HAT activities and support increased histone acetylation.

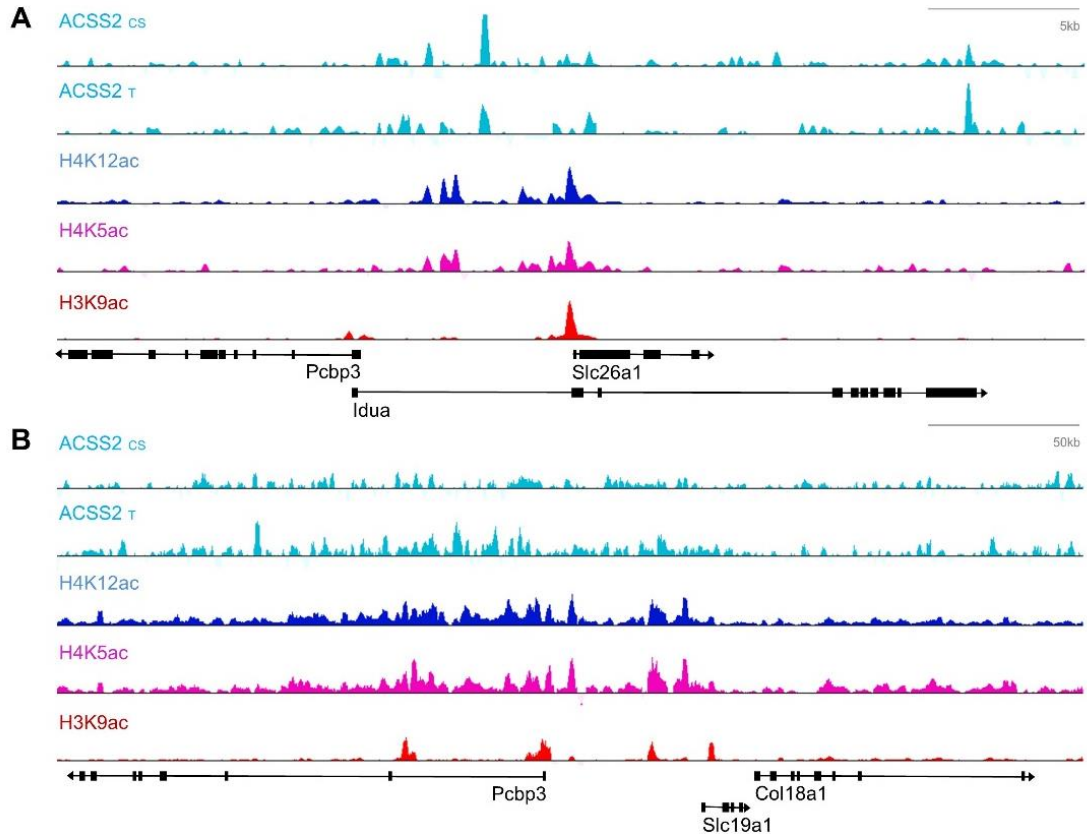


Figure 3.6. UCSC Genome Browser views of ACSS2 ChIP-seq data

(A) UCSC Genome Browser views of delta ChIP-seq tracks demonstrate that increases in H4K5, H4K12, and H3K9 acetylation co-occur with ACSS2 enrichment over the *Idua* (Alpha-L-iduronidase) gene locus upon CAD neuron differentiation. (B) At the *Slc19A1* (Solute Carrier Family 19 (Folate Transporter), Member 1) gene, elevated histone H4K5, H4K12, and H3K9 acetylation levels correspond with increasing ACSS2 enrichment in CAD neuron differentiation.

Importantly, by visual inspection of the histone acetylation and ACSS2 ChIP-seq data, we further noted the presence of both histone acetylation and ACSS2 peaks with varying shape and density of reads that are not identified in our MACS peak analysis, likely based on these variations (Fig. 3.6A, 3.6B; example genome browser track views display occupancy in delta tracks, i.e. diff subtracted undiff). One example of such enrichment occurs at the gene encoding for calcium/calmodulin-dependent protein kinase type II alpha chain (*CAMKIIA*), an enzyme that is required for hippocampal long-term potentiation (LTP) and spatial learning. At the *CAMK2A* gene locus, ACSS2 becomes bound in CAD neuron differentiation and appears to co-occur with

increases in histone H3K9, H4K5, and H4K12 acetylation, as visualized in the genome browser track view displaying ChIP occupancy in both the undifferentiated and differentiated state (Fig. 3.3I). We note that this trend is similar to that observed with MACS peaks in our previous analyses. Thus, to account for both peak and non-peak genic enrichment of histone acetylation and ACSS2, we further examined histone acetylation and ACSS2 enrichment by meta-gene analysis. First, we determined whether genes with the greatest ACSS2 enrichment are characterized by above average histone acetylation levels, to further support our peak analysis observations. Indeed, gene enrichment analysis revealed that the top 5% ACSS2-enriched genes maintain histone acetylation that is up to three-fold higher than the mean across all genes (Fig. 3.7A-D). Importantly, we then investigated whether ACSS2 enrichment patterns predict dynamic changes in histone acetylation. We examined whether ACSS2 binding during CAD neuronal differentiation correlated with more substantially increased histone acetylation. Strikingly, genes with the greatest fold-change in ACSS2 binding are distinguished by the highest histone acetylation levels in differentiated neurons, particularly histone H4 acetylation (Fig. 3.3J-L, Fig. 3.7E-H). Importantly, these top ACSS2-bound genes that experience the largest acetylation gains are neuron specific, as evident by GO term enrichment analysis (Fig. 3.3H).

In addition, to further show that ACSS2 enrichment is linked to gene expression, we implemented a multiple linear regression analysis and visualized the interaction between gene expression changes in the differentiation and binding of ACSS2 to chromatin (Fig. 3.7I). The contour plot of this model is displayed with the scatter plot of the independent gene expression variables, predicting higher levels of ACSS2 enrichment in red and lower levels in blue. Indeed, this fitted regression model confirms a remarkable relationship between higher ACSS2 enrichment and increased gene expression, and displays upregulated genes in correspondence with elevated ACSS2 enrichment in red (Fig. 3.7I). Thus, taken together with the ACSS2 and histone acetylation peak analyses, and the RNA-seq results, these genomic data demonstrate that dynamic ACSS2 enrichment in differentiated neurons is involved in transcriptional regulation, and that ACSS2 binding is linked to increases in histone acetylation at upregulated genes.

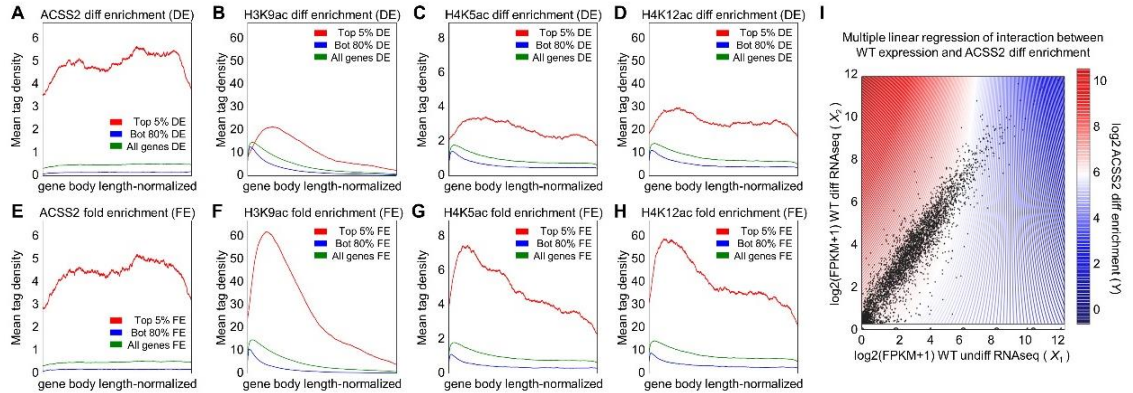


Figure 3.7. Genic enrichment of ACSS2 corresponds to increased gene expression.

(A-D) Meta-gene enrichment analysis shows ChIP occupancy for ACSS2 (A), H3K9ac (B), H4K5ac (C), and for H4K12ac (D) across the top 5% of genes enriched for ACSS2 in differentiated CAD neurons (Top 5% DE; red). The bottom 80% of genes (Bot 80% DE) is shown in blue, and the average signal across all genes (All genes DE) is shown in green. (E-H) Meta-gene enrichment analysis shows ChIP occupancy for ACSS2 (E), H3K9ac (F), H4K5ac (G), and for H4K12ac (H) at the top 5% of genes that become dynamically bound by ACSS2 upon neuronal differentiation (Top 5% DE; red). The bottom 80% of genes (Bot 80% DE) is shown in blue, and the average signal across all genes (All genes DE) is shown in green. (I) Multiple linear regression analysis was implemented to model the interaction between genic ACSS2 enrichment and WT gene expression changes. The contour plot of this fitted regression model displays high levels of ACSS2 enrichment in red and low levels in blue, and is overlaid with the scatter plot of the independent gene expression variables. The visualized model demonstrates that high ACSS2 enrichment corresponds to increased gene expression in the CAD neuronal differentiation.

### ACSS2 functions in neuronal histone acetylation

The results presented above suggest that nuclear ACSS2 expression supports neuronal histone acetylation, and indicate a requirement for ACSS2 in regulating histone acetylation and neuron-specific gene expression in differentiated neurons. To test whether acetyl-CoA biosynthesis by ACSS2 is important for neuronal chromatin acetylation, we attenuated ACSS2 expression in CAD neurons and examined global histone acetylation levels by western blot. ACSS2 knockdown indeed resulted in general reduction of most tested histone acetylation modifications including dramatically reduced histone acetylation at H4K12 (Fig. 3.8A). In contrast, ACL knockdown did not affect global levels of histone H4K12 acetylation (Fig. 3.8A), providing

further evidence that ACSS2 may be the dominant acetyl CoA supplier for histone acetylation associated with neuronal gene induction. We note that these ACL results are in contrast to previously reported data from proliferating non-neuronal cell lines, which have been shown to primarily depend on ACL to supply acetyl-CoA that participates in histone acetylation <sup>37</sup>. Therefore, it appears that contribution of the catalytic functions of ACL versus ACSS2 to the supply of nuclear acetyl-CoA required for histone acetylation on chromatin is contingent on both cell type and state of cellular differentiation. Further, ACSS2 knockdown not only substantially impairs global H4 acetylation, but also affects histone H3 acetylation, which is linked to transcriptional activation and typically mediated by HAT enzymes implicated in hippocampal LTP and memory formation – specifically Gcn5, CBP, and p300 (Fig. 3.8B). These changes show certain specificity, as global levels of H4K16 or H3K122ac acetylation were not affected by ACSS2 knockdown (Fig. 3.8B). Additionally, we performed ACSS2 co-IP experiments and found, in support of our ChIP-seq analyses that ACSS2 pulls down histone proteins and ACSS2 is preferentially bound to acetylated chromatin (Fig. 3.8C, SN = supernatant).

We explored a potential mechanism by which ACSS2 becomes chromatin-bound and recruited to transcriptionally active regions leading to increased histone acetylation. As shown above, ACSS2 knockdown resulted in the pronounced decrease of H3K9 and H3K27 acetylation (Fig. 3.8B). We reasoned that ACSS2 might physically associate with transcriptional co-activators, such as CBP, which has broad spectrum histone acetyltransferase activity, catalyzing acetylation of H3K9 and H3K27, as well as other histone lysine residues <sup>140,141</sup>. Furthermore, as described above, CBP is prominently involved in transcriptional activities that underlie the formation of long-term memories<sup>52,69,142,143</sup>. To test whether endogenous ACSS2 interacts with CBP, we performed co-IP experiments using an antibody against ACSS2. By western blot, we found that ACSS2 pulls down the co-activator CBP (Fig. 3.8D). Hence, ACSS2 physically binds to acetylated histones and to CBP, and these associations are consistent with a direct role of ACSS2 in regulating chromatin to induce neuronal gene expression.

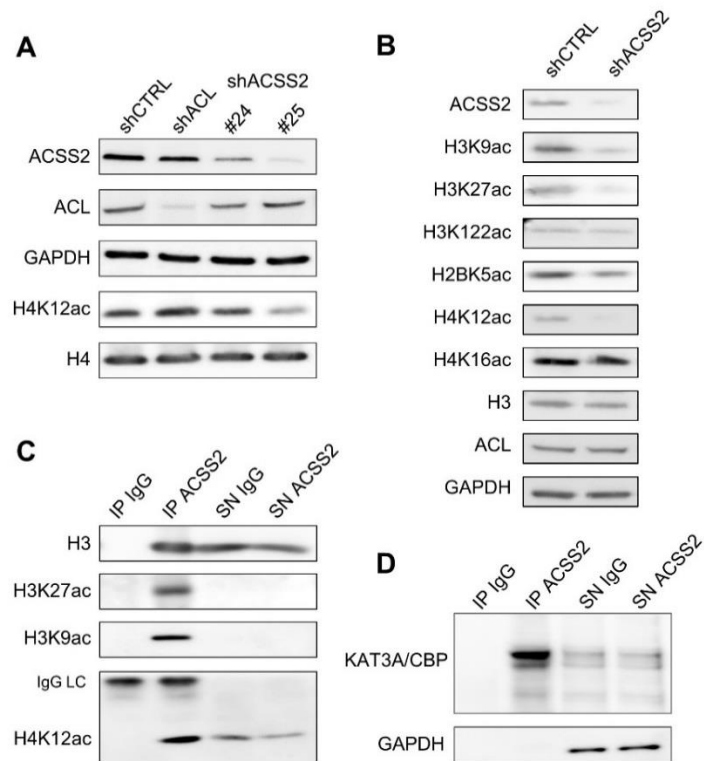


Figure 3.8. ACSS2 functions in neuronal histone acetylation.

(A) Western blot analysis of whole cell lysates after lentiviral shRNA-mediated knockdown demonstrates that ACSS2 - but not ACL - reduction lowers H4K12 acetylation. (B) ACSS2 knockdown results in decreased levels of H3K9 and H3K27 acetylation. Western blot analysis shows that ACSS2 knockdown results in decreased levels of H3K9 and H3K27 acetylation (whole cell lysates obtained from shCTRL and shACSS2 #25 knockdown cells). (C) Western blot analysis on eluates and supernatants of IgG control and ACSS2 co-IP experiments indicates that ACSS2 preferentially pulls down acetylated histone proteins. (D) Western blot analysis of IP eluates shows that CBP is coimmunoprecipitated in the ACSS2 IP, but not in the control IgG IP.

### ACSS2 regulates long-term memory storage

Based on our observations in CAD cells, we hypothesized that ACSS2 may play a role in memory *in vivo* through support for histone acetylation and transcriptional regulation, which are required during memory consolidation. ACSS2 is highly expressed in the hippocampal formation (HPF), including the dorsal CA1 region of the hippocampus proper (Suppl. Fig.6A, right: ACSS2 RNA *in situ* hybridization on CA1 sagittal section, left: reference atlas; adapted from Allen Brain

Atlas<sup>132</sup>), a brain region that is critical for contextual and spatial memory formation<sup>144–146</sup>.

Therefore, we tested the requirement for ACSS2 in long-term spatial memory formation, a hippocampus-dependent process that involves increased histone acetylation and neuronal gene transcription<sup>62,64,143,147</sup>. We attenuated hippocampal ACSS2 expression in adult mice by shRNA-mediated knockdown. We delivered a viral vector, AAV9-ACSS2 knockdown, into the dorsal CA1 area of the hippocampus, via intracranial injections using stereotactic surgery (Fig. 3.10A; AP, -2.0mm; DV, -1.4mm; ML, +/-1.5mm; C57BL/6J, N = 10 per group). Behavioral studies began three weeks post-surgery, at which point Western blot analysis showed reduced ACSS2 expression in the dorsal hippocampus, but not in the ventral hippocampus (Fig. 3.10B). Importantly, neither control vector injection nor ACSS2 shRNA knockdown injection led to no apparent deficits in locomotion or coordination (visual inspection), or in body weight by quantification (Fig. 9B;  $p = ns$ , N = 10 per group). Similarly, the mice did not display increased anxiety, as measured in the open field test<sup>148</sup> (Fig. 3.10C,  $\Delta$  mean =  $-13.7 \pm 17.2$ ,  $p = ns$ ; Fig. 9C). These results indicate that ACSS2 knockdown does not cause major, broad alterations in behavior.

To determine the role of hippocampal ACSS2 in transcription-dependent memory, we assessed long-term spatial memory in control or knockdown mice using an established object-location memory task<sup>149,150</sup>. In this assay, animals explore an arena with three different objects during training. To test long-term memory formation, the animals are re-exposed to the same arena 24h later with one object moved to a novel location (see schematic Fig. 3.10A, right). To diminish preference biases, we performed the spatial memory test on control AAV and ACSS2 knockdown mice on the same day in the same arena, using every combination of location of objects (N = 10 per group). In the retrieval test, control AAV-eGFP-injected animals displayed a significant preference for the object moved to a novel location, indicating normal long-term spatial memory (Fig. 3.10D).

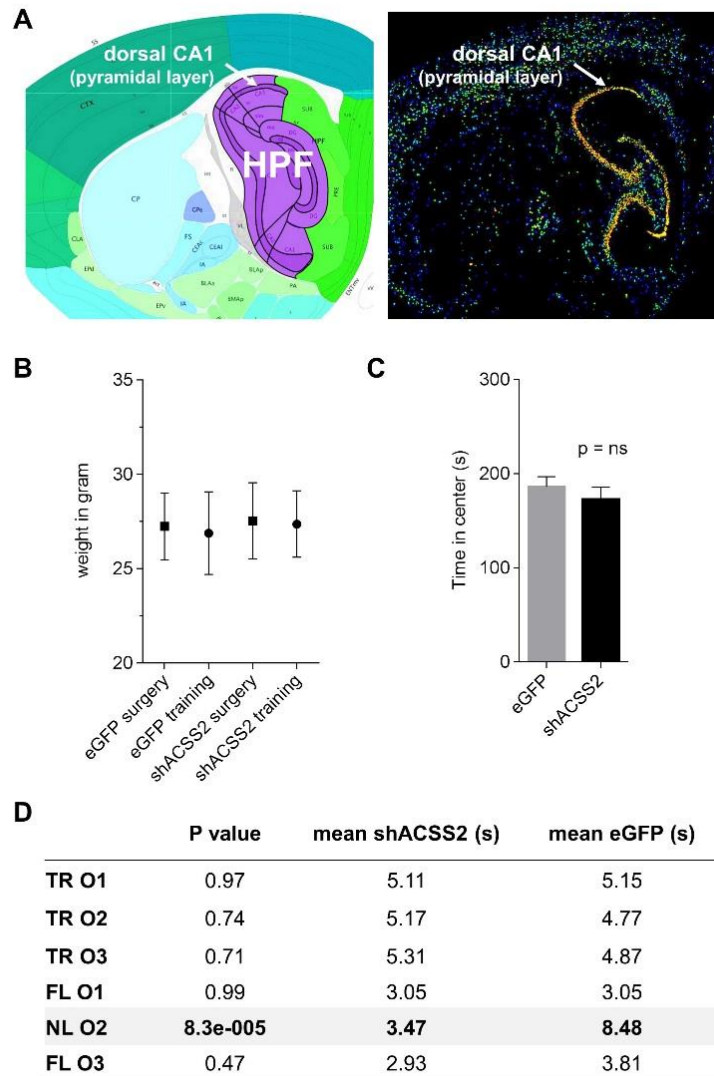


Figure 3.9. ACSS2 is highly expressed in the dorsal CA1 region of the hippocampus

(A) ACSS2 RNA *in situ* hybridization on CA1 sagittal section ACSS2 (right; left: reference atlas). From: Allen Mouse Brain Atlas<sup>132</sup>. (B) Plot shows weight of eGFP-AAV9 control and shACSS2-AAV9 knockdown mice before intracranial surgery, and following recovery before OLM task training ( $p = ns$ ,  $N = 10$  per group). (C) Bar-plot displays the averaged recorded time the eGFP-AAV9 control and shACSS2-AAV9 knockdown animals explored the center of the arena in the open field test over five minutes. (D) Table of the exploration times by eGFP-AAV9 control and shACSS2-AAV9 knockdown mice recorded for the three objects (O1-3) during the first OLM training session (TR – Training) and the 24h retention test (NL – object in novel location, FM – objects remained in former location).

Strikingly, hippocampal knockdown of ACSS2 led to an impairment in hippocampus-dependent spatial object memory (Fig. 3.10D, Fig. 9D; mean  $\Delta = -5.01 \pm 1.21$ ;  $p = 8.3e-05$ ). Importantly, ACSS2 knockdown animals showed a reduction in total object exploration during the test session suggesting that ACSS2 mice recognized all objects from the training sessions and express this recognition memory as reduced exploration (mean  $\Delta = -6.13 \pm 2.15$ ;  $p = 0.02$ ). This spatial memory defect in ACSS2 knockdown animals manifested in significantly lowered discrimination index ( $\% DI = (t \text{ novel} - t \text{ familiar}) / (t \text{ novel} + t \text{ familiar})$ ) when compared to control AAV-eGFP-injected mice (Fig. 3.10E;  $\% \Delta DI = -29.5 \pm 11.4$ ;  $p = 0.02$ ). These results indicate that ACSS2 is required in the dorsal hippocampus for long-term object-location memory.

Next, we sought to test a type of memory acquisition in the same animals that is predicted to not be affected by knockdown of ACSS2 in the dorsal CA1. Relevantly, in contrast to long-term spatial memory, standard contextual fear conditioning is not dependent on the dorsal hippocampus<sup>151</sup>, but instead highly engages the ventral hippocampus<sup>152-154</sup>. Importantly, as we targeted only the dorsal CA1 in our AAV-vector injections, the ventral hippocampus expressed normal levels of ACSS2 protein, as shown by western (Fig. 3.10B, VH or ventral hippocampus). The fear conditioning paradigm is a task in which an aversive stimulus (1.5 mA electrical shock) is associated with a neutral context. Re-exposure to the context prompts retrieval of the memory for the context-shock association, and is scored as motion freezing. We tested the control-injected and ACSS2 knockdown animals in this assay (N = 10 per group); the ACSS2 knockdown mice showed no defect compared to the control vector in contextual fear memory, with average freezing of 50% after context re-exposure (Fig. 3.10F). Hence, specific knockdown of ACSS2 in the dorsal hippocampus does not lead to ventral-specific alteration of a fear conditioned memory response. The results from the two assays show that ACSS2 may play a critical role in the formation and maintenance of long-term spatial memory - a process that involves rapid elevation of histone acetylation leading to transcription of immediate-early genes<sup>69,143,147,155</sup>.

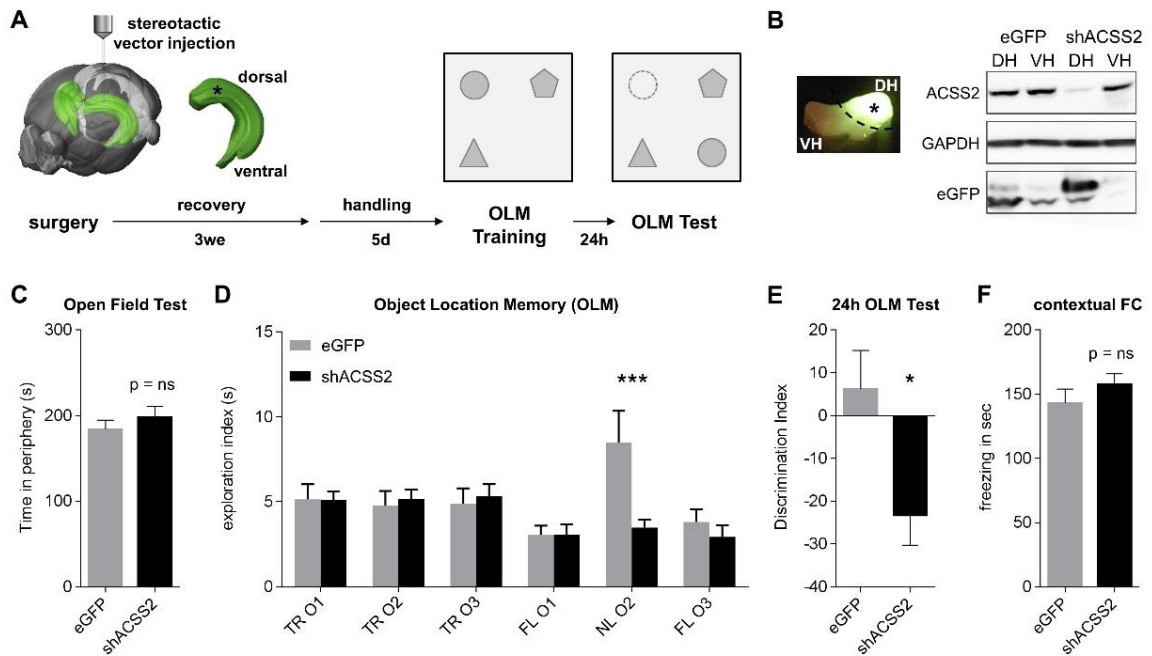


Figure 3.10. ACSS2 knockdown in dorsal hippocampus impairs object location memory.

(A) Stereotactic surgery was performed to deliver AAV9 knockdown vector into the dorsal hippocampus (AP, -2.0mm; DV, -1.4mm; ML, +/-1.5mm); four weeks later habituated mice received training for object location memory (four training sessions of 5 min each in arena with three different objects). 24 hours later the mice were given a retention test in which one object was moved to a novel location (n = 10 per cohort). (B) Western blot analysis of hippocampal tissue harvested from animals injected dorsally with either control or ACSS2 knockdown AAV9 (DH – dorsal hippocampus, VH – ventral hippocampus). (C) ACSS2 knockdown animals showed no defect in the open field test, in which the time the animal explore the periphery of the arena is recorded over five minutes. (D) Both eGFP-control and shACSS2-AAV9 mice displayed no preference for any of the three objects (O1-3) during the first OLM training session (TR – Training). During the 24h retention test, mice that received the shACSS2 knockdown vector displayed no preference for the object move to a novel location (NL) over the objects that remained in their former location (FM), in contrast to mice injected with the control eGFP-AAV9 (mean  $\Delta = -5.01 \pm 1.21$ ; t-ratio = 4.14, p = 8.3e-05). (E) Lowered discrimination index (% DI = (t NL – t FL) / (t NL + t FL)) indicates spatial memory defect in ACSS2 knockdown animals ( $\Delta$ DI =  $-29.5 \pm 11.4$ ; p = 0.02). (F) Compared to the control eGFP-AAV9 mice, ACSS2 knockdown mice show no defect in contextual fear memory. Fear memory was measured as the freezing response after re-exposure to the context 1 day after contextual fear conditioning (1.5 mA electrical shock).

## **ACSS2 regulates dynamic upregulation of early response genes *in vivo***

Following memory acquisition, dynamic changes in gene expression occur within a sensitive time window to enable the consolidation of long-term memory<sup>156</sup>. Similarly, following retrieval of the memory trace, gene transcription is necessary for memory reconsolidation – a process that is prevented by inhibiting mRNA synthesis during the sensitive post-retrieval period<sup>157,158</sup>. We hypothesized that ACSS2 is needed for dynamic upregulation of genes that mediate hippocampal memory formation and reconsolidation. Genome-wide approaches that examine memory-related changes in gene expression have long been frustrated by confounding factors unique to neural tissue, such as extraordinary cell type heterogeneity and functionally important transcript changes that are far smaller than those observed in peripheral tissues<sup>159</sup>. However, newer studies identified a core gene set that is regulated by contextual conditioning in the mouse hippocampus during consolidation and post-retrieval<sup>156,160</sup>.

To test whether the induction of these genes is reliant on ACSS2, we performed mRNA-seq on the dorsal hippocampus, i.e. the region targeted in our AAV injections. Hippocampal tissue was collected from both shACSS2 knockdown and eGFP control animals during the established sensitive period of one hour after contextual memory retrieval (RT)). Injected animals that were handled but not trained were dissected at the same time of day in order to control for circadian gene expression (CC). We focused our transcript analyses on the set of identified early response genes that have been validated in several studies, and that are regulated during the sensitive period following memory retrieval<sup>156,160–162</sup>.

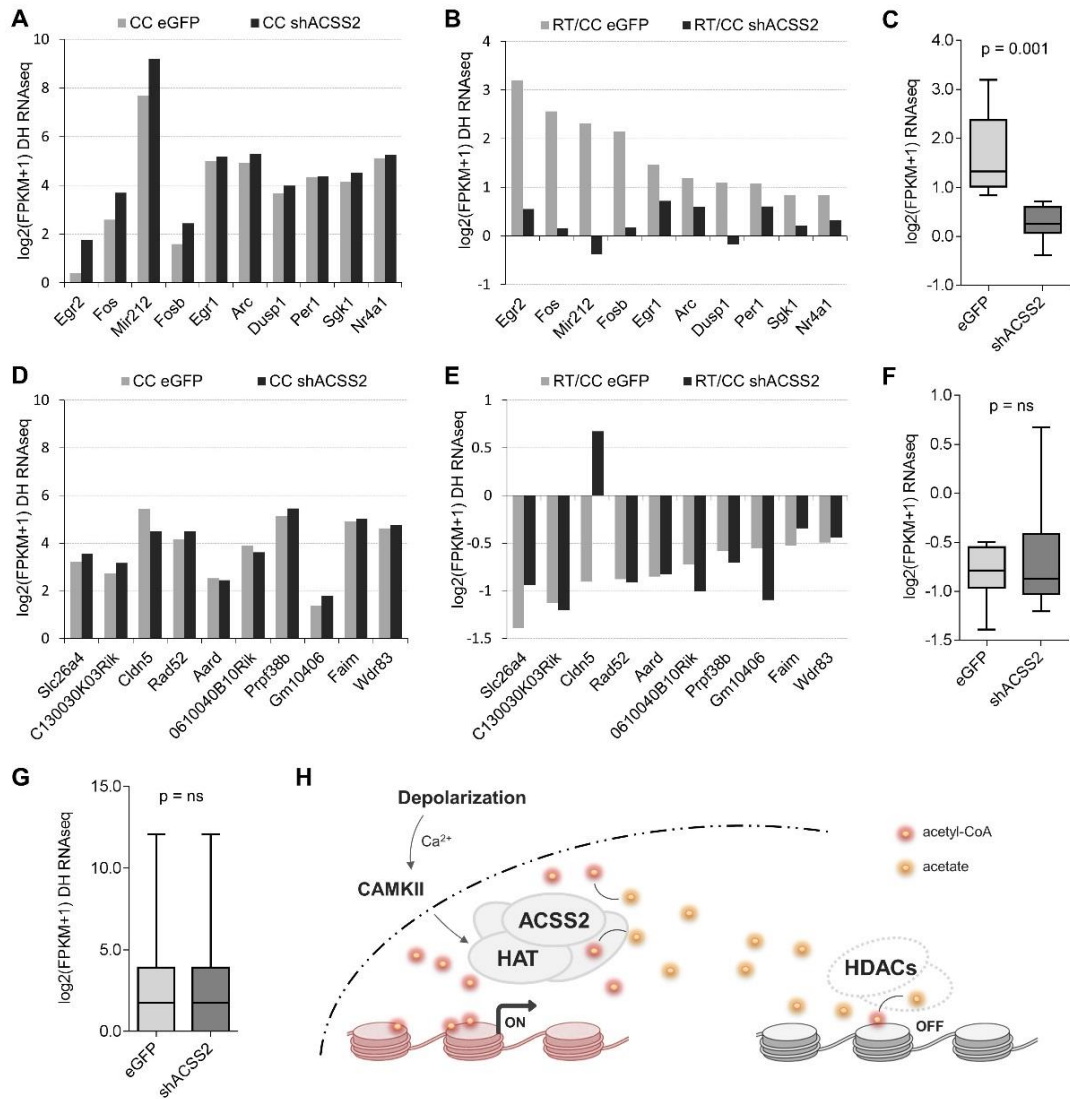


Figure 3.11. ACSS2 regulates retrieval-induced upregulation of immediate-early genes in vivo.

(A) Genome-wide RNA-seq was performed on the dorsal hippocampus of eGFP control and shACSS2 knockdown animals. The baseline expression of immediate-early genes in untrained animals is not changed in shACSS2-AAV9 mice when compared to eGFP-AAV9 control mice (CC – circadian control). (B) During the sensitive period following contextual memory retrieval (RT), immediate-early genes are upregulated in control injected animals. In contrast, the retrieval-induced expression of these early response genes is absent in ACSS2 knockdown animals ( $p = 0.001$ , Paired T test). (C) Boxplot shows the induction defect of immediate early genes in shACSS2-AAV9 injected animals (RT/CC). (D) The baseline expression of genes that are downregulated following contextual memory retrieval is not altered in ACSS2 knockdown animals. (E) Downregulation of retrieval-responsive genes occurs both in eGFP control and ACSS2 knockdown mice. (F) Boxplot compares retrieval-responsive downregulation of retrieval-responsive genes in the dorsal

hippocampus in eGFP control versus shACSS2 knockdown (RT/CC). (G) Boxplot of global transcript levels shows that genome-wide expression levels following contextual memory retrieval are not affected by ACSS2 knockdown in the dorsal hippocampus. (H) Model: ACSS2 functions as a chromatin-bound coactivator to locally provide acetyl-CoA to promote histone acetylation and the activity-induced upregulation of immediate-early genes. Accordingly, ACSS2 operates in a salvage pathway to recover both acetate and CoA, the respective byproducts of the catalytic actions of HDAC and HAT enzymes, and therefore implicates acetate metabolism in transcription regulation.

Interestingly, baseline expression of these memory-associated genes in the untrained mice was remarkably similar when comparing shACSS2 knockdown to eGFP control hippocampus (Fig. 3.11A). In clear contrast, following memory retrieval, expression of these genes was strongly upregulated in the dorsal hippocampus of eGFP control animals, during the sensitive period following contextual memory retrieval (Fig. 3.11B and 3.11C). Remarkably, this dynamic retrieval-induced transcription was absent from most of these early response genes after knockdown of ACSS2 ( $p = 0.001$ , Paired T test; Fig. 3.11B and 3.11C). In contrast, retrieval-responsive genes that are typically downregulated during this same period were not affected by knockdown of ACSS2 (Fig. 3.11D, 3.11E, 3.11F), with the exception of *Cldn5*. Additionally, global expression profiles were strikingly similar across all samples, whereas the group of immediate-early genes was significantly decreased in expression (compare global in Fig. 3.11G to IE genes in 3.11C). Together, these results demonstrate a crucial role for ACSS2 in the dynamic and exquisitely timed upregulation of genes that function in long-term memory.

## DISCUSSION

A compelling body of evidence suggests an intimate relationship between metabolic state and chromatin regulation. This link is manifested in key metabolites that participate in biochemical pathways as intermediates, and function as cofactors to regulate chromatin modifying enzymes<sup>18,163</sup>. Most interesting is the metabolite acetyl-CoA, given its central role as an intermediate of cellular energy metabolism and a key determinant of all chromatin acetylation<sup>37,38,88</sup>. Hence, how nuclear acetyl-CoA is regulated to control histone acetylation is

under investigation, and holds promise for increased understanding of molecular mechanisms that adapt gene expression to internal and external stimuli. Our study reveals a previously unknown function of the central metabolic acetyl-CoA source ACSS2 as a chromatin-bound transcriptional coactivator that stimulates histone acetylation and gene expression.

In recent years, studies have shown that optimal acetyltransferase activity involves increases in acetyl-CoA. In fact, both the catalytic activity and specificity of HAT enzymes can be determined by the local acetyl-CoA to CoA ratio<sup>130,131</sup>. For instance, the substrate selectivity of the HAT enzymes p300 (E1A binding protein p300) and CBP change with distinct acetyl-CoA levels<sup>164</sup>. Adding yet another layer of metabolic regulation of histone acetylation is the polyamine spermidine – a ubiquitous metabolite involved in chromatin condensation – which competes with acetyl-CoA for binding to HAT enzymes<sup>165</sup>. Collectively, these findings suggest that nuclear-localized metabolic enzymes could increase the local acetyl-CoA concentration by fueling catalytic activities of proximate histone acetyltransferases and hence promoting gene transcription. Indeed, in yeast, the nucleocytoplasmic acetyl-CoA synthetase interacts with subunits of SESAME (Serine-responsive SAM-containing Metabolic Enzyme complex), a protein complex that is recruited to chromatin by the Set1 methyltransferase<sup>166</sup>. In addition, the mitochondrial pyruvate dehydrogenase complex translocates to the nucleus to support histone acetylation<sup>167</sup>, and associates with p300 on chromatin to locally supply acetyl-CoA for histone acetylation and instantaneously recycle CoA<sup>168</sup>. Our study provides the first evidence that localization of an acetyl-CoA metabolic enzyme, ACSS2, directly to specific genes, leads to upregulation of neuronal histone acetylation and transcription.

Notably, ACSS2 was previously shown to partially localize to the nuclear compartment of cells<sup>37,83</sup>, and to contribute to global histone acetylation in low glucose conditions<sup>37</sup>. Curiously, in adipose and malignant cell lines, the major source of nuclear acetyl-CoA contributing to histone acetylation is ACL, not ACSS2<sup>37</sup>. In contrast, our findings reveal that post-mitotic CAD neurons preferentially rely on ACSS2 for their supply of acetyl-CoA that feeds into chromatin acetylation.

These results are consistent with a body of evidence that acetyl-CoA metabolism is highly cell and tissue specific, and is frequently dysregulated in disease. For example, malignant transformation renders tumor cells dependent on acetate, and tumors characterized by high ACSS2 levels are associated with poor disease outcome<sup>32,169,170</sup>.

Here, we demonstrate that the metabolic enzyme ACSS2 localizes to nuclei of neuronal cells, and directly associates with chromatin. Intriguingly, such direct regulation of chromatin acetylation allows for potential rapid and widespread tissue-specific adaptation to changing environment and metabolic states. In particular, recruiting ACSS2 to chromatin provides a mechanism for sustaining histone acetylation and gene transcription locally in an otherwise restrictive metabolic state of low glycolysis, when acetyl-CoA production by citrate-dependent ACL is reduced. States of low metabolism are produced by fasting, calorie restriction, or exercise, which promote hepatic  $\beta$ -oxidation of fatty acids and thus increase circulation levels of  $\beta$ -hydroxybutyrate ( $\beta$ -OHB), a ketone body that contributes to peripheral acetyl-CoA pools and plays a central role as an HDAC inhibitor. Interestingly, whereas fasting results in significantly reduced acetyl-CoA and protein acetylation in most tissues, acetyl-CoA levels in the brain remain unchanged<sup>171</sup>. Accordingly, ACSS2 expression may be of particular importance for brain function in the fasted state, allowing ketone bodies to be sourced for acetyl-CoA production in order to sustain transcriptionally permissive chromatin and regulated gene expression. Thus, taken together, our findings are relevant to an adverse set of physiologically normal and abnormal states, and inform upcoming studies of disease conditions characterized by altered chromatin acetylation and acetate dependence, including cancer and neurodegenerative disease.

Overall, our study befits the emerging paradigm that metabolite pools function in chromatin regulation and gene transcription, and specifically tightens the link between acetate metabolism and neuronal histone acetylation. Relevantly, activity-dependent increases in histone acetylation mediate the transcription of memory-related neuroplasticity genes that function in long-term memory. Here, we show that ACSS2 is critically important in the formation of long-term

spatial memory *in vivo*, a process that has been previously demonstrated to require dynamic increases in histone acetylation. Our results further show that ACSS2 promotes the transcription of early response genes with key functions in neuronal plasticity and memory. To our knowledge, this is the first demonstration that ACSS2 has a critical role in memory consolidation, and that ACSS2 functions in dynamic gene induction in neuronal cells. Taken together, our findings advance understanding of the molecular mechanisms involved in neuronal gene expression and memory, and provide new insight into how metabolic activities link to epigenetic and transcriptional regulation in the brain. Here, our results suggest a model wherein neuronal activation in the context of learning triggers  $\text{Ca}^{2+}$ -stimulated transcriptional events that rely on the conversion of acetate to acetyl-CoA by ACSS2 for coordinated histone acetylation. In this view, ACSS2 operates in a chromatin-localized salvage pathway to increase the local acetyl-CoA concentration by recycling CoA and acetate that derive from enzymatic activity of HATs and HDACs, respectively, to ultimately support the dynamic upregulation of immediate-early genes that manifest memory storage (Fig. 3.11H).

Epigenetic mechanisms continue to become recognized as principal regulators of neural function and behavior, and have been implicated in the pathophysiology of neuropsychiatric disease, including anxiety disorders and depression. In establishing ACSS2 as a key regulator at the interface of metabolic environment and neuronal chromatin, our study provides a novel enzymatic target in therapies of such neurological and cognitive disorders.

## EXPERIMENTAL PROCEDURES

**Cell Culture.** CAD cells (Cath.-a-differentiated; generously donated from the Holzbaur Lab at the University of Pennsylvania) were grown in DMEM:HAMS F12 (1:1), supplemented with 2mM Glutamine, 1% penicillin/streptomycin, and 10% Fetal Bovine Serum (FBS). To induce neuronal differentiation, sub-confluent CAD cell cultures (50-60%) were transferred to serum-free media (DMEM:HAMS F12 (1:1) supplemented with 2mM Glutamine) and maintained in 15 cm<sup>2</sup> culturing dishes for 5 days. For knockdown experiments, CAD cells were infected with lentiviral hairpin constructs (TRC collection) designed against ACL (#TRCN0000055217) or ACSS2 (#TRCN0000076124, #TRCN0000076125) in medium containing 8 mg/mL polybrene and 10% FBS for 24 h. Cells then underwent selection in culture medium supplemented with 0.5 mg/mL puromycin for 5 days to obtain a stably infected population.

**RNA-seq.** To generate libraries for RNA-seq, polyA<sup>+</sup> RNA was extracted using the Dynabeads mRNA Direct kit (Ambion) according to the manufacturer's instructions. RNA-seq libraries for scrambled control (referred to in text as WT), shACL, and shACSS2 were made using a ScriptSeq v2 RNA-seq Library Preparation Kit from Epicentre (now Illumina). The quantity and quality of the libraries were assessed by BioAnalyzer (Agilent) and qPCR (Kapa Biosystems). The multiplexed libraries were pooled and sequenced on a single lane on the Illumina NextSeq 500 platform (50bp, single-end reads). All RNA seq data was prepared for analysis as follows: NextSeq sequencing data was demultiplexed using bcl2fastq2-v02.14.01.07. Demultiplexed FASTQs were aligned by RNA-STAR 2.3.0.e using the genome index mm10 generated from iGenome UCSC mm10 FASTQ genome sequence. The aligned reads were mapped to genomic features using cufflinks-2.2.1, (-G parameter to only quantitate known features), and iGenomes mm10 UCSC genomic transcript loci. The rRNA, mRNA, and tRNA of the mouse genome were downloaded from the goldenPath UCSC FTP and were masked from the transcript quantification. After quantification all data processing was done using python pandas library v.0.14.0

**Chromatin immunoprecipitation followed sequencing (ChIP-seq).** CAD cells were fixed in 1% Formaldehyde for 10 minutes and fixation was quenched with the addition of glycine to 125mM for an additional 5 minutes. Cells were harvested by scraping from plates, and washed twice in 1x PBS before storage at -80°C. ChIP was performed as previously described (Shah, P.P., et al. 2013), except that chromatin was sheared to an average size of <500 bp using the Covaris S220 Ultrasonicator. Equal aliquots of sonicated chromatin from undifferentiated and differentiated CAD neurons were used per immunoprecipitation reaction, and 10% of the amount was saved as input. ACSS2 ChIPs were performed using 2000 µg of extract and 4 µg of antibody per sample; all other ChIPs were performed using 500 µg of extract and 4 µg of antibody per sample. Immunoprecipitation was performed using protein A Dynabeads (Life Technologies). Sequencing libraries were prepared using NEBNext Ultra library preparation procedure, and then assessed for quality and quantity by BioAnalyzer (Agilent) and qPCR (Kapa Biosystems). Sequencing was performed on the Illumina NextSeq 500 platform. All ChIP-seq data was prepared for analysis as follows: NextSeq sequencing data was demultiplexed using bcl2fastq. All reads were aligned to the mm10 reference genome using bowtie2.2.1. 1 alignment was allowed per read and 1 mismatch was allowed in the seed region (-N1 -k1). Reads were tabulated in fixed windows or to genes provided in the iGenome mm10 UCSC annotations using featureCounts from the subread1.4.6 software package. ACSS2 ChIP-seq data was normalized to input controls, while all histone acetylation ChIP-seq data was H3-subtracted. Tracks were visualized using the UCSC genome browser.

**Western blots.** Cells were lysed in buffer containing 50mM Tris pH 8.0, 0.5mM EDTA, 150mM NaCl, 1% NP40, 1% SDS, supplemented with protease inhibitor cocktail (Life Technologies, #78446). For subcellular fractionation experiments, the cell were processed using the subcellular fractionation kit for cultured cells (Thermo Scientific 78840) according to the manufacturer instructions. Protein concentration was determined by BCA protein assay (Life Technologies, number 23227), and equal amounts of protein were used in co-immunoprecipitation experiments or directly loaded on polyacrylamide gels. The endogenous co-immunoprecipitation (co-IP)

experiments were performed using antibody-conjugated protein A Dynabeads (Life Technologies) in buffer containing: 20 mM Tris, pH 8.0, 137 mM NaCl, 1 mM MgCl<sub>2</sub>, 1 mM CaCl<sub>2</sub>, 1% NP-40, 10% glycerol, with protease and phosphatase inhibitors, and 12.5 U ml<sup>-1</sup>benzonase (Novagen, 70746). Proteins or co-IP eluates were loaded and separated on 4-12% Bis-Tris polyacrylamide gels (NuPAGE). After transfer to nitrocellulose membrane, 3% BSA in TBS supplemented with 0.1% Tween 20 (TBST) was used to block the membrane at room temperature for 1 hour. Primary antibodies were diluted in TBST, and incubated at 4°C overnight. Primary antibodies are listed below. The membrane was washed 3 times with TBST, each for 10 minutes, followed by incubation of HRP-conjugated secondary antibodies at room temperature for 1 hour, in TBST. The membrane was washed again 3 times, and imaged by Fujifilm LAS-4000 imager.

**Immunofluorescence.** Cells were fixed in 4% PFA in PBS for 20 minutes at room temperature. Cells were washed twice with PBS, and permeabilized with 0.5% Triton X-100 in PBS for 10 minutes. After washing two times, cells were blocked in 10% BSA in PBS for 1 hour at room temperature. Cells were incubated with primary antibodies in 5% BSA in PBS supplemented with 0.1% Tween 20 (PBST) overnight at 4°C. Antibodies are listed below. Then cells were washed four times with PBST, each for 10 minutes, followed by incubation with fluorophore-conjugated secondary antibody in 5% BSA in PBST for 1 hour at room temperature. F-actin was labeled using Alexa Fluor® 488 Phalloidin (Thermo A12379). Cells were then washed three times in PBST, once with PBS, and incubated with 1 µg/ml of DAPI for 5 minutes. The cells were then washed twice with PBS, and mounted with ProLong Gold (Invitrogen). The slides were observed and imaged using a Nikon Eclipse microscope. Microscopy settings were unchanged between samples.

**Antibodies.** Antibodies included Anti-H2BK5ac (Active Motif 39124), Anti-H3 (Abcam ab1791), Anti-H3K9ac (Abcam ab4441), Anti-H3K27ac (Abcam ab4729), Anti-H3K122ac (Abcam ab33308), Anti-H4 (Millipore 05-858), Anti-H4K5ac (Millipore 39-584), Anti-H4K12ac (Abcam ab1761), Anti-H4K16ac (Millipore 07-329), Anti-ACSS2 (T) (Thermo MA5-145810), Anti-ACSS2

(CS) (Cell Signaling 3658), Anti-ACL (Proteintech 15421-1-AP), Anti- $\alpha$ -Tubulin (Sigma T8328), Anti-GAPDH (Fitzgerald Industries 10R-G109A), Anti-KAT3A/CBP (Abcam ab2832).

**Intracranial injection of viral vector.** Adult mice (8+ weeks of age) were anesthetized with isoflurane gas (1-5% to maintain surgical plane) and placed in a sterile field within a stereotaxic device. Animals received an injection of bupivacaine (2.5mg/Kg) for local anesthesia before the skin was disinfected with betadine solution and the skull exposed with a short incision using sterile surgical equipment. Artificial tears were applied to eyes to ensure sufficient lubricating. A small hole (about 0.5 millimeters) was be drilled in the skull over the target area using a stereotax and a stereotactic drill. A micro-syringe filled with viral vector was inserted into the dorsal hippocampus and slowly removed following injection (AP, -2.0mm; DV, -1.4mm; ML, +/-1.5mm; AAV2/9.U6.shACSS2.CMV.EGFP = ACSS2 knockdown vector; AAV2/9.CMV.EGFP.polyA = eGFP-control vector). All animals received a single dose of subcutaneous meloxicam (5 mg/kg) as analgesia (pain medicine) at induction and one dose per day for two days post-operatively as needed.

**Object location memory (OLM) task.** The OLM procedure is used to test spatial memory. The procedure consists of a training phase and a testing phase. Prior to training, each mouse was handled for 3 minutes a day for 3 days. During the training day, mice are placed in an arena (approx. 1 square foot) containing 3 different objects. The objects used were a glass bottle, a metal tower (5H x 2W x 2L inches), and a plastic cylinder. Mice were habituated to an empty arena with a black and white striped spatial cue on the wall, followed by object exposure in three 6 minute trials with and interval of 3 minutes. The arena and objects were cleaned with 70% EtOH between trials. After 24 hours, the individual mice were placed back in the arena used in the testing phase. For testing, one of the objects was moved to different location in the arena. Mice were allowed to freely explore for 5 minutes. Each session was recorded using a video camera and time spent exploring (approaches and sniffing) each object was assessed offline.

**Contextual fear conditioning.** The animal was placed in the conditioning chamber (Med Associates) for 5 min before the onset of the unconditioned stimulus (US), a 1.5 mA of continuous foot shock. A mild 2 sec., 1.5 mA foot shock is used as an aversive stimulus, which does not injure the mice in any way but provides the transient, yet startling and aversive, stimulus that is necessary for conditioning. After an additional 30 s in the chamber, the mouse was returned to its home cage. Twenty four hours later, the mouse was tested for a freezing response to the chamber (contextual) where training occurred. Time spent freezing in the chamber (motionless except for respiratory movements) in the chamber was assessed for 5 consecutive minutes.

**CHAPTER 4**  
**GENERAL DISCUSSION AND CONCLUSIONS**

## **Chromatin-localized acetyl-CoA metabolism functions in regulated gene expression**

Epigenetic enzymes have critical roles for chromatin regulatory events in normal cellular development and plasticity. A major question in the epigenetics field is how metabolic changes signal to chromatin. We explored the roles of histone acetylation and methylation as putative energy sensors, in the context of massive metabolic and transcriptional reprogramming during cell cycle re-entry of quiescent yeast. We measured changes in global histone acetylation and methylation by Western blot and SILAC-mass spectrometry, and used RNAseq and ChIP-seq to examine changes in local genic modification patterns. In each of these experimental approaches we compared histone methylation dynamics to histone acetylation, which undergoes dramatic fluctuations in cell cycle exit and re-entry. Our results are the first comprehensive and systematic investigation of how histone methylation responds to metabolic change in the context of cell cycle re-entry from quiescence.

We conclude that the functions of histone methylation and histone acetylation are remarkably distinct during nutrient-induced cell cycle return. Growth-related genes in proliferating cells are marked with acetylation and methylation modifications associated with active transcription. These same genes are inactive in quiescent cells, and have lost acetylation and have lower levels of H3K4, K36, and K79 methylation. Conversely, stress genes, which are active in quiescent cells, are enriched for acetylation and methylation. When quiescent cells are induced to re-enter the cell cycle upon nutrient addition, acetylation is lost from stress genes and rapidly re-established at growth genes, correlating with the massive upregulation of transcription at this time. Accordingly, histone acetylation serves as a broad energy sensing modification that rapidly adapts gene transcription relative to metabolic state.

Remarkably, our findings indicate that methylation functions very differently from acetylation in re-activation into the cell cycle, and is independent of metabolic state. Instead, the patterns of histone methylation found in quiescent cell remain unchanged for an extended period of time, and do not increase until new histones are synthesized during the first S phase. This *de-*

*novo* methylation occurs almost exclusively at growth genes. Thus, instead of functioning as an energy sensor, our studies suggest that histone methylation may serve a memory mark to help re-establish the growth gene expression program during early quiescence exit.

Our findings support the following model of gene regulation by metabolic state: direct control of histone acetylation and global gene transcription via the key metabolite acetyl-CoA. In yeast, during growth on glucose, the entire pool of nucleocytoplasmic acetyl-CoA that is being used in histone acetylation is produced by catalytic Acs2p<sup>87,88</sup>. Accordingly, Acs2p is a key enzyme positioned at the very interface of cellular carbon metabolism and chromatin structure regulating gene expression. Relevantly, metabolic production of acetyl-CoA leading to histone acetylation is centrally involved in cancer<sup>32,37,85,172,173</sup>, yet whether production of acetyl-CoA has a more general role in inducible gene regulation remains a question of debate. We set out to examine a new paradigm of transcriptional regulation, by which chromatin-localized acetyl-CoA biosynthesis could locally support catalytic HAT activity to promote gene expression. Recent evidence and our findings from yeast indicate that the nuclear acetyl-CoA source Acs2p may partake in such chromatin-based gene regulation. We thus investigated the importance of its highly conserved mammalian homolog ACSS2 for histone acetylation and gene expression, in the fascinating context of neuronal differentiation and, *in vivo*, learning and memory. No such link has been previously elucidated.

Our extensive genome-wide and functional studies *in vitro* in differentiating neuronal cells provide a comprehensive understanding of mechanism underlying metabolic signaling to chromatin, far beyond previous knowledge even in the context of cancer. Our results show that ACSS2 indeed directly associates with chromatin, increasing nearby histone acetylation to activate genes. In key functional data, we investigated the function of ACSS2 *in vivo*, and discovered a novel role of this central metabolic enzyme in the formation of long-term spatial memory, via upregulation of important neuronal genes. Our major results are the first evidence that metabolic acetyl-CoA production plays a critical role in long-term memory, via neuronal gene

regulation. These results provide an intriguing model in which ACSS2 is a chromatin-based epigenetic factor that increases the local acetyl-CoA concentration by recycling CoA and acetate derived from enzymatic activity of HATs and HDACs, respectively. Together, our study provides a much-needed mechanism to explain the observed link between metabolism and epigenetic plasticity, and further demonstrates a link to neural function. By linking acetate metabolism to neuronal gene expression, our findings describe an entirely novel pathway in memory formation. In the future, it will be interesting to determine the molecular targets and pathways that are affected by ACSS2 in brain regions outside the hippocampal formation. Interestingly, in the brain, N-Acetylaspartate (NAA) has been found to act in part as an extensive reservoir of acetate for acetyl coenzyme A synthesis<sup>174</sup>. It will be of interest to investigate the importance of ACSS2 in the mobilization and activation of these acetate pools, in particular after brain injury. Accordingly, NAA metabolism and catalytic ACSS2 may support post-injury neuroenergetics, lipid synthesis, and protein acetylation – in that case indicating novel therapeutic treatments such as acetate supplementation following trauma.

### **Role of ACSS2 in neuronal histone acetylation linked to alcohol consumption**

Our studies show that acetyl-CoA metabolism by ACSS2 regulates neuronal histone acetylation and gene expression. Intriguingly, neuronal histone acetylation may therefore be under the influence of extracellular levels of acetate, the substrate used by ACSS2 to generate acetyl-CoA<sup>169,175</sup>. One physiological source of acetate is alcohol metabolism in hepatic cells. Although the liver – as the site of alcohol metabolism – is particularly sensitive to alcohol exposure, acute and chronic alcohol consumption also leads to changes in other tissues, in particular the brain<sup>176,177</sup>. Recent advances in understanding the pleiotropic effects of ethanol have been possible because of the development of relevant and controlled animal studies of acute and chronic ethanol exposure<sup>178</sup>. One of the themes arising in recent studies that investigate the mechanisms of ethanol action on target tissues is the impact of ethanol on regulated gene expression.

Notably, acute alcohol consumption results in highly elevated blood acetate levels, raising up to 5-fold<sup>179–182</sup>, and has been linked to increased histone acetylation in neuronal tissues<sup>183</sup>. Interestingly, in alcoholics and heavy drinkers, the rate of EtOH metabolism is more rapid, resulting in acetate plateau levels 2-fold higher in alcohol-tolerant individuals than in controls<sup>184</sup>, suggesting greater availability of acetate as a substrate for brain metabolism. Curiously, direct supplementation of acetate – the main product of hepatic ethanol metabolism – increases histone acetylation in liver tissue, the heart, and the brain<sup>175</sup>. Relevantly, ACSS2 is the only known source of nuclear acetyl-CoA deriving from the activation of nucleocytoplasmic acetate.

Unquestionably, EtOH directly binds neuronal channel proteins and thus affects synaptic communication and cognition, causing psychotropic effects that change along a dose continuum<sup>185,186</sup>. Such direct manipulation of neurons may well trigger nuclear signaling events that result in increased histone acetylation associated with ethanol consumption. However, it remains unknown whether alcohol-induced histone acetylation might also be driven by increasing acetyl-CoA from acetate that is activated by neuronal ACSS2, or via EtOH-triggered signaling events that cascade into the nucleus, leading to acetylation of target genes. In order to elucidate whether neuronal histone acetylation linked to alcohol intake is mediated by metabolic ACSS2, we tracked the fate of isotopically labeled EtOH carbons using SILAC-based mass spec. The SILAC approach is able to distinguish histone acetylation that originated in labeled deuterated EtOH-d<sub>6</sub> metabolized to acetate by hepatic alcohol dehydrogenase (ADH) and aldehyde dehydrogenase (ALDH), from histone acetylation using other sources of acetyl-CoA (Appendix; Figure A1, A2).

To our knowledge, our data are the first to establish that histone acetylation in the brain is directly manipulated by products of hepatic alcohol breakdown (Appendix; Figure A3). By SILAC mass spec, we revealed that acute alcohol intake not only contributes to dynamic chromatin acetylation in liver and brain (Appendix; Figure A2, A3), but also drives global increases in

particular sites of histone acetylation in both hippocampus and cortex (data not shown). Thus, our preliminary results support the hypothesis that histone acetylation is influenced by metabolic state, and establish a connection between alcohol intake and neuronal chromatin alterations via liver metabolism. It will be important to investigate whether histone acetylation in other tissues is similarly affected by hepatic ethanol metabolism. Furthermore, to firmly establish that neuronal histone acetylation linked to alcohol ingestion is indeed mediated by ACSS2-dependent activation of acetate originating from hepatic ADH, EtOH-d6-SILAC must be repeated in animals following knockdown of neuronal ACSS2.

Of interest, hypothetical models of alcohol addiction that are discussed in the literature involve histone acetylation mechanisms in the amygdala to operate in the disease<sup>187</sup>. It has been proposed that the first drinking episode may cause more histone acetylation due to HDAC inhibition that results in an open chromatin structure leading to euphoric effects such as anxiolysis<sup>187</sup>. Repeated exposure to alcohol may lead to neuroadaptive changes in epigenetic mechanisms that translate into the development of chronic tolerance. Consequentially, cessation from drinking may precipitate withdrawal-related anxiety due to epigenetic causes, for instance hypoacetylation due to increased HDAC activity further condensing the chromatin structure. To relieve these dysphoric symptoms, subjects tend to self-medicate, resulting in alcohol abuse and dependence. Interestingly, this cycle of withdrawal leading to self-medication can be broken with HDAC inhibitors, which promote histone acetylation and can lead to a normal behavioral state<sup>188-190</sup>. By the same token, modulation of ACSS2 activity may present another avenue to affect the positive and negative states that arise due to alcohol exposure and withdrawal, and help to further elucidate the epigenetic alterations underlying the pathogenesis of alcoholism.

### **ACSS2 as a therapeutic target in neuropsychiatric disorders**

An important clinical implication of this work is the modulation of neuronal histone acetylation via ACSS2 as a novel therapeutic approach in neuropsychiatry. For instance, epigenetic regulation has been implicated in the development of post-traumatic stress disorder

(PTSD), a prevalent yet difficult to treat disorder that is characterized by severe social and occupational impairment<sup>191,192</sup>. Recent studies showed that development of PTSD is facilitated by a failure to contain the biologic stress response at the time of the trauma. Specifically, PTSD has been linked to decreased cortisol levels that can prolong the availability of norepinephrine to synapses, resulting in the enhanced consolidation of traumatic memory<sup>192,193</sup>. In traumatized persons, adrenergic activation and low cortisol levels will thus strongly encode the event memory, associating it with strong feelings of distress. Following the traumatic event, unintended retrieval of intrusive memories and the generalization of such fear memory results in worsening of symptoms and manifestation of PTSD<sup>193</sup>.

Importantly, the initial acquisition of such traumatic long-term memory is mediated by dynamic epigenetic mechanisms involving histone acetylation<sup>192,194</sup>. Drugs that target this process in the 'golden hours' are expected to be greatly useful to prevent the consolidation of traumatic event memories and development on PTSD<sup>191</sup>. Relevantly, our studies revealed that hippocampal ACSS2 expression is essential for cognitive plasticity and long-term memory formation. Thus, it is reasonable to speculate that attenuation of ACSS2 using a small molecule inhibitor may be of potential usefulness to negatively regulate cognition, in order to counteract acquisition of trauma memory by temporarily preventing cortico-amygdala plasticity. Pharmacological targeting of ACSS2 within hours of a traumatic event could in principle function as an amnesiac to prevent trauma memory consolidation causing PTSD. Interestingly, modern treatment interventions for PTSD and addiction involve extinction therapy paradigms that focus on fear extinction learning to rescue cognitive deficits. In fact, epigenetics-based clinical trials use HDAC inhibitors in conjunction with cognitive behavioral therapy to augment fear extinction learning<sup>191,195</sup>.

However, the original trauma memory is not erased by fear extinction learning and newly conditioned responses, and often followed by recurrence of disease symptoms such as intrusion memories<sup>192,193</sup>. Theoretically, augmenting psychotherapy with medication during exposure-based 'windows of opportunity' could modify the trauma memory post-retrieval. Used in such re-

exposure settings, inhibiting histone acetylation and neuronal gene expression by pharmacological targeting of ACSS2 could prevent reconsolidation of fear memories underlying PTSD. Similarly, in the context of substance abuse and drug addiction, ACSS2 inhibition could prevent drug seeking behaviors if the associative memories that underlie drug addiction are disrupted by preventing reconsolidation following re-exposure. How exactly epigenetic mechanisms interact to regulate transcription in memory consolidation and reconsolidation will be an exciting area of future study, and promises new therapeutic avenues and targets in neuropsychiatry.

## APPENDIX

### Histone H4 peptide aa 4-17

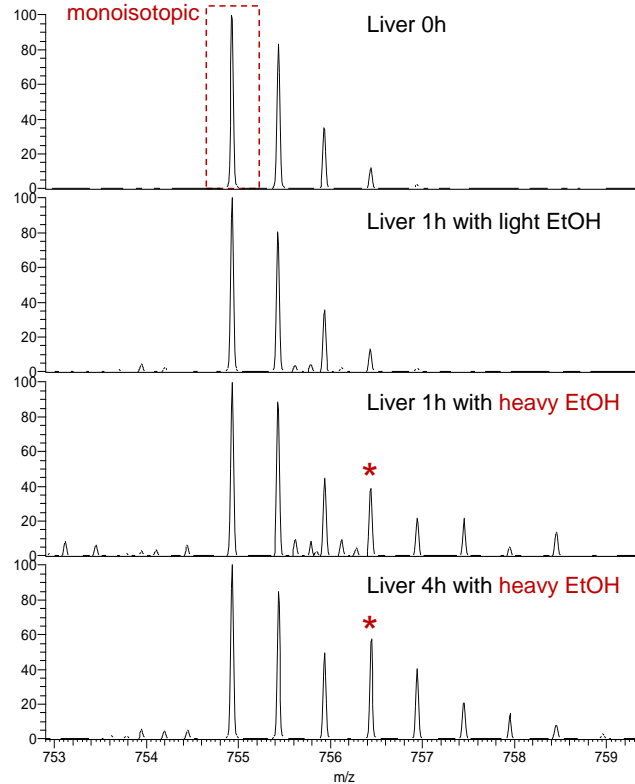


### Figure A1. Histone H4 acetylation labeling in SILAC with heavy EtOH

Full mass spectra of ions from the H4 peptide GKGKGLGKGGAKR showing representative label incorporation into single isotope heavy acetylated H4 aa 4-17 peptide 1h and 4h post EtOH-administration, deriving from metabolized deuterated EtOH-d<sub>6</sub> (obtained from Sigma-Aldrich, product #186414). The appropriate injection volume is based upon the weight of the animal and the desired blood alcohol level of 300 mg/dL (calculated based upon the following formula: volume of ethanol in milliliters = [(weight of the mouse in grams) × (desired blood alcohol level in mg/dL + 31)]/19529), and administered via intraperitoneal injection into the lower left abdominal quadrant close to the midline at a 30° angle. In humans, blood alcohol levels of around 300 mg/dL are associated with clinical sign and symptoms that include confusion, disorientation, impaired balance, and slurred speech.

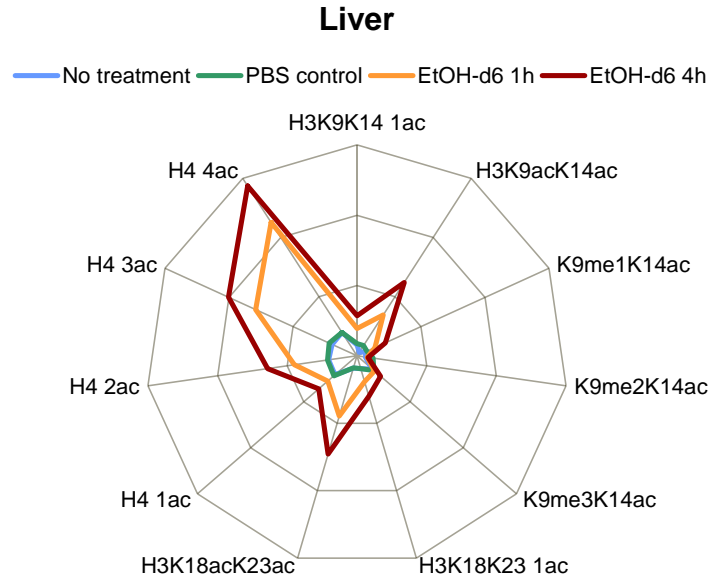


**Figure A2. Heavy EtOH-SILAC – Histone acetylation labeling in liver**

Visualized is the relative labeling of acetylated peptide species in a radar chart with each spoke representing the indicated modified peptide in different treatments. The data length of a spoke is proportional to the relative labeling of the acetylation in the indicated peptide modification variant. The three circles represent 30%, 60% and 90% of the isotope intensity. The natural isotope distribution detected in untreated mice remains unchanged in PBS-injected control animals. Following administration of heavy EtOH-d6, isotopic labeling of specific histone acetylation occurs within 1h, and increases further at 4h post-injection.

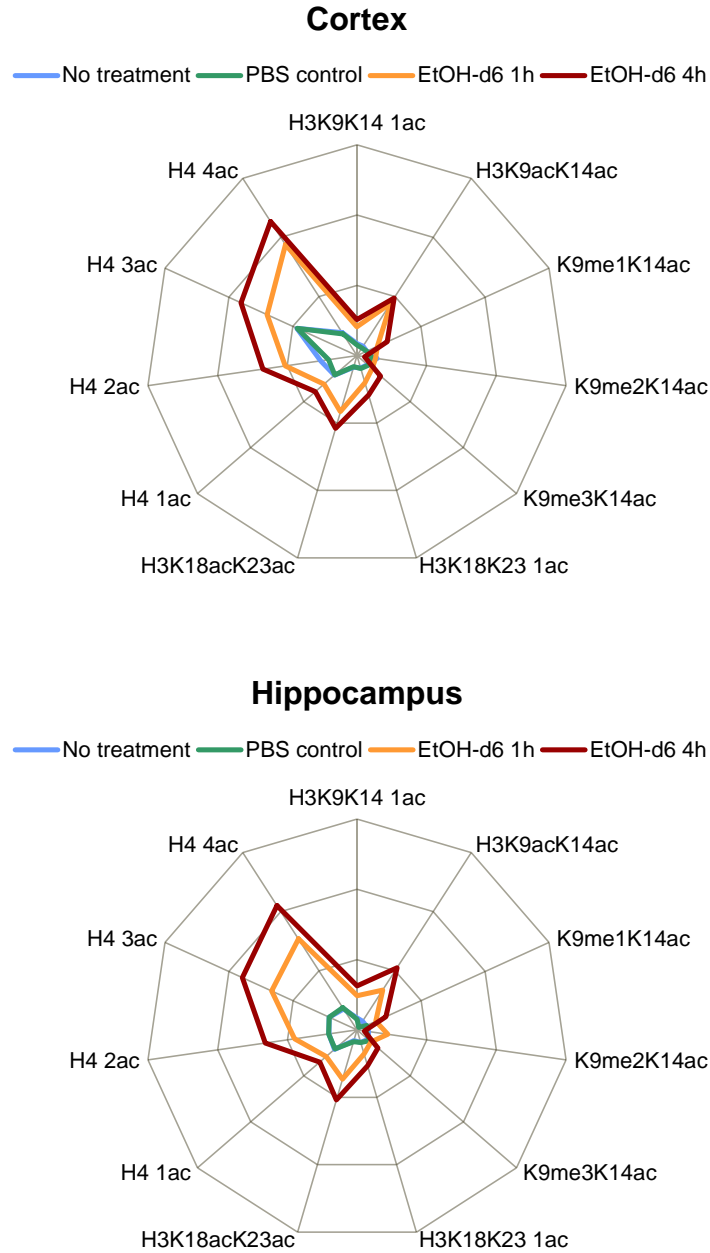


**Figure A3. Heavy EtOH-SILAC – Histone acetylation labeling in cortex and hippocampus**

Visualized is the relative labeling of acetylated peptide species in a radar chart with each spoke representing the indicated modified peptide in different treatments. The data length of a spoke is proportional to the relative labeling of the acetylation in the indicated peptide modification variant. The three circles represent 30%, 60% and 90% of the isotope intensity. The natural isotope distribution detected in untreated mice remains unchanged in PBS-injected control animals. Following administration of heavy EtOH-d6, isotopic labeling of specific histone acetylation occurs within 1h, and increases further at 4h post-injection.

## BIBLIOGRAPHY

1. Waddington, C. H. The strategy of the genes. A discussion of some aspects of theoretical biology. With an appendix by H. Kacser. *Strateg. genes A Discuss. some ...* ix +262 . (1957). doi:10.1007/3-540-32786-X\_7
2. Goldberg, A. D., Allis, C. D. & Bernstein, E. Epigenetics: A Landscape Takes Shape. *Cell* **128**, 635–638 (2007).
3. Borrelli, E., Nestler, E. J., Allis, C. D. & Sassone-Corsi, P. Decoding the epigenetic language of neuronal plasticity. *Neuron* **60**, 961–74 (2008).
4. Levenson, J. M. & Sweatt, J. D. Epigenetic mechanisms in memory formation. *Nat. Rev. Neurosci.* **6**, 108–18 (2005).
5. Khorasanizadeh, S. The Nucleosome: From Genomic Organization to Genomic Regulation. *Cell* **116**, 259–272 (2004).
6. Berger, S. L. The complex language of chromatin regulation during transcription. *Nature* **447**, 407–12 (2007).
7. Bhaumik, S. R., Smith, E. & Shilatifard, A. Covalent modifications of histones during development and disease pathogenesis. *Nat. Struct. Mol. Biol.* **14**, 1008–16 (2007).
8. Kouzarides, T. Chromatin modifications and their function. *Cell* **128**, 693–705 (2007).
9. Shahbazian, M. D. & Grunstein, M. Functions of site-specific histone acetylation and deacetylation. *Annu. Rev. Biochem.* **76**, 75–100 (2007).
10. Berndsen, C. E. & Denu, J. M. Catalysis and substrate selection by histone/protein lysine acetyltransferases. *Curr. Opin. Struct. Biol.* **18**, 682–9 (2008).
11. Burdge, G. C. & Lillycrop, K. a. Nutrition, epigenetics, and developmental plasticity: implications for understanding human disease. *Annu. Rev. Nutr.* **30**, 315–39 (2010).
12. Bannister, A. J. & Kouzarides, T. Regulation of chromatin by histone modifications. *Cell Res.* **21**, 1–15 (2011).
13. Filippakopoulos, P. & Knapp, S. Targeting bromodomains: epigenetic readers of lysine acetylation. *Nat. Rev. Drug Discov.* **13**, 337–356 (2014).
14. Feige, J. N. & Auwerx, J. Transcriptional coregulators in the control of energy homeostasis. *Trends Cell Biol.* **17**, 292–301 (2007).
15. Kaelin, W. G. & McKnight, S. L. Influence of metabolism on epigenetics and disease. *Cell* **153**, 56–69 (2013).
16. Wellen, K. E. & Thompson, C. B. A two-way street: reciprocal regulation of metabolism and signalling. *Nat. Rev. Mol. Cell Biol.* **13**, 270–276 (2012).
17. Everett, L. J. & Lazar, M. A. Nuclear receptor Rev-erba: Up, down, and all around. *Trends in Endocrinology and Metabolism* **25**, 586–592 (2014).
18. Katada, S., Imhof, A. & Sassone-Corsi, P. Connecting Threads: Epigenetics and

- Metabolism. *Cell* **148**, 24–8 (2012).
19. Gut, P. & Verdin, E. The nexus of chromatin regulation and intermediary metabolism. *Nature* **502**, 489–98 (2013).
  20. Shen, H. & Laird, P. W. Interplay between the cancer genome and epigenome. *Cell* **153**, 38–55 (2013).
  21. Baylin, S. B. & Jones, P. a. A decade of exploring the cancer epigenome — biological and translational implications. *Nat. Rev. Cancer* **11**, 726–734 (2011).
  22. Rivera, C. M. & Ren, B. Mapping human epigenomes. *Cell* **155**, 39–55 (2013).
  23. Ong, S. E. *et al.* Stable isotope labeling by amino acids in cell culture, SILAC, as a simple and accurate approach to expression proteomics. *Mol. Cell. Proteomics* **1**, 376–386 (2002).
  24. Ong, S.-E. & Mann, M. A practical recipe for stable isotope labeling by amino acids in cell culture (SILAC). *Nat. Protoc.* **1**, 2650–2660 (2006).
  25. Zee, B. M., Levin, R. S., Dimaggio, P. a & Garcia, B. a. Global turnover of histone post-translational modifications and variants in human cells. *Epigenetics Chromatin* **3**, 22 (2010).
  26. Zee, B. M. *et al.* In vivo residue-specific histone methylation dynamics. *J. Biol. Chem.* **285**, 3341–50 (2010).
  27. Mews, P. *et al.* Histone methylation has dynamics distinct from those of histone acetylation in cell cycle reentry from quiescence. *Mol. Cell. Biol.* **34**, 3968–80 (2014).
  28. Maddocks, O. D. K., Labuschagne, C. F., Adams, P. D. & Vousden, K. H. Serine Metabolism Supports the Methionine Cycle and DNA/RNA Methylation through De Novo ATP Synthesis in Cancer Cells. *Molecular Cell* (2015). doi:10.1016/j.molcel.2015.12.014
  29. Chi, P., Allis, C. D. & Wang, G. G. Covalent histone modifications--miswritten, misinterpreted and mis-erased in human cancers. *Nat. Rev. Cancer* **10**, 457–69 (2010).
  30. Greer, E. L. & Shi, Y. Histone methylation: a dynamic mark in health, disease and inheritance. *Nat. Rev. Genet.* **13**, 343–57 (2012).
  31. Lu, C. *et al.* IDH mutation impairs histone demethylation and results in a block to cell differentiation. *Nature* **483**, 474–8 (2012).
  32. Comerford, S. A. *et al.* Acetate Dependence of Tumors. *Cell* **159**, 1591–1602 (2014).
  33. Carrer, A. & Wellen, K. E. Metabolism and epigenetics: a link cancer cells exploit. *Curr. Opin. Biotechnol.* **34**, 23–29 (2014).
  34. Yanagida, M. Cellular quiescence: are controlling genes conserved? *Trends Cell Biol.* **19**, 705–15 (2009).
  35. Gray, J. V. J. *et al.* 'Sleeping beauty': quiescence in *Saccharomyces cerevisiae*. *Microbiol. Mol. Biol. Rev.* **68**, 187–206 (2004).
  36. Zaman, S., Lippman, S. I., Zhao, X. & Broach, J. R. How *Saccharomyces* responds to nutrients. *Annu. Rev. Genet.* **42**, 27–81 (2008).

37. Wellen, K. E. *et al.* ATP-citrate lyase links cellular metabolism to histone acetylation. *Science* **324**, 1076–80 (2009).
38. Cai, L., Sutter, B. M., Li, B. & Tu, B. P. Acetyl-CoA induces cell growth and proliferation by promoting the acetylation of histones at growth genes. *Mol. Cell* **42**, 426–37 (2011).
39. Friis, R. M. N. *et al.* A glycolytic burst drives glucose induction of global histone acetylation by picNuA4 and SAGA. *Nucleic Acids Res.* **37**, 3969–80 (2009).
40. Klose, R. J. & Zhang, Y. Regulation of histone methylation by demethylation and demethylation. *Nat. Rev. Mol. Cell Biol.* **8**, 307–18 (2007).
41. Smith, B. C. & Denu, J. M. Chemical mechanisms of histone lysine and arginine modifications. *Biochim. Biophys. Acta* **1789**, 45–57 (2009).
42. Cavuoto, P. & Fenech, M. F. A review of methionine dependency and the role of methionine restriction in cancer growth control and life-span extension. *Cancer Treatment Reviews* **38**, 726–736 (2012).
43. Cao, X. J., Zee, B. M. & Garcia, B. A. Heavy methyl-SILAC labeling coupled with liquid chromatography and high-resolution mass spectrometry to study the dynamics of site-specific histone methylation. *Methods Mol. Biol.* **977**, 299–313 (2013).
44. Gräff, J. & Tsai, L.-H. Histone acetylation: molecular mnemonics on the chromatin. *Nat. Rev. Neurosci.* **14**, 97–111 (2013).
45. Nelson, E. D. & Monteggia, L. M. Epigenetics in the mature mammalian brain: Effects on behavior and synaptic transmission. *Neurobiol. Learn. Mem.* **96**, 53–60 (2011).
46. Dulac, C. Brain function and chromatin plasticity. *Nature* **465**, 728–35 (2010).
47. Day, J. J. & Sweatt, J. D. Epigenetic mechanisms in cognition. *Neuron* **70**, 813–29 (2011).
48. Sweatt, J. D. The emerging field of neuroepigenetics. *Neuron* **80**, 624–32 (2013).
49. Wood, M. a, Hawk, J. D. & Abel, T. Combinatorial chromatin modifications and memory storage: a code for memory? *Learn. Mem.* **13**, 241–4 (2006).
50. Levenson, J. M. *et al.* Regulation of Histone Acetylation during Memory Formation in the Hippocampus. *J. Biol. Chem.* **279**, 40545–40559 (2004).
51. Alarcón, J. M. *et al.* Chromatin acetylation, memory, and LTP are impaired in CBP<sup>+/-</sup> mice: A model for the cognitive deficit in Rubinstein-Taybi syndrome and its amelioration. *Neuron* **42**, 947–959 (2004).
52. Korzus, E., Rosenfeld, M. G. & Mayford, M. CBP histone acetyltransferase activity is a critical component of memory consolidation. *Neuron* **42**, 961–972 (2004).
53. Fass, D. M. *et al.* Crebinostat: a novel cognitive enhancer that inhibits histone deacetylase activity and modulates chromatin-mediated neuroplasticity. *Neuropharmacology* **64**, 81–96 (2013).
54. Robison, A. J. & Nestler, E. J. Transcriptional and epigenetic mechanisms of addiction. *Nat. Rev. Neurosci.* **12**, 623–37 (2011).
55. Peña, C. J., Bagot, R. C., Labonté, B. & Nestler, E. J. Epigenetic Signaling in Psychiatric

- Disorders. *J. Mol. Biol.* **426**, 3389–3412 (2014).
56. Rudenko, A. & Tsai, L.-H. Epigenetic modifications in the nervous system and their impact upon cognitive impairments. *Neuropharmacology* 1–13 (2014). doi:10.1016/j.neuropharm.2014.01.043
  57. Lubin, F. D. Epigenetic gene regulation in the adult mammalian brain: Multiple roles in memory formation. *Neurobiol. Learn. Mem.* **96**, 68–78 (2011).
  58. Brownell, J. E. *et al.* Tetrahymena histone acetyltransferase A: A homolog to yeast Gcn5p linking histone acetylation to gene activation. *Cell* **84**, 843–851 (1996).
  59. Schmitt, M. & Matthies, H. Biochemical studies on histones of the central nervous system. III. Incorporation of [<sup>14</sup>C]-acetate into the histones of different rat brain regions during a learning experiment. *Acta Biol. Med. Ger.* **38**, 683–689 (1979).
  60. Rogge, G. a & Wood, M. a. The role of histone acetylation in cocaine-induced neural plasticity and behavior. *Neuropsychopharmacology* **38**, 94–110 (2013).
  61. White, A. O. & Wood, M. a. Does stress remove the HDAC brakes for the formation and persistence of long-term memory? *Neurobiol. Learn. Mem.* (2013). doi:10.1016/j.nlm.2013.10.007
  62. Gräff, J., Woldemichael, B. T., Berchtold, D., Dewarrat, G. & Mansuy, I. M. Dynamic histone marks in the hippocampus and cortex facilitate memory consolidation. *Nat. Commun.* **3**, 991 (2012).
  63. Schneider, A. *et al.* Acetyltransferases (HATs) as targets for neurological therapeutics. *Neurotherapeutics* **10**, 568–88 (2013).
  64. Oliveira, A. M. M. *et al.* Subregion-specific p300 conditional knock-out mice exhibit long-term memory impairments. *Learn. Mem.* **18**, 161–169 (2011).
  65. Bannerman, D. M. *et al.* Hippocampal synaptic plasticity, spatial memory and anxiety. *Nat. Rev. Neurosci.* **15**, 181–92 (2014).
  66. Bourtchouladze, R. *et al.* Different Training Procedures Recruit Either One or Two Critical Periods for Contextual Memory Consolidation, Each of Which Requires Protein Synthesis and PKA. *Learn. Mem.* **5**, 365–374 (1998).
  67. Wang, F., Marshall, C. B. & Ikura, M. Transcriptional/epigenetic regulator CBP/p300 in tumorigenesis: Structural and functional versatility in target recognition. *Cellular and Molecular Life Sciences* **70**, 3989–4008 (2013).
  68. Fischer, A. Epigenetic memory: The Lamarckian brain. *EMBO J.* **33**, 945–967 (2014).
  69. Wood, M. a. *et al.* Transgenic mice expressing a truncated form of CREB-binding protein (CBP) exhibit deficits in hippocampal synaptic plasticity and memory storage. *Learn. Mem.* **12**, 111–119 (2005).
  70. McNulty, S. E. *et al.* Differential roles for Nr4a1 and Nr4a2 in object location vs. object recognition long-term memory. *Learn. Mem.* **19**, 588–92 (2012).
  71. Stefanko, D. P., Barrett, R. M., Ly, A. R., Reolon, G. K. & Wood, M. a. Modulation of long-term memory for object recognition via HDAC inhibition. *Proc. Natl. Acad. Sci. U. S. A.* **106**, 9447–52 (2009).

72. Fischer, A., Sananbenesi, F., Mungenast, A. & Tsai, L.-H. Targeting the correct HDAC(s) to treat cognitive disorders. *Trends Pharmacol. Sci.* **31**, 605–17 (2010).
73. Haettig, J. *et al.* HDAC inhibition modulates hippocampus-dependent long-term memory for object location in a CBP-dependent manner. *Learn. Mem.* **18**, 71–79 (2011).
74. Gräff, J. & Tsai, L.-H. The potential of HDAC inhibitors as cognitive enhancers. *Annu. Rev. Pharmacol. Toxicol.* **53**, 311–30 (2013).
75. Park, C. S., Rehrauer, H. & Mansuy, I. M. Genome-wide analysis of H4K5 acetylation associated with fear memory in mice. *BMC Genomics* **14**, 539 (2013).
76. Hsieh, J. & Eisch, A. J. Epigenetics, hippocampal neurogenesis, and neuropsychiatric disorders: Unraveling the genome to understand the mind. *Neurobiol. Dis.* **39**, 73–84 (2010).
77. Sharma, S. K. Protein acetylation in synaptic plasticity and memory. *Neurosci. Biobehav. Rev.* **34**, 1234–1240 (2010).
78. Tsankova, N., Renthal, W., Kumar, A. & Nestler, E. J. Epigenetic regulation in psychiatric disorders. *Nat. Rev. Neurosci.* **8**, 355–367 (2007).
79. Pietrocola, F., Galluzzi, L., Bravo-San Pedro, J. M., Madeo, F. & Kroemer, G. Acetyl Coenzyme A: A Central Metabolite and Second Messenger. *Cell Metab.* **21**, 805–821 (2015).
80. Comerford, S. a *et al.* Acetate dependence of tumors. *Cell* **159**, 1591–602 (2014).
81. Ikeda, Y. *et al.* Transcriptional regulation of the murine acetyl-CoA synthetase 1 gene through multiple clustered binding sites for sterol regulatory element-binding proteins and a single neighboring site for Sp1. *J. Biol. Chem.* **276**, 34259–69 (2001).
82. Hallows, W. C., Lee, S. & Denu, J. M. Sirtuins deacetylate and activate mammalian acetyl-CoA synthetases. *Proc. Natl. Acad. Sci. U. S. A.* **103**, 10230–5 (2006).
83. Ariyannur, P. S. *et al.* Nuclear-cytoplasmic localization of acetyl coenzyme a synthetase-1 in the rat brain. *J. Comp. Neurol.* **518**, 2952–77 (2010).
84. Chypre, M., Zaidi, N. & Smans, K. ATP-citrate lyase: a mini-review. *Biochem. Biophys. Res. Commun.* **422**, 1–4 (2012).
85. Zaidi, N., Royaux, I., Swinnen, J. V & Smans, K. ATP citrate lyase knockdown induces growth arrest and apoptosis through different cell- and environment-dependent mechanisms. *Mol. Cancer Ther.* **11**, 1925–35 (2012).
86. Rae, C., Fekete, A. D., Kashem, M. a, Nasrallah, F. a & Bröer, S. Metabolism, compartmentation, transport and production of acetate in the cortical brain tissue slice. *Neurochem. Res.* **37**, 2541–53 (2012).
87. van den Berg, M. a *et al.* The two acetyl-coenzyme A synthetases of *Saccharomyces cerevisiae* differ with respect to kinetic properties and transcriptional regulation. *J. Biol. Chem.* **271**, 28953–9 (1996).
88. Takahashi, H., McCaffery, J. M., Irizarry, R. a & Boeke, J. D. Nucleocytosolic acetyl-coenzyme a synthetase is required for histone acetylation and global transcription. *Mol. Cell* **23**, 207–17 (2006).

89. Sang, L., Coller, H. a & Roberts, J. M. Control of the reversibility of cellular quiescence by the transcriptional repressor HES1. *Science* **321**, 1095–1100 (2008).
90. Pardee, a B. A restriction point for control of normal animal cell proliferation. *Proc. Natl. Acad. Sci. U. S. A.* **71**, 1286–90 (1974).
91. Martinez, M. J. *et al.* Genomic Analysis of Stationary-Phase and Exit in *Saccharomyces cerevisiae* : Gene Expression and Identification of Novel Essential Genes. *Mol. Biol. Cell* **15**, 5295–5305 (2004).
92. Slattery, M. M. G. & Heideman, W. Coordinated Regulation of Growth Genes in *Saccharomyces cerevisiae*. *Cell Cycle* 1210–1219 (2007).
93. Radonjic, M. *et al.* Genome-Wide Analyses Reveal RNA Polymerase II Located Upstream of Genes Poised for Rapid Response upon *S. cerevisiae* Stationary Phase Exit. *Mol. Cell* **18**, 171–183 (2005).
94. Lu, C. & Thompson, C. B. Metabolic regulation of epigenetics. *Cell Metab.* **16**, 9–17 (2012).
95. Laporte, D. *et al.* Metabolic status rather than cell cycle signals control quiescence entry and exit. *J. Cell Biol.* **192**, 949–57 (2011).
96. Fox, C. J., Hammerman, P. S. & Thompson, C. B. Fuel feeds function: energy metabolism and the T-cell response. *Nat. Rev. Immunol.* **5**, 844–52 (2005).
97. Taplick, J., Kurtev, V., Lager, G. & Seiser, C. Histone H4 acetylation during interleukin-2 stimulation of mouse T cells. *FEBS Lett.* **436**, 349–52 (1998).
98. Evertts, A. G. *et al.* Quantitative dynamics of the link between cellular metabolism and histone acetylation. *J. Biol. Chem.* **288**, 12142–51 (2013).
99. Teperino, R., Schoonjans, K. & Auwerx, J. Histone methyl transferases and demethylases; can they link metabolism and transcription? *Cell Metab.* **12**, 321–7 (2010).
100. Katoh, Y. *et al.* Methionine Adenosyltransferase II Serves as a Transcriptional Corepressor of Maf Oncoprotein. *Mol. Cell* **41**, 554–66 (2011).
101. Shyh-Chang, N. *et al.* Influence of threonine metabolism on S-adenosylmethionine and histone methylation. *Science* **339**, 222–6 (2013).
102. Fabrizio, P. & Longo, V. D. The chronological life span of *Saccharomyces cerevisiae*. *Aging Cell* **2**, 73–81 (2003).
103. Ong, S.-E. Stable Isotope Labeling by Amino Acids in Cell Culture, SILAC, as a Simple and Accurate Approach to Expression Proteomics. *Mol. Cell. Proteomics* **1**, 376–386 (2002).
104. Wang, Y. *et al.* Ras and Gpa2 mediate one branch of a redundant glucose signaling pathway in yeast. *PLoS Biol.* **2**, E128 (2004).
105. Gasch, a P. *et al.* Genomic expression programs in the response of yeast cells to environmental changes. *Mol. Biol. Cell* **11**, 4241–57 (2000).
106. Byvoet, P., Shepherd, G. R., Hardin, J. M. & Noland, B. J. The distribution and turnover of labeled methyl groups in histone fractions of cultured mammalian cells. *Arch. Biochem.*

- Biophys.* **148**, 558–567 (1972).
107. Byvoet, P. In vivo turnover and distribution of radio-N-methyl in arginine-rich histones from rat tissues. *Arch. Biochem. Biophys.* **152**, 887–888 (1972).
  108. Anand, R. & Marmorstein, R. Structure and mechanism of lysine-specific demethylase enzymes. *J. Biol. Chem.* **282**, 35425–9 (2007).
  109. Tsukada, Y. *et al.* Histone demethylation by a family of JmjC domain-containing proteins. *Nature* **439**, 811–6 (2006).
  110. Pokholok, D. K. *et al.* Genome-wide map of nucleosome acetylation and methylation in yeast. *Cell* **122**, 517–27 (2005).
  111. Li, B., Carey, M. & Workman, J. L. The role of chromatin during transcription. *Cell* **128**, 707–19 (2007).
  112. Heintzman, N. D. *et al.* Distinct and predictive chromatin signatures of transcriptional promoters and enhancers in the human genome. *Nat. Genet.* **39**, 311–8 (2007).
  113. Guenther, M. G., Levine, S. S., Boyer, L. a, Jaenisch, R. & Young, R. a. A chromatin landmark and transcription initiation at most promoters in human cells. *Cell* **130**, 77–88 (2007).
  114. Ulanovskaya, O. a, Zuhl, A. M. & Cravatt, B. F. NNMT promotes epigenetic remodeling in cancer by creating a metabolic methylation sink. *Nat. Chem. Biol.* **9**, 300–6 (2013).
  115. Liang, G. & Zhang, Y. Embryonic stem cell and induced pluripotent stem cell: an epigenetic perspective. *Cell Res.* **23**, 49–69 (2013).
  116. Ang, Y.-S. *et al.* Wdr5 mediates self-renewal and reprogramming via the embryonic stem cell core transcriptional network. *Cell* **145**, 183–97 (2011).
  117. Kizer, K. O., Xiao, T. & Strahl, B. D. Accelerated nuclei preparation and methods for analysis of histone modifications in yeast. *Methods* **40**, 296–302 (2006).
  118. Recht, J. *et al.* Histone chaperone Asf1 is required for histone H3 lysine 56 acetylation, a modification associated with S phase in mitosis and meiosis. *Proc. Natl. Acad. Sci. U. S. A.* **103**, 6988–93 (2006).
  119. Lin, S. & Garcia, B. a. *Examining histone posttranslational modification patterns by high-resolution mass spectrometry. Methods in enzymology* **512**, (Elsevier Inc., 2012).
  120. Bajad, S. U. *et al.* Separation and quantitation of water soluble cellular metabolites by hydrophilic interaction chromatography-tandem mass spectrometry. *J. Chromatogr. A* **1125**, 76–88 (2006).
  121. Zee, B. M., Britton, L.-M. P., Wolle, D., Haberman, D. M. & Garcia, B. a. Origins and formation of histone methylation across the human cell cycle. *Mol. Cell. Biol.* **32**, 2503–14 (2012).
  122. Trapnell, C., Pachter, L. & Salzberg, S. L. TopHat: discovering splice junctions with RNA-Seq. *Bioinformatics* **25**, 1105–11 (2009).
  123. Trapnell, C. *et al.* Transcript assembly and quantification by RNA-Seq reveals unannotated transcripts and isoform switching during cell differentiation. *Nat. Biotechnol.*

- 28**, 511–5 (2010).
124. Wyce, A. *et al.* H2B ubiquitylation acts as a barrier to Ctk1 nucleosomal recruitment prior to removal by Ubp8 within a SAGA-related complex. *Mol. Cell* **27**, 275–88 (2007).
  125. Langmead, B., Trapnell, C., Pop, M. & Salzberg, S. L. Ultrafast and memory-efficient alignment of short DNA sequences to the human genome. *Genome Biol.* **10**, R25 (2009).
  126. Kandel, E. R., Dudai, Y. & Mayford, M. R. The molecular and systems biology of memory. *Cell* **157**, 163–186 (2014).
  127. Rogerson, T. *et al.* Synaptic tagging during memory allocation. *Nat. Rev. Neurosci.* **15**, 157–69 (2014).
  128. Zovkic, I. B., Guzman-Karlsson, M. C. & Sweatt, J. D. Epigenetic regulation of memory formation and maintenance. *Learn. Mem.* **20**, 61–74 (2013).
  129. Valor, L. M. *et al.* Ablation of CBP in forebrain principal neurons causes modest memory and transcriptional defects and a dramatic reduction of histone acetylation but does not affect cell viability. *J. Neurosci.* **31**, 1652–63 (2011).
  130. Albaugh, B. N., Arnold, K. M. & Denu, J. M. KAT(ching) Metabolism by the Tail: Insight into the Links between Lysine Acetyltransferases and Metabolism. *Chembiochem* **53706**, 290 – 298 (2010).
  131. Pietrocola, F., Galluzzi, L., Bravo-San Pedro, J. M., Madeo, F. & Kroemer, G. Acetyl Coenzyme A: A Central Metabolite and Second Messenger. *Cell Metab.* **21**, 805–821 (2015).
  132. Lein, E. S. *et al.* Genome-wide atlas of gene expression in the adult mouse brain. *Nature* **445**, 168–176 (2007).
  133. Li, Y., Hou, L. X.-E., Aktiv, A. & Dahlström, A. Studies of the central nervous system-derived CAD cell line, a suitable model for intraneuronal transport studies? *J. Neurosci. Res.* **85**, 2601–2609 (2007).
  134. Qi, Y., Wang, J. K., McMillian, M. & Chikaraishi, D. M. Characterization of a CNS cell line, CAD, in which morphological differentiation is initiated by serum deprivation. *J. Neurosci.* **17**, 1217–1225 (1997).
  135. Castaneda-castellanos, D. R. *et al.* Short communication CNS voltage-dependent Na<sup>+</sup> channel expression and distribution in an undifferentiated and differentiated CNS cell line. *New York* **866**, 281–285 (2000).
  136. Harvey, V. L., Saul, M. W., Garner, C. & McDonald, R. L. A role for the volume regulated anion channel in volume regulation in the murine CNS cell line, CAD. *Acta Physiol. (Oxf)*. **198**, 159–68 (2010).
  137. Huang, W.-H., Mai, R.-T. & Lee, Y.-H. W. Transcription factor YY1 and its associated acetyltransferases CBP and p300 interact with hepatitis delta antigens and modulate hepatitis delta virus RNA replication. *J. Virol.* **82**, 7313–7324 (2008).
  138. Aoyama, T. *et al.* Histone modifiers, YY1 and p300, regulate the expression of cartilage-specific gene, chondromodulin-I, in mesenchymal stem cells. *J. Biol. Chem.* **285**, 29842–50 (2010).

139. Mokrani, H., Sharaf el dein, O., Mansuroglu, Z. & Bonnefoy, E. Binding of YY1 to the Proximal Region of the Murine Beta Interferon Promoter Is Essential To Allow CBP Recruitment and K8H4/K14H3 Acetylation on the Promoter Region after Virus Infection. *Mol. Cell. Biol.* **26**, 8551–8561 (2006).
140. Jin, Q. *et al.* Distinct roles of GCN5/PCAF-mediated H3K9ac and CBP/p300-mediated H3K18/27ac in nuclear receptor transactivation. *EMBO J.* **30**, 249–262 (2011).
141. Henry, R. a., Kuo, Y. M. & Andrews, A. J. Differences in specificity and selectivity between CBP and p300 acetylation of histone H3 and H3/H4. *Biochemistry* **52**, 5746–5759 (2013).
142. Vecsey, C. G. *et al.* Histone Deacetylase Inhibitors Enhance Memory and Synaptic Plasticity via CREB: CBP-Dependent Transcriptional Activation. *J. Neurosci.* **27**, 6128–6140 (2007).
143. Barrett, R. M. *et al.* Hippocampal focal knockout of CBP affects specific histone modifications, long-term potentiation, and long-term memory. *Neuropsychopharmacology* **36**, 1545–56 (2011).
144. O'Keefe, J. & Burgess, N. Theta activity, virtual navigation and the human hippocampus. *Trends Cogn. Sci.* **3**, 403–406 (1999).
145. Fanselow, M. S. Contextual fear, gestalt memories, and the hippocampus. *Behav. Brain Res.* **110**, 73–81 (2000).
146. Maren, S. & Holt, W. The hippocampus and contextual memory retrieval in Pavlovian conditioning. *Behav. Brain Res.* **110**, 97–108 (2000).
147. Poplawski, S. G. *et al.* Object-location training elicits an overlapping but temporally distinct transcriptional profile from contextual fear conditioning. *Neurobiol. Learn. Mem.* **116**, 90–5 (2014).
148. Stanford, S. C. The Open Field Test: reinventing the wheel. *J. Psychopharmacol.* **21**, 134–135 (2007).
149. Oliveira, A. M. M., Hawk, J. D., Abel, T. & Havekes, R. Post-training reversible inactivation of the hippocampus enhances novel object recognition memory. *Learn. Mem.* **17**, 155–160 (2010).
150. Balderas, I. *et al.* The consolidation of object and context recognition memory involve different regions of the temporal lobe. *Learn. Mem.* **15**, 618–624 (2008).
151. Matus-Amat, P. The Role of the Dorsal Hippocampus in the Acquisition and Retrieval of Context Memory Representations. *J. Neurosci.* **24**, 2431–2439 (2004).
152. Maren, S., Aharonov, G. & Fanselow, M. S. Neurotoxic lesions of the dorsal hippocampus and Pavlovian fear conditioning in rats. *Behav. Brain Res.* **88**, 261–274 (1997).
153. Zhu, H. *et al.* Chemogenetic Inactivation of Ventral Hippocampal Glutamatergic Neurons Disrupts Consolidation of Contextual Fear Memory. *Neuropsychopharmacology* **39**, 1880–1892 (2014).
154. Rogers, J. L., Hunsaker, M. R. & Kesner, R. P. Effects of ventral and dorsal CA1 subregional lesions on trace fear conditioning. *Neurobiol. Learn. Mem.* **86**, 72–81 (2006).
155. Barrett, R. M. & Wood, M. a. Beyond transcription factors: the role of chromatin modifying

- enzymes in regulating transcription required for memory. *Learn. Mem.* **15**, 460–7 (2008).
156. Peixoto, L. L. *et al.* Memory acquisition and retrieval impact different epigenetic processes that regulate gene expression. *BMC Genomics* **16**, S5 (2015).
  157. Mamiya, N. *et al.* Brain Region-Specific Gene Expression Activation Required for Reconsolidation and Extinction of Contextual Fear Memory. *J. Neurosci.* **29**, 402–413 (2009).
  158. Vianna, M. R., Igaz, L. M., Coitinho, A. S., Medina, J. H. & Izquierdo, I. Memory extinction requires gene expression in rat hippocampus. *Neurobiol. Learn. Mem.* **79**, 199–203 (2003).
  159. Maze, I. *et al.* Analytical tools and current challenges in the modern era of neuroepigenomics. *Nat. Neurosci.* **17**, (2014).
  160. Levenson, J. M. A Bioinformatics Analysis of Memory Consolidation Reveals Involvement of the Transcription Factor c-Rel. *J. Neurosci.* **24**, 3933–3943 (2004).
  161. Cheval, H. *et al.* Distinctive features of Egr transcription factor regulation and DNA binding activity in CA1 of the hippocampus in synaptic plasticity and consolidation and reconsolidation of fear memory. *Hippocampus* **22**, 631–42 (2012).
  162. Keeley, M. B. Differential transcriptional response to nonassociative and associative components of classical fear conditioning in the amygdala and hippocampus. *Learn. Mem.* **13**, 135–142 (2006).
  163. Wallace, D. C. & Fan, W. Energetics, epigenetics, mitochondrial genetics. *Mitochondrion* **10**, 12–31 (2010).
  164. Henry, R. A., Kuo, Y., Bhattacharjee, V., Yen, T. J. & Andrews, A. J. Changing the Selectivity of p300 by Acetyl-CoA Modulation of Histone Acetylation. (2015).
  165. Pietrocola, F. *et al.* Spermidine induces autophagy by inhibiting the acetyltransferase EP300. *Cell Death Differ.* **22**, 509–516 (2015).
  166. Li, S. *et al.* Serine and SAM Responsive Complex SESAME Regulates Histone Modification Crosstalk by Sensing Cellular Metabolism. *Mol. Cell* **60**, 408–421 (2015).
  167. Sutendra, G. *et al.* A nuclear pyruvate dehydrogenase complex is important for the generation of Acetyl-CoA and histone acetylation. *Cell* **158**, 84–97 (2014).
  168. Matsuda, S. *et al.* Nuclear pyruvate kinase M2 complex serves as a transcriptional coactivator of arylhydrocarbon receptor. *Nucleic Acids Res.* gkv967 (2015). doi:10.1093/nar/gkv967
  169. Mashimo, T. *et al.* Acetate Is a Bioenergetic Substrate for Human Glioblastoma and Brain Metastases. *Cell* **159**, 1603–1614 (2014).
  170. Schug, Z. T. *et al.* Acetyl-CoA Synthetase 2 Promotes Acetate Utilization and Maintains Cancer Cell Growth under Metabolic Stress. *Cancer Cell* **27**, 57–71 (2015).
  171. Mariño, G. *et al.* Regulation of autophagy by cytosolic acetyl-coenzyme A. *Mol. Cell* **53**, 710–25 (2014).
  172. Pietrocola, F., Galluzzi, L., Bravo-San Pedro, J. M., Madeo, F. & Kroemer, G. Acetyl

- Coenzyme A: A Central Metabolite and Second Messenger. *Cell Metab.* **21**, 805–821 (2015).
173. Yoshii, Y. *et al.* Cytosolic acetyl-CoA synthetase affected tumor cell survival under hypoxia: the possible function in tumor acetyl-CoA/acetate metabolism. *Cancer Sci.* **100**, 821–827 (2009).
  174. Moffett, J. R., Arun, P., Ariyannur, P. S. & Namboodiri, A. M. a. N-Acetylaspartate reductions in brain injury: impact on post-injury neuroenergetics, lipid synthesis, and protein acetylation. *Front. Neuroenergetics* **5**, 11 (2013).
  175. Soliman, M. L. & Rosenberger, T. a. Acetate supplementation increases brain histone acetylation and inhibits histone deacetylase activity and expression. *Mol. Cell. Biochem.* **352**, 173–80 (2011).
  176. Jiang, L. & Gulanski, B. Increased brain uptake and oxidation of acetate in heavy drinkers. *J. Clin. ...* **123**, (2013).
  177. Bhatt, D. P., Houdek, H. M., Watt, J. a & Rosenberger, T. a. Acetate supplementation increases brain phosphocreatine and reduces AMP levels with no effect on mitochondrial biogenesis. *Neurochem. Int.* **62**, 296–305 (2013).
  178. Plackett, T. P. & Kovacs, E. J. Acute models of ethanol exposure to mice. *Methods Mol. Biol.* **447**, 3–9 (2008).
  179. Zakhari, S. Alcohol metabolism and epigenetics changes. *Alcohol Res.* **35**, 6–16 (2013).
  180. Starkman, B. Epigenetics—Beyond the genome in alcoholism. *Alcohol Res. ...* 293–305 (2011).
  181. Shukla, S. D. *et al.* Emerging role of epigenetics in the actions of alcohol. *Alcohol. Clin. Exp. Res.* **32**, 1525–1534 (2008).
  182. Kendrick, S. F. W. *et al.* Acetate, the key modulator of inflammatory responses in acute alcoholic hepatitis. *Hepatology* **51**, 1988–97 (2010).
  183. Kim, J.-S. & Shukla, S. D. Acute in vivo effect of ethanol (binge drinking) on histone H3 modifications in rat tissues. *Alcohol Alcohol* **41**, 126–32 (2006).
  184. Jiang, L. *et al.* Increased brain uptake and oxidation of acetate in heavy drinkers. *J. Clin. Invest.* **123**, 1605–1614 (2013).
  185. Ponomarev, I., Wang, S., Zhang, L., Harris, R. A. & Mayfield, R. D. Gene coexpression networks in human brain identify epigenetic modifications in alcohol dependence. *J. Neurosci.* **32**, 1884–97 (2012).
  186. Shibasaki, M., Mizuno, K., Kurokawa, K. & Ohkuma, S. Enhancement of histone acetylation in midbrain of mice with ethanol physical dependence and its withdrawal. *Synapse* **65**, 1244–50 (2011).
  187. Krishnan, H. R., Sakharkar, A. J., Teppen, T. L., Berkel, T. D. M. & Pandey, S. C. *The Epigenetic Landscape of Alcoholism.* *Epigenetics* **115**, (Elsevier Inc., 2014).
  188. Arora, D. S. *et al.* Hyposensitivity to gamma-aminobutyric acid in the ventral tegmental area during alcohol withdrawal: reversal by histone deacetylase inhibitors. *Neuropsychopharmacology* **38**, 1674–84 (2013).

189. Pandey, S. C., Ugale, R., Zhang, H., Tang, L. & Prakash, A. Brain chromatin remodeling: a novel mechanism of alcoholism. *J. Neurosci.* **28**, 3729–37 (2008).
190. You, C., Zhang, H., Sakharkar, A. J., Teppen, T. & Pandey, S. C. Reversal of deficits in dendritic spines, BDNF and Arc expression in the amygdala during alcohol dependence by HDAC inhibitor treatment. *Int. J. Neuropsychopharmacol.* **17**, 313–22 (2014).
191. Pizzimenti, C. L. & Lattal, K. M. Epigenetics and memory: causes, consequences and treatments for post-traumatic stress disorder and addiction. *Genes, Brain Behav.* **14**, 73–84 (2015).
192. Zannas, A. S., Provençal, N. & Binder, E. B. Epigenetics of Posttraumatic Stress Disorder: Current Evidence, Challenges, and Future Directions. *Biol. Psychiatry* **78**, 1–9 (2015).
193. Yehuda, R. *et al.* Post-traumatic stress disorder. *Nat. Rev. Dis. Prim.* 15057 (2015). doi:10.1038/nrdp.2015.57
194. Lattal, K. M. & Wood, M. a. Epigenetics and persistent memory: implications for reconsolidation and silent extinction beyond the zero. *Nat. Neurosci.* **16**, 124–9 (2013).
195. Kwapis, J. L. & Wood, M. a. Epigenetic mechanisms in fear conditioning : implications for treating post-traumatic stress disorder. *Trends Neurosci.* **37**, 706–720 (2014).